Activity Regulation of the Apoptosis and Autophagy Executioners Caspase-9 and ULK1

Inaugural-Dissertation

zur Erlangung des Doktorgrades
der Mathematisch-Naturwissenschaftlichen Fakultät
der Heinrich-Heine-Universität Düsseldorf

vorgelegt von

Stefan Drießen
aus Geldern

Düsseldorf, April 2015

aus dem Institut für Molekulare Medizin
der Heinrich-Heine-Universität Düsseldorf

Gedruckt mit der Genehmigung der
Mathematisch-Naturwissenschaftlichen Fakultät der
Heinrich-Heine-Universität Düsseldorf

Referent: Prof. Dr. Sebastian Wesselborg

Korreferent: Prof. Dr. Dieter Willbold

Tag der mündlichen Prüfung: 10.06.2015

Eidesstattliche Erklärung

Ich versichere an Eides Statt, dass die Dissertation von mir selbständig und ohne unzulässige fremde Hilfe unter Beachtung der „Grundsätze zur Sicherung guter wissenschaftlicher Praxis an der Heinrich-Heine-Universität Düsseldorf“ erstellt worden ist.

Remarks

The results depicted in Figure 5-3 A and partially Figure 5-5 were obtained by Quynh Nguyen during her bachelor thesis that was supervised by Stefan Drießen. The results depicted in Figure 5-12 B were obtained by Dr. Sebastian Schultz (Department of Biochemistry, Institute for Cancer Research, The Norwegian Radium Hospital, Oslo, Norway).The results depicted in Figure 5-18 C were obtained by Petter Holland (Institute of Basic Medical Sciences, Faculty of Medicine, University of Oslo, Norway). The results depicted in Figure 5-19 B were obtained by Niklas Berleth. The results depicted in Figure 5-20 A were partially obtained by Nora Hieke. The results depicted in Figure 5-20 B were partially performed by Olena Friesen. The mass spectrometric analysis and 2D-gel analysis were performed by Dr. Anja Stefanski (Molecular Proteomics Laboratory, BMFZ, University of Düsseldorf, Germany).

Table of contents

Abbreviations

Δ	deletion
λPP	lambda protein phosphatase
3-MA	3-methyladenine
aa	amino acid
Ab	antibody
Abl	Abelson murine leukemia viral oncogene homolog 1
Ad 5	adenovirus type 5
ADP	adenosine diphosphate
AKT	RAc-alpha serine/threonine-protein kinase
ALV	avian leukosis virus
AMBRA1	activating molecule in Beclin1-regulated autophagy
Amp	ampicillin
AMPK	adenosine 5'-monophosphate-activated protein kinase
APAF1	apoptotic protease-activating factor 1
AP	alkaline phosphatase
APS	ammonium persulphate
ATG	autophagy-related gene/protein
ATP	adenosine triphosphate
ATPase	adenosine triphosphatase
BAG2	BAG family molecular chaperone regulator 2
Baf A_1	bafilomycin A1 (from *Streptomyces griseus*)
Barkor	Beclin-1-associated autophagy-related key regulator
Bcl-2	B-cell lymphoma 2
Beclin1	Coiled-coil myosin-like BCL2-interacting protein
Bcr	breakpoint cluster region
Bif-1	Bax interacting factor-1
Bor	bortezomib
β-ME	beta-mercaptoethanol
bp	base pair
BSA	bovine serum albumine
CAD	caspase-activated DNase
CaMKK	Ca^{2+}/calmodulin-dependent protein kinase kinase
CARD	caspase activation and recruitment domain
CASP3	caspase-3
C9	caspase-9

CASP9	caspase-9
CCL	cleared cell lysate
cDNA	complementary DNA/ copy DNA
CTD	carboxy-terminal domain
CHAPS	3-[(3-Cholamidopropyl)dimethylammonio]-1-propanesulfonate
CMA	chaperone-mediated autophagy
CMV	cyto-megalo-virus
cyt c	cytochrome c
Da	Dalton
ddH_2O	double distilled H_2O
DD	death domain
DED	death effector domain
DFCP1	double FYVE domain containing protein 1
def	deficient
DIABLO	direct IAP binding protein with low pl
DIGE	difference gel electrophoresis
DMEM	Dulbecco's modified Eagle's medium
DMSO	dimethylsulfoxide
DNA	deoxyribonucleic acid
dNTP	2'-deoxynucleoside-5'-trisphosphate
Dox	doxycycline
dsDNA	double strand DNA
DTT	1,4-dithiothreitol
DUB	deubiquitinase
EBSS	Earle's balanced salt solution
E. coli	*Escherichia coli*
EDTA	ethylenediamine tetraacetic acid
EGFP	enhanced GFP
EGTA	ethylene-glycol-bis(2-aminoethyl ether)-N,N,N',N'- tetraacetic acid
env	gene encoding glycoprotein 160 (envelope protein)
Em	emission
ER	endoplasmic reticulum
EtOH	ethanol
Ex	excitation
FADD	Fas-accociated death domain
FAK	focal adhesion kinase
FCS	fetal calf serum

FIP200	FAK family-interacting protein of 200 kDa
Flp	flippase
FPLC	fast protein liquid chromatography
FRT	flippase recognition target
$GABA_A$	gamma-aminobutyric acid A
GABARAP	$GABA_A$-receptor associated protein
gag	gene encoding p55 (core protein)
GAPDH	glyceraldehyde-3-phosphate dehydrogenase
GATE-16	Golgi-associated ATPase enhancer of 16 kDa
GFP	green fluorescent protein
GST	glutathione- S-transferase
GTPase	guanosine triphosphatase
HA	peptide from influenza hemagglutinin protein (YPYDVPDYA)
HDAC6	histone deacetylase 6
HEK	human embryonic kidney
HeLa	Henrietta Lacks
HEPES	2-[4-(2-Hydroxyethyl)-1-piperazinyl]-ethanesulfonic acid
HPV18	human papillomavirus 18
HSP	heat shock protein
IAP	inhibitors of apoptosis
IB	immunoblot
IBM	IAP-binding motif
Ig	immunoglobulin
IgL	immunoglobulin light chain
IL	interleukin
IP	immunopurification
IP_3	inositol-(1,4,5)-trisphosphate
IP_3R	IP_3 receptor
IPTG	isopropyl-β-D-thiogalactopyranoside
IRES	internal ribosomal entry site
JAK2	Janus kinase 2
JAMM	JAB1/MPN/MOV34 metalloenzymes
Kan	Kanamycin
kd	kinase-dead
LB	lysogeny broth
LC3	short for MAP1LC3 (microtubule-associated protein light chain 3)
LC3-I	cytosolic, unlipidated LC3 (apparent MW ~18 kDa)

LC3-II	membrane bound, PE-conjugated LC3 (apparent MW ~16 kDa)
LKB1	liver kinase B
LPC	lysophosphatidylcholine
mAb	monoclonal antibody
MBP	myelin basic protein
M(ed)	medium
MEF	mouse embryonic fibroblast
MeOH	methanol
Mito	mitomycin C
MMLV	Moloney murine leukemia virus
MOMP	mitochondria outer membrane permeabilization
mRNA	messenger RNA
MS	mass spectrometry
mRFP	monomeric red fluorescent protein
MTOC	microtubule organizing center
(m)TOR	(mammalian/mechanistic) target of rapamycin
mTORC1/2	mammalian/mechanistic target of rapamycin complex 1/2
MW	molecular weight
NCBI	National Center for Biotechnology Information
NOD	nucleotide-binding and oligomerisation domain
OTU	ovarian tumor protease
P	phosphate
p	protein (as prefix or suffix) or phospho (as prefix)
^{32}P	phosphate containing the radioactive ^{32}P isotope of phosphorus
PAGE	polyacrylamide gel electrophoresis
PARP	Poly (ADP-ribose) polymerase
PAS	pre-autophagosomal structure
PBS	phosphate-buffered saline
PCR	polymerase chain reaction
PDK1	phosphatidylinositol 3-dependent kinase
PE	phosphatidylethanolamine
PI	phosphatidylinositol
PI3K	phosphatidylinositol 3-kinase
$PI(3,4)P_2$	phosphatidylinositol 3,4-bisphosphate
$PI(4,5)P_2$	phosphatidylinositol 4,5-bisphosphate
$PI(3,4,5)P_3$	phosphatidylinositol 3,4,5-trisphosphate
PMSF	phenylmethanesulfonyl fluoride

pol	gene encoding protease, reverse transcriptase and integrase
polybrene	1,5-dimethyl-1,5-diazaundecamethylene polymethobromide
PP	protein phosphatase
PS	phosphatidylserine
PTEN	phosphatase and tensin homolog
PTM	post translational modification
PVDF	polyvinylidene fluoride
QVD	Q-VD-OPh hydrate
rAAV	recombinant adeno-associated virus
Raptor	regulatory-associated protein of mTOR
RAV-1	Rous associated virus 1
RB1	retinoblastoma 1
RB1CC1	RB1-inducible coiled-coil protein 1
rec	reconstituted
REDD1	protein regulated in development and DNA damage response 1
rfu	relative fluorescent unit
Rheb	Ras homolog enriched in brain
Rictor	rapamycin insensitive companion of mTOR
RNA	ribonucleic acid
RPMI	Roswell Park Memorial Institute
RT	room temperature
RTK	receptor tyrosine kinases
SD	standard deviation
SDS	sodium dodecylsulfate
SESN1/2	sestrin 1/2
siRNA	small interfering RNA
Smac	second mitochondria-derived activator of caspases
SNAP-29	synaptosomal-associated protein 29
SNARE	N-ethylmaleimide-sensitive factor attachment protein receptor
SNP	single nucleotide polymorphism
STAT3	Signal transducer and activator of transcription 3
STK36/FUSED	Serine/threonine protein kinase 36
STS	staurosporine
Stx17	syntaxin 17
t	time
T	temperature
TAE	Tris acetate EDTA buffer

TAK1	TGF-beta activated kinase 1
TBS	Tris-buffered saline
TEMED	N,N,N',N'-tetramethylethylene-diamine
Tet	tetracycline
TNF-R	tumor necrosis factor receptor
TRADD	TNF-R1-associated death domain
TRAIL	TNF-related apoptosis-inducing ligand
Tris	Tris-(hydroxymethyl)-aminomethane
Triton X-100	4-(1,1,3,3-Tetramethylbutyl)phenyl-polyethylene glycol
TSC1/2	tuberous sclerosis 1/2 protein
TUBE	tandem ubiquitin binding entities
Tween®	polyoxyethylene(20) sorbitan monolaurate
U	Units
Ub	ubiquitin
UCH	ubiquitin C-terminal hydrolases
ULK1/2	Unc-51-like kinase 1/2
UPS	ubiquitin-proteasome system
USP	ubiquitin-specific protease
VSV-G	vesicular stomatitis virus glycoprotein
UVRAG	UV radiation resistance-associated gene protein
VAMP8	SNARE vesicle-associated membrane protein 8
v/v	volume per volume
WIPI	WD repeat domain phosphoinositide-interacting protein
WCL	whole cell lysate
w/o	without
WP	WP1130
w/v	weight per volume
wt	wild type
x	times (multiplication)
X-Gal	5-bromo-4-chloro-3-indoxyl-β-D-galactopyranoside

Prefixes

p (pico)	10^{-12}
n (nano)	10^{-9}
µ (micro)	10^{-6}
m (milli)	10^{-3}

c (centi)	10^{-2}
k (kilo)	10^{3}
M (mega)	10^{6}

Units

s	second	Da	Dalton
min	minute	V	volt
h(rs)	hour(s)	A	ampere
g/ *g*	gram or local gravity	pH	$-\log10(a_{H+})$
l	litre	°C	degree Celsius
M	molar (mole/l)	rpm	rounds per minute
U	enzyme unit		

Amino acids

	single-letter	**three-letter code**
Alanine	A	Ala
Cysteine	C	Cys
Aspartic acid	D	Asp
Glutamic acid	E	Glu
Phenylalanine	F	Phe
Glycine	G	Gly
Histidine	H	His
Isoleucine	I	Ile
Lysine	K	Lys
Leucine	L	Leu
Methionine	M	Met
Asparagine	N	Asn
Proline	P	Pro
Glutamine	Q	Gln
Arginine	R	Arg
Serine	S	Ser
Threonine	T	Thr
Valine	V	Val
Tryptophan	W	Trp
Tyrosine	Y	Tyr

Deoxyribonucleotides

		single-letter code
2’-Deoxyadenosine 5‘-monophosphate	dAMP	A
2’-Deoxycytidine 5‘-monophosphate	dCMP	C
2’-Deoxyguanosine 5‘-monophosphate	dGMP	G
2‘-Deoxythymidine 5‘-monophosphate	dTMP	T

1 Summary

In the first part of the thesis, apoptotic processes were examined. Apoptosis, a form of programmed cell death, is essential *inter alia* for cell homeostasis, embryogenesis and elimination of tumor cells. Apoptosis is mainly activated via the extrinsic death receptor pathway and the intrinsic mitochondrial pathway, which is characterized by mitochondria outer membrane permeabilization (MOMP), apoptosome formation that induces the activation of the initiator apoptosis executioner caspase-9 (cysteine aspartate-specific protease 9), and effector caspase activation, ultimately leading to cell death. Most common, cancer therapeutics induce cell death via the intrinsic apoptosis pathway by genotoxic stress, and in turn tumor cells gain radio- and chemotherapy resistance by disrupting the intrinsic apoptosis pathway. The broad-range kinase inhibitor staurosporine (STS) has the ability to induce caspase-9 activation bypassing the canonical intrinsic apoptosis pathway and thereby enabling the elimination of radio- and chemotherapy resistant tumor cells.

Using STS, it could be shown that caspase-9 activation bypassing the intrinsic apoptosis pathway relies on the caspase activation and recruitment domain (CARD). In contrast, other proteases like calpains, cathepsins, and capsase-4 were not involved. In addition, caspase-9 phosphorylation status is not important for STS induced caspase-9 activation, but its activation by another macro-molecular complex employing CARD to CARD interaction is assumable, in which putatively BAG2 plays a crucial role. The further understanding of alternative caspase-9 activation mechanisms increases the chance for overcoming chemo- and radiotherapy resistance in tumor cells.

In the second part of the thesis, autophagic processes were examined. (Macro)autophagy is a highly conserved pro-survival cellular process responsible for the degradation of long-lived proteins and old/damaged organelles. Autophagy maintains cellular homeostasis and supports adaption to cellular stress conditions like starvation. The central complex for regulating autophagy initiation is the ULK1 complex consisting of the Ser/Thr kinases ULK1/2, and the accessory proteins ATG13, RB1CC1, and ATG101. Under normal conditions the complex is kept inactivated by phosphorylation through mTORC1, whereas activated under cellular stress conditions via dephosphorylation/phosphorylation processes. Based on previous findings it has been proposed that ULK1 stability is regulated by ubiquitination, however deubiquitinases (DUBs) regulating ULK1 ubiquitination have not been characterized yet.

Using the partially selective DUB-inhibitor WP1130, it was confirmed that ULK1 is post-translationally modified by ubiquitination, which induces the aggregation of ULK1/2 and its transfer to perinuclear aggresomes. Furthermore, upon aggregation, ULK1/2 kinase activity was abrogated leading ultimately to autophagy inhibition by WP1130 treatment. Collectively, these results strongly indicate that deubiquitinases regulate ULK1 stability, activity, and overall autophagy. Accordingly, regulation of ULK1 ubiquitination might be an effective approach to modulate the autophagic response that can be of advance in combinatorial anticancer therapies.

1.1 Zusammenfassung

Der erste Teil der Dissertation beschäftigt sich mit der Untersuchung apoptotischer Prozesse. Apoptose, eine Form des programmierten Zelltods, ist unter anderem entscheidend für die Erhaltung der Zellhomöostase, der Embryogenese und der Eliminierung von Tumorzellen. Apoptose wird hauptsächlich durch den extrinsischen Todesrezeptorsignalweg und den intrinsischen mitochondrialen Signalweg aktiviert. Letzterer ist gekennzeichnet durch die Permeabilisierung der äußeren Mitochondrienmembran, der Apoptosomformation, welche die Aktivierung der Initiatorcaspase Caspase-9 induziert, und die Effektorcaspasen Aktivierung, die schlussendlich zum Zelltod führt. Hauptsächlich induzieren Krebstherapeutika den Zelltod über den intrinsischen Apoptosesignalweg durch genotoxischen Stress. Im Gegenzug werden Tumorzellen Strahlungs- und Chemotherapie-resistent durch die Blockierung des intrinsischen Apoptosesignalwegs. Der Breitband Kinaseinhibitor Staurosporin (STS) hat die Möglichkeit, Caspase-9 Aktivierung zu induzieren, die unabhängig vom kanonischen intrinsischen Apoptosesignalweg abläuft und dadurch die Eliminierung therapieresistenter Tumorzellen ermöglicht.

Es konnte gezeigt werden, dass die Staurosporin induzierte Caspase-9 Aktivierung von der *caspase activation and recruitment domain* (CARD) abhängig ist. Im Gegensatz sind andere Proteasen wie Calpaine, Cathepsine oder Caspase-4 nicht involviert. Des Weiteren hat der Caspase-9 Phosphorylierungsstatus keinen Einfluss auf die STS induzierte Aktivierung von Caspase-9. Es ist jedoch naheliegend, dass die Aktivierung durch einen anderen makromolekularen Komplex mittels CARD-CARD Interaktion stattfindet, in welchem möglicherweise BAG2 eine entscheidende Rolle spielt. Das weitere Verständnis der alternativen Caspase-9 Aktivierung könnte einen entscheidenden Beitrag liefern Strahlungs- und Chemotherapie-Resistenzen zu überwinden.

Der zweite Teil der Dissertation beschäftigt sich mit der Untersuchung autophagischer Prozesse. (Makro)autophagie ist ein hochkonservierter, zellulärer Prozess, der sich positiv auf das Überleben der Zelle auswirkt. Während der Autophagie werden langlebige Proteine und beschädigte/alte Organelle abgebaut, um die zelluläre Homöostase zu gewährleisten. Darüber hinaus werden akute zelluläre Stressbedingungen wie Nährstoffunterversorgung adaptiert. Der zentrale Komplex zur Regulierung der Autophagieinitiation ist der ULK1 Komplex bestehend aus den Ser/Thr Kinasen ULK1/2 und den Proteinen ATG13, RB1CC1 und ATG101. Unter Normalbedingungen ist der Komplex durch mTORC1 abhängige Phosphorylierung inaktiviert, wohingegen unter zellulären Stressbedingungen der Komplex durch Dephosphorylierung/Phosphorylierung aktiviert wird. Basierend auf vorherigen Ergebnissen wurde gezeigt, dass ULK1-Stabilität durch Ubiquitinierung reguliert wird. Bisher wurden jedoch keine beteiligten Deubiquitinasen (DUB) charakterisiert.

Mit Hilfe des partiell selektiven DUB-inhibitors WP1130 wurde bestätigt, dass ULK1 posttranslational durch Ubiquitinierung modifiziert wird, wodurch die Aggregierung von ULK1/2

und der anschließende Transfer zu perinukleären Aggresomen induziert wird. Des Weiteren führt die Aggregierung zum Verlust der ULK1/2 Kinaseaktivität und zur Autophagie-Inhibition. Zusammenfassend belegen diese Ergebnisse die Regulierung der Stabilität und der Aktivität von ULK1 und allgemein der Autophagie durch Deubiquitinierungsprozesse. Demzufolge könnte die Regulierung von ULK1 durch Ubiquitinierung ein möglicher Ansatz sein, um autophagische Prozesse zu modulieren und generell kombinatorische Krebstherapien zu optimieren.

2 Introduction

This thesis is divided into two main parts, dealing on the one hand with the apoptotic initiator caspase-9 and on the other hand with the Ser/Thr kinase ULK1 involved in autophagy initiation. Therefore, the apoptotic and autophagic parts are introduced separately.

2.1 Apoptosis

The term apoptosis has Greek origin, which can be translated as “falling off” describing analogously the falling off of leaves from a tree (Kerr et al., 1972). Nowadays, apoptosis is synonymously used for programmed cell death type I, a genetically form of cell death. Under normal physiological conditions, apoptosis can be considered as the counterpart of mitosis and cell proliferation. In human adults about 10 billion cells die every day, to balance the number of new cells generated by stem cells (Renehan et al., 2001; Elmore, 2007). Besides remaining cell homeostasis, apoptosis plays a crucial role in embryogenesis, the elimination of autoreactive lymphocytes, virus-infected cells, or tumor cells. Accordingly, dysregulation of apoptosis contributes to various diseases, such as degenerative disorders, cancer, and infectious diseases. The process of apoptosis is highly conserved throughout metazoan species. In addition, the existence of programmed cell death has also been observed in unicellular organism, i.e. *Saccharomyces cerevisiea* (Madeo et al., 1997). Apoptosis is characterized by several morphological and biochemical processes. Kerr et al. described apoptosis taking place at two morphologic discrete stages, first the formation of a number of membrane-bound cell fragments and second the elimination of these so-called apoptotic bodies by phagocytosis (Kerr et al., 1972). The first stage is characterized by nuclear and cellular shrinkage, which is caused by condensation of chromatin and cytoplasm (Kerr et al., 1972; Elmore, 2007). Additionally, the chromosomal DNA is cleaved between nucleosomes, resulting in DNA units with a length of 180 bp, which is accomplished by caspase-activated DNase (CAD) (Nagata et al., 2010). Further hallmarks are the reduction of mitochondrial membrane potential and intracellular acidification (Ly et al., 2003; Nilsson et al., 2006). The formation of apoptotic bodies is mediated by plasma membrane blebbing of varying size, which contain the condensed cytoplasm, tightly packed organelles, and nuclear fragments (Elmore, 2007). The second morphological stage, the clearance of apoptotic cells, is characterized by the externalization of “find-me” and “eat-me” signals, e.g. lysophosphatidylcholine (LPC) and phosphatidylserine (PS), respectively (Fadok et al., 1992; Lauber et al., 2003). Notably, during apoptosis cellular contents are not released from the

cell, hence avoiding the generation of an inflammatory response and secondary necrosis (Nagata et al., 2010; Ravichandran, 2011).

2.1.1 Apoptotic signaling pathways

In mammalian cells, apoptosis can be activated by two main signaling pathways, i.e. the extrinsic death receptor pathway and the intrinsic mitochondrial pathway. The extrinsic apoptosis pathway is characterized by the activation of death receptors localized in the plasma-membrane sensing signals from outside the cell upon binding to their respective ligands, whereas the intrinsic pathway is activated within the cell, e.g. by cellular or chromosomal damage. Both pathways are executed via activation of intracellular cysteine aspartate-specific proteases, termed caspases. To date, 15 different mammalian caspases have been reported, which can be subdivided into two groups, one regulating inflammatory processes (caspase-1, -4, -5, -11, -13, and -14) and the others regulating apoptosis (caspase-2, -3, -6, -7, -8, -9, -10, and -15) (Chowdhury et al., 2008; McIlwain et al., 2013). The apoptosis regulating caspases can be further divided into initiator caspases (caspase-2, -8, -9, and -10) and effector caspases (caspase-3, -6, and -7). Of note, caspase-12 is a pseudo caspase and caspase-11 and -15 are absent in humans (Lamkanfi et al., 2004; Chowdhury et al., 2008). Hereinafter, only the apoptosis relevant caspases will be described. Caspases are synthesized as inactive pro-forms, the so-called procaspases. For caspase activation the proteolytic processing at two specific aspartic residues is necessary. Thereby, the pro-domain is removed (except for initiator caspases), which results in the formation of a small and large subunit of approximately 10 and 20 kDa (p10, p20). Those subunits form a heterotetramer of two p10 and two p20 subunits (Chowdhury et al., 2008). The large subunit contains the catalytic center, whereas the small subunit is crucial for substrate binding (Pop & Salvesen, 2009).

Generally, initiator caspases are activated in large macromolecular complexes, e.g. the death-inducing signaling complex (DISC) regarding the extrinsic apoptosis pathway and the apoptosome in the intrinsic mitochondrial pathway.

To date, it is reported that approximately 1,000 proteins are cleaved by caspases (Crawford & Wells, 2011). The processing of effector caspases results in the cleavage of multiple proteins belonging to various types of proteins, e.g. cytoskeleton and structural proteins, nuclear proteins, DNA-synthesis and DNA-repair proteins, cell cycle proteins and many more. The inactivation of those proteins results in cell cycle arrest, loss of cell-to-cell adhesion, membrane blebbing, tagging the cell for phagocytosis, and attraction of phagocytes, which ultimately leads to the elimination of the cell (Fischer et al., 2003).

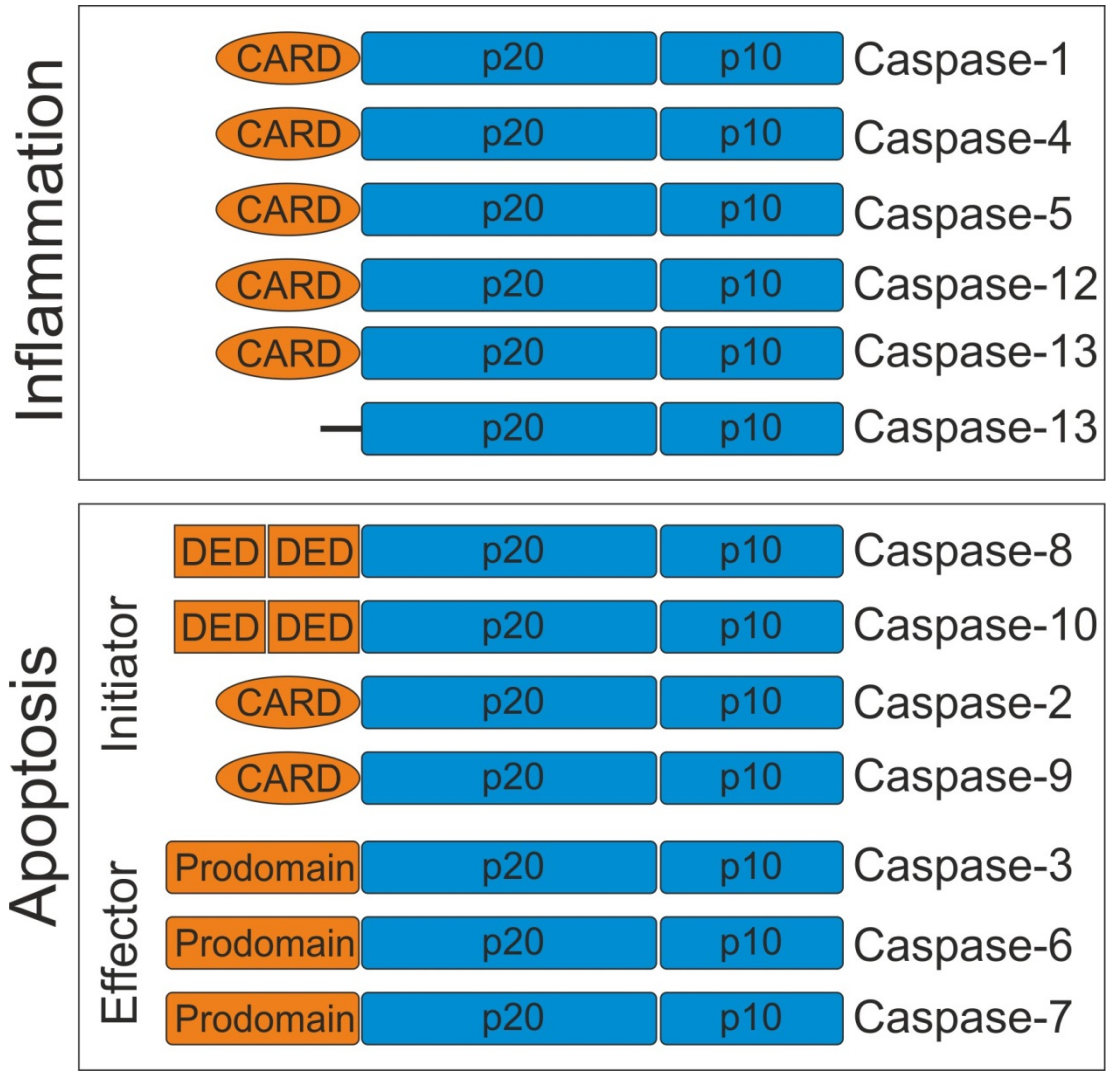

Figure 2-1: Overview of mammalian caspases. Caspases can be subdivided into inflammatory and apoptotic caspases. The latter can be further subdivided into initiator and effector caspases. Caspases consists of a small (p10) and a large (p20) subunit, as well as other domains, such as the death effector domain (DED) and the caspase activation and recruitment domain (CARD), which are important for homotopic cell-to-cell interaction.

2.1.1.1 Extrinsic apoptosis pathway

The extrinsic apoptosis pathway is induced by the binding of death receptor ligands to their corresponding death receptor in the plasma membrane of the cell. The death receptors belong to the tumor necrosis factor receptor (TNF-R) superfamily, containing an intracellular death domain (DD), which is crucial for signal transduction. To date, six DD-containing death receptors are reported, namely TNF-R1 (also termed DR1, CD120a, p55, p60), CD95 (also termed DR2, FAS, APO-1), TRAIL-R1 (also termed DR4, APO-2), TRAIL-R2 (also termed DR5, KILLER, TRICK2), TRAMP (also termed DR3, APO-3, LARD, WSL-1), and DR6. These receptors are activated upon binding to their respective ligand, namely TNF, CD95L (also termed FasL, APO-1L), TRAIL (also termed APO-1L), and TL1A (Lavrik et al., 2005; Kantari & Walczak, 2011). The death receptors can be subdivided into two groups. The first is characterized by recruiting the adapter protein Fas-accociated death domain (FADD) in the cytoplasm to

CD95, TRAIL-R1, or TRAIL-R2 upon binding to their respective ligand, which enables the formation of the DISC. The second group is characterized by the recruitment of the adapter protein TNF-R1-associated death domain (TRADD) to TNF-R1, TRAMP, and DR6 upon binding to their respective ligands (Lavrik et al., 2005; Kantari & Walczak, 2011). The TRADD-death receptors function in the regulation of transcription, and apoptosis via NF-κB and JNK activation, and a programmed form of necrosis the so-called necroptosis (reviewed in (Declercq et al., 2009; Vandenabeele et al., 2010; Cabal-Hierro & Lazo, 2012; Kaczmarek et al., 2013)). One of the best characterized ligand activated death receptor signaling pathways is the binding of ligands to CD95 and TRAIL-R1/2, thereby inducing the formation of the DISC in the cell, which consists of probably trimerized receptors, the DD-containing FADD, procaspase-8/10, and the FLICE inhibitory proteins ($FLIP_{L/S}$) (Peter & Krammer, 2003). CD95 and TRAIL-R1/2 probably trimerize upon ligand binding, thus enabling the recruitment of FADD via homotopic DD binding, whereas FADD binds again via homotopic interaction with its death effector domain (DED) to procaspase-8 and procaspase-10 (Lavrik et al., 2005). Procaspase-8 is activated concerning the induced proximity model, by local aggregation of procaspase-8 at the DISC that leads to its subsequent autoproteolytic activation (Salvesen & Dixit, 1999). Upon the activation of the initiator caspase-8, the effector caspase-3, -6, and -7 are activated, resulting in apoptosis. The contribution of caspase-10 to apoptosis, which is the closest relative of caspase-8, is still unclear and conflicting results have been reported (McIlwain et al., 2013).

The extrinsic apoptosis pathway is connected with the intrinsic apoptosis pathway by caspase-8 dependent cleavage and activation of the pro-apoptotic Bcl-2 protein Bid, generating a truncated form (tBid). tBid translocates to mitochondria and activates the intrinsic apoptosis pathway. This additional way of apoptosis induction can be seen as an activation loop increasing the apoptosis rate (Li et al., 1998). Of note, it has been reported that two types of CD95 apoptotic pathways exists (Scaffidi et al., 1998; Lavrik & Krammer, 2012). In type I cells, caspase-8 is activated by the DISC within seconds, which cannot be blocked by the overexpression of anti-apoptotic Bcl-2 proteins (Bcl-2, Bcl-x_L). In contrast, apoptosis can be blocked via overexpression of anti-apoptotic Bcl-2 proteins in type II cells. DISC-formation is reduced in those cells, and activation of caspase-3 is mainly dependent on the mitochondrial activation loop via cleavage of Bid by caspase-8 (Yin et al., 1999; Kaufmann et al., 2007; Lavrik & Krammer, 2012).

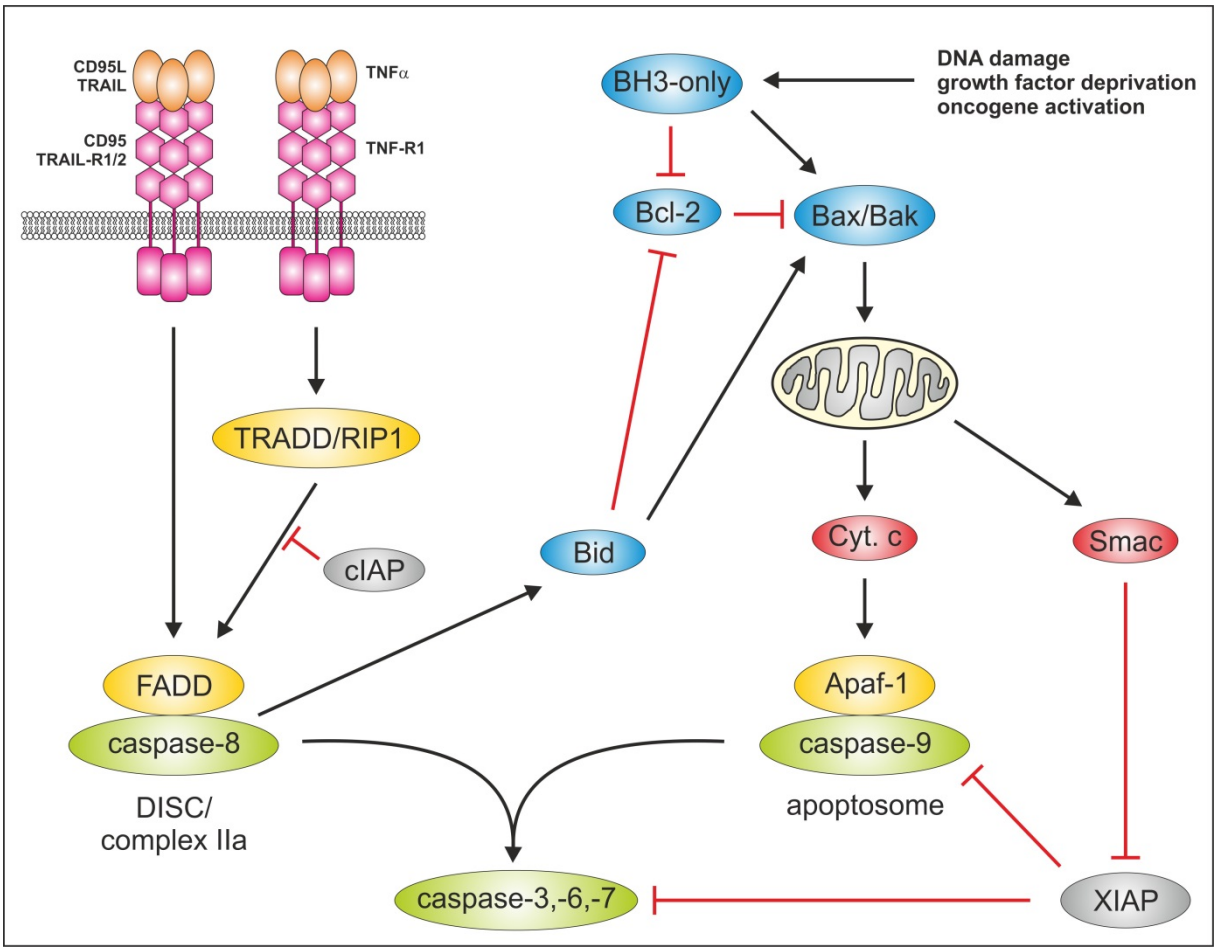

Figure 2-2: Signaling pathways of the extrinsic death receptor pathway and the intrinsic mitochondrial pathway. (modified from the postdoctoral thesis (Habilitation) of PD Dr. Björn Stork, 2013)

2.1.1.2 Intrinsic apoptosis pathway

The intrinsic mitochondrial pathway is activated under stress conditions in the cell, e.g. chromosomal damage or oncogene activation. The central organelle in this pathway is the mitochondrion, which is able to release pro-apoptotic factors upon cellular stress conditions, e.g. DNA-damage and oxidative stress, and moreover UV- and γ-radiation, which also leads to DNA-damage. The central regulators of the intrinsic apoptosis pathway are the B-cell lymphoma 2 (Bcl-2) proteins, which can be divided into pro-apoptotic, i.e. Bcl-2, Bcl-x_L, Mcl-1, A1/Bfl-1, and Bcl-w (Vaux et al., 1988; Boise et al., 1993; Kozopas et al., 1993; Lin et al., 1993; Choi et al., 1995; Gibson et al., 1996); and anti-apoptotic members, i.e. the multidomain proteins Bak, Bax, and Bok/Mtd, and the BH3-only proteins Bid, Bad, Bik/Nbk, Bim/Bod, Noxa, Puma/Bbc3, Bmf, and Hrk/DP5 (Lomonosova & Chinnadurai, 2008; Strasser et al., 2011; Happo et al., 2012). The function of Bcl-2 proteins regulating apoptosis will be explained in detail in chapter 2.1.2.1..

Upon the above described cellular stress conditions, the transcription factor p53 can induce the up-regulation of anti-apoptotic Bcl-2 proteins, e.g. Bax, Puma, and Noxa, resulting in mitochondria outer membrane permeabilization (MOMP). The main result of MOMP is the

release of different apoptogenic factors, such as cytochochrome c and Smac/DIABLO (Liu et al., 1996; Oda et al., 2000; Nakano & Vousden, 2001; Vaux, 2011). Cytochrome c is a 12 kDa protein, which is under normal healthy conditions localized between the outer and inner mitochondrial membrane, shuttling electrons between complex III and complex IV of the respiratory chain (Kulikov et al., 2012). When Cytochrome c is released under apoptosis inducing conditions, it binds apoptotic protease-activating factor 1 (APAF1) at the WD-40 repeat and induces a conformational change that potentially causes hydrolysis of a bound (d)ATP and enables the formation of a heptamer. APAF1 consists of three functional domains, namely the N-terminal CARD, the C-terminal WD-40 repeats, and the central nucleotide-binding and oligomerization domain (NOD). The N-terminal CARD region of APAF1 forms a central ring, and the seven NODs are laterally associated to form a hub. Subsequently, procaspase-9 is recruited to this macromolecular ring complex via CARD-to-CARD interaction, ultimately forming the apoptosome, which is able to activate procaspase-9 and induces the caspase cascade leading to apoptosis (Saleh et al., 1999; Acehan et al., 2002; Yu et al., 2005; Riedl & Salvesen, 2007).
Generally, there exist two models how procaspase-9 is activated in the apoptosome, the proximity-induced dimerization model and the proximity-induced association/allosteric model (Reubold & Eschenburg, 2012). In the proximity-induced dimerization model procaspase-9 is activated when two procaspase-9 proteins are brought into close contact, *ergo* close steric proximity (Renatus et al., 2001; Boatright et al., 2003; Pop et al., 2006). In the proximity-induced association/allosteric model, the APAF1 recruitment of procaspase-9 induces a conformational change resulting in its activation (Rodriguez & Lazebnik, 1999; Shiozaki et al., 2002; Chao et al., 2005). Which of these models holds true is still under debate. However, caspase-9 comprises only substantial catalytic activity when bound to the apoptosome.

For the sake of completeness, it has to be mentioned, that procaspase-2, the other initiator caspase of the intrinsic apoptosis pathway besides caspase-9, is also activated in a macromolecular complex termed the PIDDosome. Thereby, p53-induced protein with a death domain (PIDD) interacts via a DD with the adapter protein RIP-associated ICH-1/CED-3 homologous protein with a death domain (RAIDD) that can recruit procaspase-2 via a CARD. Procaspase-2 is activated by this interaction and can initiate apoptosis upon genotoxic stress (Tinel & Tschopp, 2004). To date, several PIDD-containing complexes are reported, which are involved in DNA repair, cell cycle regulation, and nuclear factor-κB signaling (Janssens & Tinel, 2012).

2.1.2 Regulation of Apoptosis

Apoptosis is tightly regulated, since either an increased or a decreased rate of apoptosis possibly leads to severe diseases such as neurodegeneration or cancer. Furthermore, disturbed apoptosis during embryogenesis can lead to abnormal development of the brain, other organs, and physiognomic defects (Brill et al., 1999).

2.1.2.1 Bcl-2 proteins

Members of the Bcl-2 protein family are central regulators of the mitochondrial intrinsic apoptosis pathway. Their main function is the regulation of the mitochondrial outer-membrane permeabilization (MOMP). The Bcl-2 protein family can be subdivided regarding their inducing (pro-apoptotic) or inhibiting (anti-apoptotic) role in apoptosis, i.e. the pro-apoptotic Bcl-2, Bcl-$x_{L,}$ Mcl-1, A1/Bfl-1, and Bcl-w proteins, and the anti-apoptotic multidomain proteins Bak, Bax, and Bok/Mtd, and the BH3-only proteins Bid, Bad, Bik/Nbk, Bim/Bod, Noxa, Puma/Bbc3, Bmf, and Hrk/DP5 (Moldoveanu et al., 2014). The protein family members Bak, Bax, and Bok (the role of Bok is uncertain) are the so-called effectors of MOMP, which are directly inhibited via protein-protein interaction by Bcl-2, Bcl-$x_{L,}$ Mcl-1, A1/Bfl-1, and Bcl-w (Llambi et al., 2011). Those proteins comprise four Bcl-2 homology (BH) domains. The induction of MOMP is realized by a conformational change of Bak/Bax, which oligomerize in the outer mitochondrial membrane creating a pore. The BH3-only proteins, which share only the third BH domain, regulate the pro-apoptotic and anti-apoptotic multidomain Bcl-2 proteins presumably via two models either by directly activating the pro-apoptotic effectors or by blocking the activity of the anti-apoptotic proteins and thereby activating the pro-apoptotic effectors in an indirect way. tBid, Bim, and PUMA potentially activate Bak/Bax directly, whereas Bad, Bik, Bmf, Hrk, and Noxa disrupted the existing anti-apoptotic complex by binding of anti-apoptotic proteins. The latter are called de-repressors or sensitizers (Czabotar et al., 2014; Moldoveanu et al., 2014).

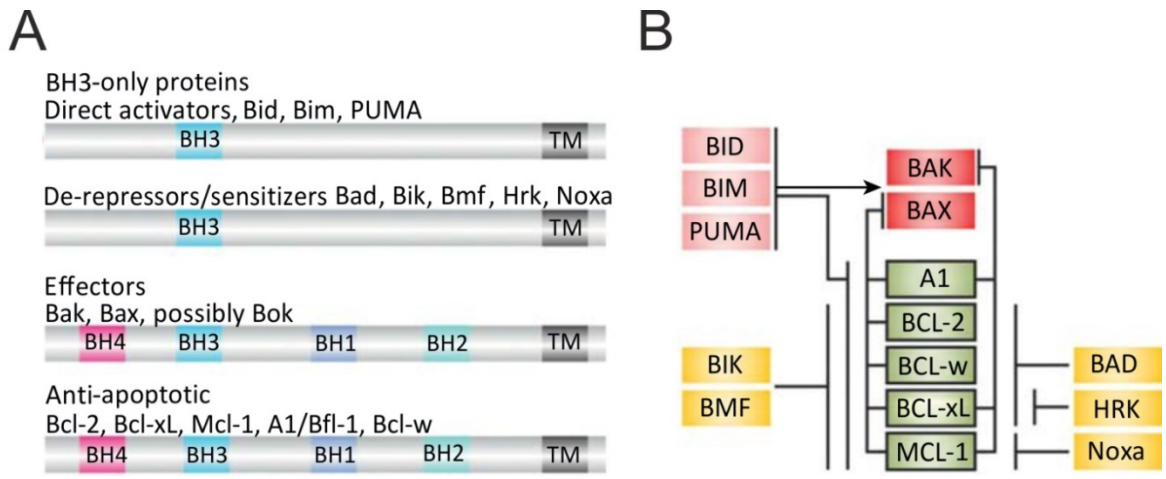

Figure 2-3: The Bcl-2 protein family and its regulation. (A) Schematic drawing and classification of Bcl-2 proteins. (B) Schematic drawing of Bcl-2 protein regulation. (modified from Moldoveanu et al., 2014)

2.1.2.2 IAP proteins

The inhibitors of apoptosis (IAP) proteins are a protein family counterbalancing the activity of caspases. The mammalian IAP protein family consists of eight members namely NAIP, c-IAP1, c-IAP2, XIAP, survivin, Apollon/Bruce, ML-IAP/livin, and ILP-2. (Vaux & Silke, 2003). The IAPs comprise one to three baculoviral IAP repeat (BIR) domains, a zinc binding domain with a length of about 70 amino acids that are mainly responsible for caspase binding (Hinds et al., 1999; de Almagro & Vucic, 2012). The best characterized IAP regarding the regulation of apoptosis is XIAP. The BIR2 and BIR3 domain are crucial for the inhibition of the effector caspase-3 and caspase-7 and the initiator caspase-9 (Shiozaki et al., 2003; Scott et al., 2005). In the case of caspase-9 inhibition, XIAP binds via the BIR3 domain the N-terminal peptide of the linker region between the small and the large subunit that is exposed after the autocatalytic cleavage of procaspase-9, thus inhibiting the activation of caspase-9 (Srinivasula et al., 2001). The IAPs itself can be regulated via protein phosphorylation regulating protein-protein interaction, intracellular localization, or stability (Srinivasula & Ashwell, 2008). Moreover, the inhibitory IAPs are regulated itself by other inhibitors. Proteins with IAP-binding motif (IBM) can bind IAPs at their BIR domain releasing the bound caspase or inducing the degradation of IAPs. One of these inhibitors is the second mitochondria-derived activator of caspases (Smac, also termed direct IAP binding protein with low pl, DIABLO), which is released from the mitochondria during MOMP, subsequently binding XIAP and thus releasing caspase-9 (Vaux, 2011; de Almagro & Vucic, 2012).

2.1.3 Therapeutics targeting apoptosis

One of the hallmarks of cancer, which were postulated by Hanahan and Weinberg, is the resistance to cell death (Hanahan & Weinberg, 2011). One opportunity for cancer therapy is

therefore to overcome this resistance and induce cell death in those cells via apoptosis. The targeted cancer therapeutics can be subdivided into therapeutic monoclonal antibodies and small molecules that can enter the cell and inhibit the enzymatic activity of targeted proteins. Hereafter, focus will be set on BH3 mimetics and Smac mimetics, inducing the intrinsic apoptosis pathway and monoclonal antibodies against TRAIL-R1/2 inducing the extrinsic apoptosis pathway.

One possibility to induce apoptosis in cancer cells is the activation of the intrinsic apoptosis pathway via inhibiting anti-apoptotic Bcl-2 proteins with the help of BH3 mimetics. The latter function as de-repressors that mimic the role of Bad, Bik, Bmf, Hrk, and Noxa. ABT-737 is such a BH3 mimetic, an organic molecule that inhibits Bcl-2, Bcl-x_L, and Bcl-w with high affinity, but is not able to bind the other two anti-apoptotic Bcl-2 proteins Mcl-1 and A1. Therefore, ABT-737 has little activity in tumor cells, expressing high levels of Mcl-1 or A1. Accordingly, combination with Mcl-1 downregulators has been suggested. (Oltersdorf et al., 2005; van Delft et al., 2006). However, the BH3 mimetics ABT-263 (navitoclax, oral version of ABT-737), GX15-070 (obatoclax), and AT-10 are under clinical evaluation in hematological malignancies. In contrast to ABT-737, the BH3 mimetics GX15-070 and AT-10 bind to all anti-apoptotic Bcl-2 proteins, but with rather low affinity (Khaw et al., 2011; Billard, 2012).

Another approach to induce apoptosis in cancer cells is the inhibition of IAPs, which can be achieved among others by Smac mimetics. These molecules mimic the IAP-binding motif (IBM) of Smac, which inhibits IAPs when released from the mitochondria. Smac mimetics can be applied to the cell as peptides, Smac-encoding polynucleotides, or small molecules (Chen & Huerta, 2009). The small molecules can be further subdivided into mono- or bivalent antagonists. The monovalent antagonist has one IBM, whereas the bivalent comprises two, which allows the simultaneous binding to the BIR2 and BIR3 domain that leads to more efficient caspase activation (de Almagro & Vucic, 2012). The first Smac mimetic entering human clinical trials was GDC-0152. This small molecule showed strong inhibition of XIAP, c-IAP1/2, and ML-IAP (Flygare et al., 2012). To date, several other Smac mimetics such as LCL161, HGS1029, or TL32711 are in clinical trials that will examine the safety and efficiency of IAP antagonists for the treatment of human diseases and especially as anti-tumor therapeutics (de Almagro & Vucic, 2012; Fulda & Vucic, 2012).

Adjacent to inducing the intrinsic apoptosis pathway for cancer therapy, the extrinsic death receptor pathway represents another promising opportunity. TRAIL and anti-TRAIL-R1/2 antibodies have been tested in several clinical trials, revealing apoptosis inducing effects in

some tumor cells, while normal cells were not affected (Ashkenazi et al., 1999; Walczak et al., 1999; Dimberg et al., 2013). Disappointingly, when used as monotherapy, TRAIL agonists showed minimal therapeutic effects, which is caused via multiple resistance mechanisms starting from the ligand binding until the caspase cascade by affecting the expression, stability, and function of the extrinsic apoptosis pathway (Dimberg et al., 2013). Therefore, combinatory therapies are investigated in current approaches using, e.g. the monoclonal antibodies mapatumumab against TRAIL-R1 or lexatumumab against TRAIL-R2 in combination with other cancer therapies targeting the mechanisms contributing to TRAIL resistance such as the aforementioned Smac and BH3 mimetics (Dimberg et al., 2013).

2.1.3.1 Staurosporine and derivatives

In tumor cells, parts of the apoptosis machinery are frequently inactivated which can result in chemo- and radiotherapy resistance. Most common is the disruption of the intrinsic apoptosis pathway, especially with regard to pre-mitochondrial and mitochondrial death processes e.g. mutation of *TP53* gene, pro-, or anti-apoptotic *BCL2* genes (Johnstone et al., 2002). Therefore, the investigation of therapeutics, activating apoptosis that bypass the canonical intrinsic apoptosis pathway is essential for overcoming chemo- and radiotherapy resistance.

Staurosporine was first identified and isolated in 1977 from the marine actinobacteria *Streptomyces sp.* strain AM-2282 (Omura et al., 1977). The alkaloid staurosporine is produced by a range of actinomycete species, inducing apoptosis in various cell lines. It was first identified as a specific PKC inhibitor (Tamaoki et al., 1986), but is now known as a broad-range kinase inhibitor of over 100 Ser/Thr and Tyr kinases *inter alia* AKT, PKA, CDK2/cyclin A1, or ERK1/2 (Fabian et al., 2005). A kinase screen of 121 kinases with staurosporine was performed by the MRC Protein Phosphorylation Unit in Dundee (UK). The data can be found online at http://www.kinase-screen.mrc.ac.uk/screening-compounds/349401.

Among various derivatives, STS has the strongest apoptotic potential (Harkin et al., 1998; Gescher, 2000), followed by its stereoisomer UCN-01 (7-hydroxystaurosporine), which appears to be less non-specific (Davies et al., 2000; Bain et al., 2007). Meanwhile, several clinical phase I and phase II studies were completed which investigated the impact of UCN-01 on diverse tumor types (https://clinicaltrials.gov/ct2/results?term=ucn-01). Notably, pharmacology studies revealed a low bioavailability of UCN-01 due to the high affinity to the plasma protein α1-Acid Glycoprotein (Sparreboom et al., 2004; Fuse et al., 2005). Therefore, new derivatives of UCN-01 with lower retention are currently being explored. However, despite the high binding capacity to human plasma proteins, clinical trials reported an

antitumor effect of UCN-01 when administered at 34 mg/m^2 per day for 3 days intravenous, 22 h after administration of 30 mg/m^2 cisplatin (Perez et al., 2006).
To date, it is still investigated how staurosporine induce apoptosis in detail. It is reported that staurosporine can induce apoptosis through the canonical intrinsic mitochondrial pathway, but data of our group could show that staurosporine can trigger a novel intrinsic apoptosis pathway, which allows the induction of apoptosis in anticancer drug-resistant tumor cells independently of death receptors. The staurosporine-inducible, alternative intrinsic apoptosis pathway, is characterized by the induction of apoptosis in Bcl-2 and Bcl-xL overexpressing cells as well as the independency of APAF1 and apoptosome formation, and is dependent on caspase-9 (Stepczynska et al., 2001; Manns et al., 2011).

To date, over 500 kinases have been identified to be encoded in the human genome, which play crucial roles in signaling pathways regulating for example the cell cycle, cytoskeletal formation, autophagy, apoptosis, or inflammation. Accordingly, kinase inhibitors can be used as anticancer drugs that are capable of binding target enzymes at their catalytic site and thus inhibiting or blocking the kinase function (Bharate et al., 2013). Nowadays, the protein kinase inhibitor Imatinib (Glivec) inhibiting Bcr-Abl is applied against chronic myelogenous leukemia and the tyrosine kinase inhibitors Gefitinib (Iressa) and Erlotinib (Tarceva) inhibiting EGFR signaling against lung cancer. Meanwhile, several staurosporine derivatives such as UCN-01, enzastaurin (PKC412), or midostaurin are tested in clinical phase I – phase III studies against diverse types of tumors, e.g. midostaurin against acute myeloid leukemia (Fischer et al., 2010) and enzastaurin against glioblastoma (Wick et al., 2010). A list of those clinical studies can be found at https://clinicaltrials.gov/ct2/results?term=ucn-01 (ucn-01 in the address can be replaced by midostaurin and enzastaurin).
Since protein kinases can be modulated by small molecules, which are mostly ATP competitors, the group of protein kinases has become the most studied group of drug targets after G-protein coupled receptors (GPCRs) (Bharate et al., 2013). Further analysis of how protein kinase inhibitors induce apoptosis in detail will contribute to the finding and development of potential cancer therapies with higher efficiency and less side effects.

2.2 Autophagy

Autophagy is a primarily degradative cellular process taking place in all eukaryotes (Feng et al., 2014). The term autophagy has Greek origin and is a composite, consisting of the words autos (self) and phagein (to eat), which was suggested in 1963 by Christian de Duve describing analogously the self-eating of a cell (Klionsky, 2008). In 1967 de Duve and colleagues reported the first electron microscopic images of autophagic structures (Deter et

al., 1967). Next to autophagy, the ubiquitin-proteasome system (UPS) is the second major protein degradation pathway in the cell that recycles specifically selected proteins (Wong & Cuervo, 2010). In contrast, autophagy is active on basal level in every cell enabling the degradation of long-lived proteins, macromolecules and damaged organelles, e.g. mitochondria, to maintain cellular homeostasis. Notably, autophagy can also be induced under different stress conditions including hypoxia, nutrient deprivation, or infection of cells by pathogens.

2.2.1 Different types of Autophagy and Morphology

Autophagy can be divided into three different types, namely microautophagy, chaperone-mediated autophagy (CMA) and macroautophagy. During microautophagy, parts of the cytosol are directly sequestered by lysosomes through membrane invagination, whereas CMA is characterized by the delivery of selected proteins containing a KFERQ motif into lysosomes. Macroautophagy (hereafter referred as autophagy) describes a process by which cytoplasmic cargo is engulfed within a double-membraned vesicle, termed the autophagosome (Wong & Cuervo, 2010; Mizushima et al., 2011). Subsequently, autophagosomes are transported to lysosomes and fuse with them to form autolysosomes, leading to the degradation of the sequestered cargo and the inner-autophagosomal membrane by acidic hydrolases. This catabolic recycling machinery provides building material like fatty acids and amino acids for anabolic processes or they are metabolized for energy production (He & Klionsky, 2009; Mizushima et al., 2011). In recent years also selective processes have been identified, which lead to the selective degradation of various organelles and pathogens. These selective autophagy pathways are, e.g. the degradation of endoplasmic reticulum (reticulophagy or ERphagy), peroxisomes (pexophagy), ribosomes (ribophagy), mitochondria (mitophagy), spermatozoon-inherited organelles following fertilization (allophagy), or intracellular pathogens (xenophagy) (Al Rawi et al., 2012; Reggiori et al., 2012; Fimia et al., 2013).

The formation of autophagosomes is maintained by different steps, i.e. vesicle nucleation, vesicle elongation, and the completion/closure of the double-membraned vesicle. In yeast the biogenesis of autophagosomes takes place at a specific platform, termed the pre-autophagosomal structure (PAS), which is located close to the vacuole where most of the autophagy-related (ATG) proteins are located (Suzuki et al., 2001; Suzuki et al., 2007). From there the phagophore (also termed isolation membrane, IM) arises and encloses cytoplasmic cargo, ultimately leading to the formation of an autophagosome (Suzuki et al., 2001; Mizushima et al., 2011). The source of autophagosomal membranes in mammals is still under debate, although various reports indicate the recruitment of membranes portions

from mitochondria (Axe et al., 2008; Hayashi-Nishino et al., 2009; Yla-Anttila et al., 2009), endoplasmic reticulum (Hailey et al., 2010) and also ER-mitochondrial contact sites (Hamasaki et al., 2013).

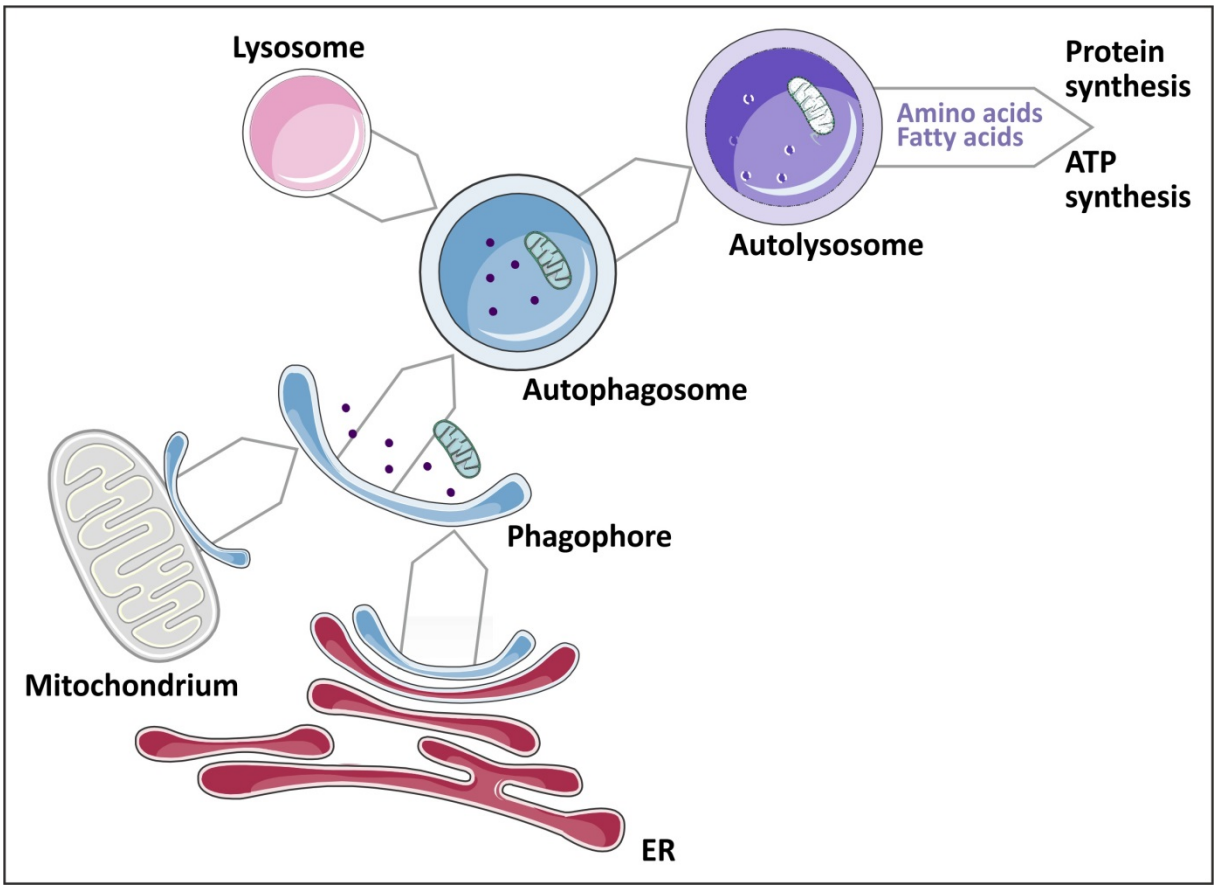

Figure 2-4: Schematic overview of Autophagy-Morphology. (modified from the doctoral thesis of Dr. Sebastian Alers, 2011)

2.2.2 Molecular Regulation of Autophagy

From the early discovery of autophagy in the 1960's it lasted about 30 years up to the first investigations of how this process is regulated. Tsukada and Ohsumi reported the isolation and characterization of the first 15 *Saccharomyces cerevisiea* mutants defective for autophagy (Tsukada & Ohsumi, 1993). To date, multiple screens for autophagy-defective mutants in yeast were performed recently leading to identification of ATG38 (Araki et al., 2013). Most of the ATG genes and core complexes required for autophagy in yeast have mammalian orthologs (Meijer et al., 2007), yet considering their higher complexity, some ATGs possess an even higher diversity with more than one homolog. In addition, different non-ATG proteins are regulating processes of autophagy, such as Bcl-2, AKT, mammalian/mechanistic target or rapamycin (mTOR), or vacuolar protein sorting protein 34 (VPS34).

Herein, focus will be set on the regulation of autophagy in mammals. Mammalian ATG proteins can be functionally grouped into six protein complexes, which are involved in

multiple steps of autophagy: involved in vesicle nucleation 1) the ULK1-ATG13-RB1CC1-ATG101 protein kinase complex, 2) the PIK3C3/VPS34-PIK3R4/VPS15-BECN1-ATG14 PtdIns3K class III complex 3) the PI3P-binding WIPI/ATG18-ATG2 complex, and 4) the multi-spanning transmembrane protein ATG9A; involved in vesicle elongation and completion, 5) the ubiquitin-like ATG12/ATG5 system, and 6) the ubiquitin-like LC3 conjugation system (Mizushima et al., 2011).

2.2.2.1 Regulation of vesicle nucleation by the PtdIns3K class III complex

The first morphological step for autophagosome formation is the vesicle nucleation and generation of the phagophore. One of the initial steps for vesicle nucleation is the generation of phosphatidylinositol 3-phosphate (PI3P), which is maintained by phosphatidylinositol 3-kinases (PI3K, PtdIns3K) (Petiot et al., 2000). In mammals this process is mainly regulated via the phosphatidylinositol 3-kinase (PI3K, PtdIns3K) class III complex. The core of this complex is built by the catalytic subunit VPS34 (PIK3C3), the adapter protein VPS15 (PIK3R4), and BECN1/Beclin-1. BECN1 functions as a scaffold protein, important for the recruitment of complex activators and repressors. Known positive regulators of autophagy are the BECN1 interacting proteins ATG14 (also termed ATG14-like, ATG14L, or Beclin-1-associated autophagy-related key regulator, Barkor), UV radiation resistance-associated gene protein (UVRAG), activation molecule in beclin-1-regulated autophagy 1 (AMBRA1), and Bax interacting factor-1 (Bif-1), whereas RUN domain protein as Beclin-1 interacting and cysteine-rich containing (Rubicon) and Bcl-2 proteins are negative regulators of autophagy. It has been reported that Rubicon negatively regulates autophagy by interaction with UVRAG and Bcl-2 proteins thereby sequestering BECN1 from the PI3K class III complex (Funderburk et al., 2010; Kang et al., 2011; Mizushima et al., 2011). The complex interacting with ATG14 is most likely the functional equivalent to yeast complex I that is involved in phagophore formation. Furthermore, ATG14 silencing leads to suppression of autophagosome formation (Zhong et al., 2009). It is hypothesized that formation of distinct protein complexes via binding of BECN1 with various proteins, a precise function of the PI3K class III complex is orchestrated, regulating autophagy at multiple steps (Kang et al., 2011).

Upon generation of the lipid PI3P, two different PI3P-binding effector proteins participate in autophagy induction. On the one hand the WD-repeat protein interacting with phosphoinositides (WIPI) protein family, whereas only WIPI-1 and WIPI-2 among the four family members are recruited to autophagosomal membranes dependent of PI3P (Proikas-Cezanne et al., 2004; Polson et al., 2010), and on the other hand the double FYVE domain containing protein 1 (DFCP1) (Axe et al., 2008). When autophagy is induced, DFCP1 accumulates at PI3P-enriched ER subdomains forming a ring-like structure, called

omegasomes, due to their Ω-like appearance. It has been speculated that newly formed autophagosomes bud from these structures (Hayashi-Nishino et al., 2009; Yla-Anttila et al., 2009).

2.2.2.2 Regulation of vesicle elongation and completion by two conjugation systems

Two ubiquitin-like conjugation systems are involved in the elongation of autophagosomes, i.e. the ATG12-ATG5 system and the LC3-phosphatidylethanolamine (PE) system. ATG12 and LC3 are the ubiquitin-like proteins in these systems, which are conjugated by E1-, E2-, and E3-like enzymatic activities to ATG5 and PE, respectively. With respect to the first system, ATG12 is conjugated to ATG5 via the E1-like enzyme ATG7 and the E2-like enzyme ATG10. So far an E3-like enzyme was not identified (Mizushima et al., 1998; Shintani et al., 1999; Geng & Klionsky, 2008). The conjugated ATG12-ATG5 is then able to interact with ATG16L to form a high molecular oligomer complex (Mizushima et al., 1999; Mizushima et al., 2003; Geng & Klionsky, 2008). With respect to the LC3-PE system, the cysteine protease ATG4 cleaves C-terminal residues from LC3 to form cytosolic LC3-I prior to conjugation. Subsequently, the generated free carboxyl group of the C-terminal glycine is conjugated to the amino group of PE by the E1-like enzyme ATG7 and E2-like enzyme ATG3 (Satoo et al., 2009). It has been speculated that the ATG12-ATG5-ATG16L conjugate has an E3-like activity for the conjugation of LC3 to PE (Hanada et al., 2007; Mizushima et al., 2011). The lipidated LC3-II is associated to the membrane of the phagophore and also at later stages to the autophagosome and autolysosome. The membrane association is facilitated by the lipidation with PE (Kabeya et al., 2004). In mammals, the existence of three families of yeast ATG8 homologs including nine proteins have been reported, i.e. the microtubule-associated protein light chain 3 (MAP1LC3, short LC3), the $GABA_A$-receptor associated protein (GABARAP), and the Golgi-associated ATPase enhancer of 16 kDa (GATE-16) subfamily (Kabeya et al., 2004). Furthermore, mammals comprise four homologs of yeast ATG4, i.e. ATG4A - ATG4D (Marino et al., 2003).

Due to the increased conversion of LC3-I to LC3-II during autophagy and the correlation between autophagosomes and LC3-II levels, this protein is a suitable marker for autophagy by immunoblotting (LC3-I to LC3-II conversion or LC3-II level detection), and in addition for fluorescence-labeled or immunostained LC3 for microscopy and flow cytometric analysis (Mizushima & Levine, 2010; Klionsky et al., 2012). Notably, due to the degradation of LC3-II during autophagy in autolysosomes under autophagy inducing conditions, the autophagic flux has to be monitored by assessing LC3-II generation in the presence and absence of lysosomal inhibitors, e.g. bafilomycin A_1 (Tanida et al., 2005; Mizushima et al., 2010).

Bafilomycin A_1 inhibits the lysosomal acidification through H^+-ATPase inhibition, which prevents lysosomal degradation, yet maintains the fusion of autophagosomes and lysosomes (Fass et al., 2006).

Additionally, the elongation of the phagophore seems to be dependent on the recruitment of the multispan transmembrane protein ATG9A. ATG9A is localized at the trans-Golgi network, endosomes, and under starvation conditions to early and late autophagosomes. ATG9A seems to shuttle among these organelles and it has been proposed to carry lipids to the omegasome (Young et al., 2006; He et al., 2008; Mizushima et al., 2011).

2.2.2.3 Autophagosome-lysosome fusion

To date, the mechanisms underlying the final stage of autophagy, autophagosome-lysosome fusion, remains largely unknown. It has been reported that syntaxin 17 (Stx17) functions as the autophagosomal soluble N-ethylmaleimide-sensitive factor attachment protein receptor (SNARE), localized at the outer membrane of autophagosomes, which interacts with synaptosomal-associated protein 29 (SNAP-29) and the lysosomal SNARE vesicle-associated membrane protein 8 (VAMP8) at the lysosome membrane, accomplishing the autolysosome (Itakura et al., 2012).

2.2.3 Regulation of starvation induced autophagy

Autophagy induction is strictly regulated, as otherwise increased or insufficient autophagy has severe effects possibly leading to several diseases. The immediate autophagy induction upon nutrient deprivation is important for the supply of energy and furthermore the supplement of building material for anabolic processes.

In mammals, autophagy is regulated by nutrient sensing and growth factor signaling pathways, which ultimately lead to the inhibition of the mammalian/mechanistic target of rapamycin complex 1 (mTORC1), consisting of the Ser/Thr kinase mTOR, mammalian lethal with sec-13 protein 8 (mLST8, also termed G protein β subunit-like, GβL), proline-rich AKT substrate of 40 kDa (PRAS40), DEP domain containing mTOR-interacting protein (DEPTOR), and the regulatory-associated protein of mTOR (RPTOR) (Hara et al., 2002; Kim et al., 2003; Sancak et al., 2007). It has been reported that the presence of nutrients regulate mTORC1 activity via two signaling pathways, on the one hand by the AMP-activated protein kinase (AMPK) pathway depending on glucose availability (Meley et al., 2006), and on the other hand by the Rag family of GTPases depending on amino acid availability (Sancak et al., 2008). The presence of amino acids leads to the switch of Rag GTPase heterodimers into their active conformation, allowing the interaction with the mTORC1 complex via RPTOR, which

causes the translocation to late endosomes and lysosomes. At their surface, the GTP-binding protein Ras homolog enriched in brain (Rheb) is located, finally activating mTORC1 (Laplante & Sabatini, 2012). Upon energy-depleted conditions, AMP levels increase and AMPK – consisting of a catalytic α- and the regulatory β- and γ-subunit – becomes activated by liver kinase B1 (LKB1) dependent phosphorylation of AMPKα at Thr172. Activated AMPK inhibits mTORC1 either by phosphorylation of RPTOR, promoting the binding of 14-3-3 proteins (Gwinn et al., 2008), or by phosphorylation of the negative regulator tuberous sclerosis 2 protein (TSC2), inducing the GAP activity of TSC1-TSC2 for Rheb (Garami et al., 2003; Inoki et al., 2006). Additionally, AMPK is also activated via several nutrient-independent signaling pathways, i.e. TRAIL-induced activation of TGF-beta activated kinase 1 (TAK1), Ca^{2+}-mediated activation of Ca^{2+}/calmodulin-dependent protein kinase kinase-beta (CaMKKβ), and DNA-damage mediated activation of sestrin 1 and 2 (SESN1/2) (Hoyer-Hansen et al., 2007; Budanov & Karin, 2008; Herrero-Martin et al., 2009). Moreover, stress signals such as hypoxia also inactivate mTORC1 either by TSC1/2 activation through AMPK or the protein regulated in development and DNA damage response 1 (REDD1) (Brugarolas et al., 2004; Reiling & Hafen, 2004; DeYoung et al., 2008). With respect to growth factor signaling that regulates autophagy, growth factors activate the PI3K/AKT pathway via binding to receptor tyrosine kinases (RTK) on the outer membrane of cells. At the cytosolic site of RTK, PI3K is recruited and activated, which leads to the generation of PIP3 and subsequently to the recruitment of phosphatidylinositol 3-dependent kinase 1 (PDK1). The translocalized PDK1 activates AKT by phosphorylation, which in turn prevents the formation of the TSC1/2 complex by phosphorylation of TSC2, ultimately leading to the activation of mTORC1 by Rheb (Huang & Manning, 2009).

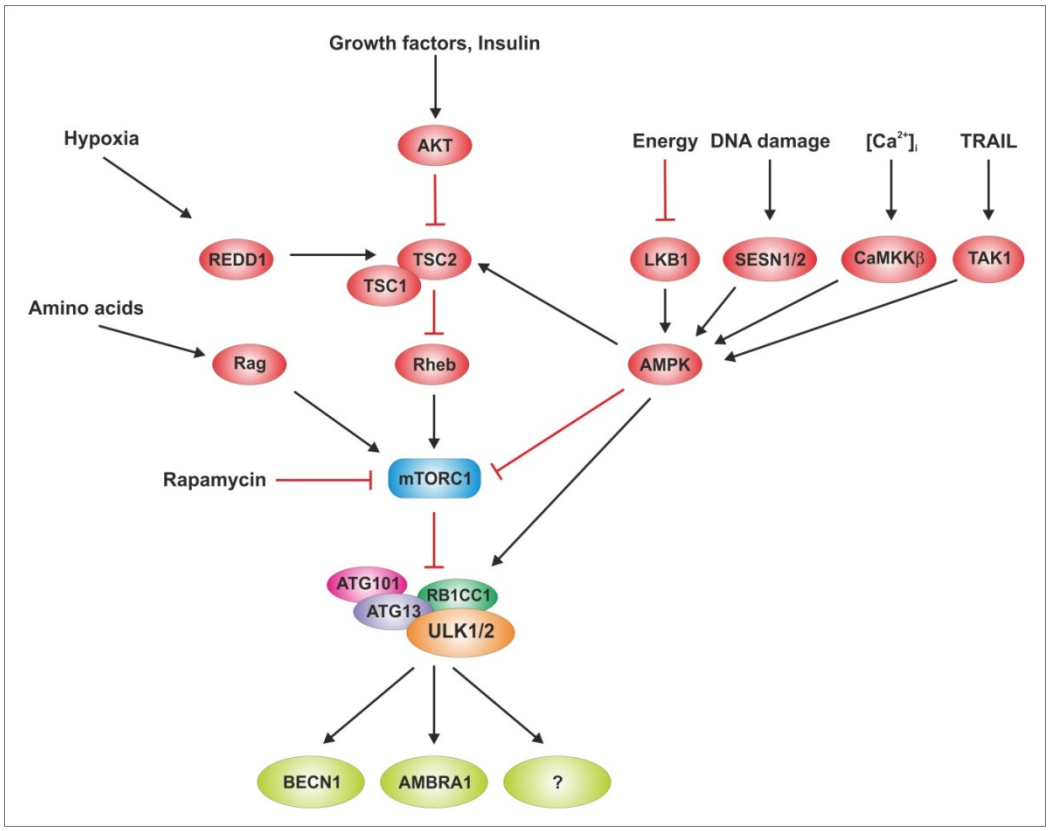

Figure 2-5: Signaling pathways up- and downstream of the ULK1 complex. (modified from the postdoctoral thesis (Habilitation) of PD Dr. Björn Stork)

2.2.3.1 Regulation via the ULK1/2-ATG13-RB1CC1-ATG101 complex

Among the functional groups of ATG proteins the ULK1 complex is the key regulator complex of autophagy induction. The ULK1 core complex consists of the Ser/Thr protein kinase Unc-51-like kinase 1/2 (ULK1/2), and the adapter proteins ATG13, RB1-inducible coiled-coil protein 1 (RB1CC1; also termed focal adhesion kinase interacting protein of 200 kDa, FIP200), and ATG101 (Behrends et al., 2010; Mizushima et al., 2011). ULK1 is one of five mammalian orthologs of yeast ATG1, which was the first identified autophagy-related gene product in a *Saccharomyces cerevisiea* screen for autophagy-defective mutants and it is the only kinase among the 38 ATGs (Tsukada & Ohsumi, 1993). Among the five mammalian orthologs ULK1, 2, 3, 4, and STK36 (also termed fused), ULK1 and ULK2 show the highest homology, whereas ULK3, 4, and STK36 are only conserved within the N-terminal catalytic domain (Chan & Tooze, 2009; Mizushima, 2010; Alers et al., 2012). Although ULK1, 2, and 3 appear to play crucial roles for autophagic processes, only ULK1 and ULK2 seem to be relevant for starvation-induced autophagy (Chan et al., 2007). Concluded from *Ulk1*-/- and *Ulk2*-/- single-knockout and double-knockout mice, it has been suggested that ULK1 and ULK2 have redundant roles, since both single-knockout mice are viable whereas the double-knockout mice die shortly after birth (Kundu et al., 2008; Cheong et al., 2011). Interestingly, ULK1 deficient mice show a delayed clearance of mitochondria from reticulocytes, whereas

ULK2 deficient mice do not show an abnormal phenotype, indicating differential roles of ULK1 and ULK2 for selective autophagy and mitophagy (Cheong et al., 2011). To date, three ULK1/2-deficient vertebrate cell systems have been reported, the *ULK1/2*-/- chicken DT40 cell line and two independently generated *Ulk1/2*-/- murine embryonic fibroblasts (MEFs) (Alers et al., 2011; Cheong et al., 2011; McAlpine et al., 2013). In two cell lines autophagy induction independently of ULK1/2 has been described. Autophagy can be induced upon amino acid starvation with EBSS in ULK1/2 deficient DT40 cells and upon glucose starvation in ULK1/2 deficient MEFs (Alers et al., 2011; Cheong et al., 2011). In contrast to the DT40 ULK1/2 deficient cells, in ULK1/2 deficient MEFs amino acid starvation is not sufficient for autophagy induction. This indicates a cell type specific role of ULK1/2 for autophagy induced by glucose and amino acid starvation.

The ULK1 complex is mainly regulated by phosphorylation executed by several kinases, e.g. mTOR as part of the mTOR complex 1 (mTORC1). Under nutrient rich conditions mTORC1 is associated with the ULK1 complex and phosphorylates ULK1 in an inhibitory manner. Under nutrient-deprived conditions mTORC1 dissociates from the ULK1 complex and the inhibitory phosphorylation sites of ULK1 become dephosphorylated which enables its autophosphorylation, transphosphorylation of RB1CC1 and ATG13, and the translocation to the phagophore (Chan et al., 2009; Ganley et al., 2009; Hosokawa et al., 2009; Jung et al., 2009; Alers et al., 2012). Several groups reported the direct phosphorylation of ULK1 by AMPK indicating the existence of mTOR-independent regulation of autophagy (Egan et al., 2011; Kim et al., 2011; Shang et al., 2011; Mack et al., 2012). In return, our group discovered the *vice versa* phosphorylation of all three subunits of AMPK by ULK1, facilitating a functional negative feedback loop, which possibly contributes to the termination of an autophagic response. Nowadays, several other ULK1 substrates have been reported that function in autophagy regulation, e.g. BECN1 and AMBRA1. BECN1 is phosphorylated by ULK1 upon amino acid starvation and mTOR inhibition, which leads to increased activity of the ATG14 containing VPS34 complex (Russell et al., 2013). AMBRA1 becomes phosphorylated under autophagy inducing conditions, thereby releasing the PI3K class III complex from dynein, which results in the translocation to the endoplasmic reticulum, enabling autophagosome nucleation (Di Bartolomeo et al., 2010; Fimia et al., 2011).

Besides phosphorylation, ULK1 is also regulated by other post translational modification including acetylation and ubiquitination and moreover by miRNA (Lin et al., 2012; Nazio et al., 2013; Pan et al., 2013). With respect to ubiquitination, it has been reported that under autophagy inducing conditions, the mTOR inhibiting AMBRA1 phosphorylation sites are dephosphorylated that leads to the interaction of AMBRA1 with the E3-Ligase TRAF6. Subsequently, TRAF6 ubiquitinates ULK1 by K63-linked ubiquitin chains, which stabilizes

ULK1 (Nazio et al., 2013). The polyubiquitination of ULK1 by K63-Ub linked chains was also observed by another group (Zhou et al., 2007).

2.2.4 WP1130 and Regulation via Deubiquitinases

WP1130, also termed degrasyn, was originally discovered in a screen for small compounds suppressing IL-3 and IL-6 activation of STAT molecules (Bartholomeusz et al., 2007). It has been reported that WP1130 mediates the inhibition of Bcr-Abl kinase activity due to K63-linked polyubiquitination of Bcr-Abl and accumulation in aggresome structures, whereas Abl and Bcr alone were not affected (Bartholomeusz et al., 2007; Sun et al., 2011). Furthermore, WP1130 induced the primarily K63-linked polyubiquitination of JAK2, its trafficking through HDAC6 to perinuclear aggresomes, thus inhibiting its kinase activity (Kapuria et al., 2011). WP1130 did not affect kinase activity directly, it rather functions as a partially selective deubiquitinase (DUB) inhibitor, directly inhibiting DUB activity of USP5, USP9X, USP14, UCH-L1 and UCH-L5, inducing the accumulation of polyubiquitinated proteins to perinuclear aggresomes (Kapuria et al., 2010).

Ubiquitination is a post-translational modification with critical roles in signal transduction, e.g. regulating enzyme activity and translocation of proteins and, moreover, determining protein stability. Ubiquitination can be classified by the generation of chains between the carboy-terminal glycine of ubiquitin and one of the seven internal lysine residues of the 76 amino acids consisting ubiquitin (K6, K11, K27, K29, K33, K48, K63) (Komander et al., 2009). So far, only K48 and K63-linked ubiquitin chains were extensively studied, predominantly K48-linked ubiquitination labels proteins for proteasomal degradation, whereas K63-linked ubiquitination has influence in signal transduction, e.g. through the NF-κB pathway, in DNA-damage response and lysosomal sorting (Ikeda & Dikic, 2008; Clague et al., 2012). The dynamic nature of ubiquitination and deubiquitination events is crucial for regulating protein stability, maintaining ubiquitin homeostasis, and the control of ubiquitin-dependent signaling pathways (Clague et al., 2012). DUBs oppose the function of the E3 ubiquitin ligases. The human genome encodes about 90 DUBs, of which 79 are predicted to be active. They can be grouped into five families: the ubiquitin-specific protease (USP) family (~55 members), the ubiquitin C-terminal hydrolases (UCHs), ovarian tumor proteases (OTUs), and members of the Josephin family. Those four groups belong to cysteine proteases, whereas the fifth DUB family comprises a group of Zn^{2+} metalloproteases, i.e. the JAB1/MPN/MOV34 metalloenzymes (JAMMs) (Nijman et al., 2005). Nowadays, several DUBs have been reported to influence protein stability and activity in apoptosis and autophagy pathways. Under normal conditions the transcription factor p53 is ubiquitinated by Mdm2 inducing the degradation of p53. The DUB USP7 (also termed HAUSP) also regulates p53 stability

counteracting Mdm2 by deubiquitination and hence stabilization of p53 (Li et al., 2002). Another DUB plays also a role in regulating an apoptosis relevant protein. USP9X stabilizes Mcl-1 by removing the K48-linked polyubiquitin chains that normally mark Mcl-1 for proteasomal degradation (Schwickart et al., 2010). Moreover, USP9X seems to play a crucial role in zymophagy, a selective form of autophagy, degrading zymogen granules upon pancreatitis-induced intracellular zymogen activation (Grasso et al., 2011). In addition, other DUBs were discovered that regulate autophagy, such as USP10 and USP13. These two DUBs regulate the deubiquitination of VPS34, the catalytic subunit of the PI3k class III complex, and stabilities of USP10 and USP13 are coordinately regulated with that of VPS34 (Liu et al., 2011). Collectively, only few DUBs were discovered that regulate stability and activity of autophagic processes. Accordingly, future studies have to reveal enzymes involved in ubiquitin conjugation/deconjugation, in order to establish a more complete model of ubiquitin-dependent regulation of autophagy.

3 Aims of work

One hallmark of cancer is the resistance of tumor cells death. Overcoming this resistance by apoptosis induction in those cells is essential for a successful cancer therapy.
Therefore, the major aim of the apoptosis part of the thesis was to further dissect apoptosis signaling pathways that bypass the canonical intrinsic apoptosis pathway especially regarding alternative activation of the initiator caspase-9 next to apoptosome dependent activation.

(1) The first aim was to elucidate the importance of the CARD and the catalytic activity of caspase-9 for an alternative activation by staurosporine (STS) that is reported to activate caspase-9 independent of the apoptosome.

(2) The second aim was to establish a cell system ideal for analysis of apoptosome independent apoptosis pathway.

(3) The third objective was to elucidate the role of caspase-9 phosphorylation for alternative activation and to find caspase-9 interaction partners that function in caspase-9 activation next to the apoptosome.

It has been proposed that anticancer drugs induce cyto-protective autophagy, leading to impaired efficiency of these compounds. Accordingly, the major aim of the autophagic part of the thesis was to further elucidate the regulation of the ULK1 complex that is crucial for regulating autophagy initiation itself. Focus was set on the investigation of the regulation of the kinase component, i.e. ULK1/2 by ubiquitinating and deubiquitinating processes and its impact on overall autophagy.

(1) The first aim was to analyze the impact of altered ULK1/2 ubiquitination on its stability and activity with the help of the partially selective deubiquitinase inhibitor WP1130.

(2) The second and last objective of the thesis was to further elucidate the impact of DUB inhibition on autophagy in general, the causal influence of ULK1 in this case and to discover the DUBs regulating ULK1/2

4 Materials and Methods

4.1 Materials

4.1.1 Vectors

Commercial vector	Application and source
pCRII®-TOPO®	TA-cloning®; Invitrogen, Life Technologies
pCR2.1®-TOPO®	TA-cloning®; Invitrogen, Life Technologies
pMSCVpuro	retroviral transfection; Clontech Laboratories
pHCMV-VSV-G	pseudotypisation of retroviruses; Clontech Laboratories
pEGFP-N3	source of EGFP cDNA for caspase-9 tagging; Clontech Laboratories

Provided vector	Application and source
pMSCVpuro-caspase-9	source of caspase-9 cDNA for molecular cloning, site directed mutagenesis and stable expression of caspase-9 [human]; Merle Daubrawa (Tübingen, Germany)
pMSCVpuro-ΔCARD-caspase-9	stable expression of ΔCARD-caspase-9; Björn Stork (Düsseldorf, Germany)
pMSCVpuro-mRFP-EGFP-rLC3	stable expression of mRFP-EGFP-rLC3; Sebastian Alers (Tübingen, Germany)
pCMVpuro-4A/HA-ubiquitin(8x)	transient expression of HA-ubiquitin; Stefan Jentsch (Martinsried, Germany)
pCDNA3.1-HA-ubiquitin	transient expression of HA-ubiquitin; MRC Protein Phosphorylation and Ubiquitylation Unit (Dundee, Scotland)
pcDNA3.1-HA-ubiquitin-K48R	transient expression of HA-ubiquitin K48R; MRC Protein Phosphorylation and Ubiquitylation Unit (Dundee, Scotland)
pcDNA3.1-HA-ubiquitin-K63R	transient expression of HA-ubiquitin K63R; MRC Protein Phosphorylation and Ubiquitylation Unit (Dundee, Scotland)
pcDNA3.1-HA-ubiquitin-K48/63R	transient expression of HA-ubiquitin K48/63R; MRC Protein Phosphorylation and Ubiquitylation Unit (Dundee, Scotland)
pcDNA3.1-HA-ubiquitin-K48only	transient expression of HA-ubiquitin K48only; MRC Protein Phosphorylation and Ubiquitylation Unit (Dundee, Scotland)

pcDNA3.1-HA-ubiquitin-K63only	transient expression of HA-ubiquitin K63only; MRC Protein Phosphorylation and Ubiquitylation Unit (Dundee, Scotland)
pcDNA3.1-HA-ubiquitin-K48/63only	transient expression of HA-ubiquitin K48/63only; MRC Protein Phosphorylation and Ubiquitylation Unit (Dundee, Scotland)
pcDNA3.1-HA-ubiquitin-KallR	transient expression of HA-ubiquitin KallR; MRC Protein Phosphorylation and Ubiquitylation Unit (Dundee, Scotland)

4.1.1.1 Generated vectors for retroviral expression

Vector	**Application**
pMSCVpuro-caspase-9-R13A	stable expression of caspase-9-R13A
pMSCVpuro-caspase-9-R56A	stable expression of caspase-9-R56A
pMSCVpuro-caspase-9-C287S	stable expression of caspase-9-C287S
pMSCVpuro-caspase-9 ΔCARD	stable expression of caspase-9 ΔCARD
pMSCVpuro-caspase-9-GFP	stable expression of caspase-9-GFP
pMSCVpuro-caspase-9-GFP-R13A	stable expression of caspase-9-GFP-R13A
pMSCVpuro-caspase-9-GFP-R56A	stable expression of caspase-9-GFP-R56A
pMSCVpuro-caspase-9-GFP-C287S	stable expression of caspase-9-GFP-C287S
pMSCVpuro-caspase-9-GFP-C287S-R13A	stable expression of caspase-9-GFP-C287S-R13A
pMSCVpuro-caspase-9-GFP-C287S-R56A	stable expression of caspase-9-GFP-C287S-R56A

4.1.2 Oligonucleotides

All oligonucleotides (primer) used in this thesis for site directed mutagenesis and DNA sequencing were synthesized by Sigma-Aldrich (St. Louis, MO, USA) or Life Technologies (Carlsbad, CA, USA). Small interfering RNAs (siRNA) were purchased from Dharmacon, GE Healthcare (Chalfont St Giles, UK).

Oligonucleotides for site directed mutagenesis

Primer name	**5´-3´sequence**
EGFP-N3_TAAtoGGA_for	CTTTAAAACATCAGGAAAAAGGGCGAATTC
EGFP-N3_TAAtoGGA_rev	GAATTCGCCCTTTTTCCTGATGTTTTAAAG
EGFP-N3_ATGtoTTG_for	GATCCATCGCCACCTTGGTGAGCAAGGGCG
EGFP-N3_ATGtoTTG_rev	CGCCCTTGCTCACCAAGGTGGCGATGGATC

CASP9_R13A_for	CTCCTGCGGCGGTGCGCGCTGCGGCTGGTGG
CASP9_R13A_rev	CCACCAGCCGCAGCGCGCACCGCCGCAGGAG
CASP9_R56A_for	GGCGGGATCAGGCCGCGCAGCTGATCATAG
CASP9_R56A_rev	CTATGATCAGCTGCGCGGCCTGATCCCGCC
CASP9_C287S_for	CATCCAGGCCAGTGGTGGGGAGCAGAAAGAC
CASP9_C287S_rev	GTCTTTCTGCTCCCCACCACTGGCCTGGATG

Oligonucleotides for DNA sequencing

pMSCVpuro_for	CCCTTGAACCTCCTCGTTCGACC
pMSCVpuro_rev	GAGACGTGCTACTTCCATTTGTC
CASP9-GFP_for1	TGGACGACATCTTTGAGCAGTGG
CASP9-GFP_for2	ATTCTCTCTCACGGCTGTCAG
pCDNA3.1_for	CGCAAATGGGCGGTAGGCGTG
pCDNA3.1_rev	TAGAAGGCACAGTCGAGG

Oligonucleotides for siRNA silencing

siRNA	**Supplier and reference number (#)**
SMARTpool: ON-TARGETplus UCH-L1 [human] siRNA	Dharmacon, #L-004309-00-0005
SMARTpool: ON-TARGETplus UCH-L5 [human] siRNA	Dharmacon, #L-006060-00-0005
SMARTpool: ON-TARGETplus USP5 [human] siRNA	Dharmacon, #L-006095-00-0005
SMARTpool: ON-TARGETplus USP9X [human] siRNA	Dharmacon, #L-006099-00-0005
SMARTpool: ON-TARGETplus USP14 [human] siRNA	Dharmacon, #L-006065-00-0005

4.1.3 Bacteria strains

***Escherichia coli* strain used for the production of vectors**

Strain	**Genotype**
DH5α	F^- *end*A1 *gln*V44 *thi*-1 *rec*A1 *rel*A1 *gyr*A96 *deo*R *nup*G Φ80d*lacZ*ΔM15 Δ(*lacZYA-argF*)U169, *hsd*R17(r_K^- m_K^+), λ–

4.1.4 Antibodies

All antibodies used for immunoblotting in this thesis were supplied by Abcam (Cambridge, UK), Bethyl Laboratories (Montgomery, TX, USA), BD Biosciences (Franklin Lakes, NJ, USA), Enzo Life Sciences (Farmingdale, NY, USA), Cell Signaling Technology (Danvers, MS, USA), CovalAb S.A.S. (Villeurbanne, France), LI-COR Biosciences (Lincoln, NE, USA), Life Technologies (Carlsbad, CA, USA), MBL International (Woburn, MA, USA), Merck Millipore

(Darmstadt, Germany), Roche Diagnostics (Rotkreuz, Switzerland), Rockland Immunochemicals (Gilbertsville, PA, USA), Santa Cruz Biotechnology (Dallas, TX, USA), or Sigma-Aldrich (St. Louis, MO, USA).

Primary antibodies

Antibody	**Supplier and reference number (#)**
Apoptosis part	
rabbit APAF1	Enzo Liefe Sciences, #ADI-AAP-300-C
mouse anti-caspase-3	BD Biosciences, #610322
rabbit anti-caspase-3	Cell Signaling Technology, #9664
rabbit anti-caspase-9	Costume-made by Charles River
mouse anti-PARP	Enzo Life Sciences, #BML-SA250
Autophagy part	
rabbit anti-AMBRA1	Covalab, #pab0224-P
mouse anti-AMPKα	Cell Signaling Technology, #2793
rabbit anti-AMPKα pT172	Cell Signaling Technology, #2531
rabbit anti-ATG101	Sigma-Aldrich, #SAB4200175
rabbit anti-ATG13	Sigma-Aldrich, #SAB4200100
rabbit anti-Beclin1	Santa Cruz Biotechnology, #11427
mouse anti-HA (12CA5)	Abcam, #ab16918
rabbit anti-FIP200/RB1CC1	Bethyl Laboratories, #A301-574A
rabbit anti-LC3	MBL International, #PM036
rabbit anti-LC3B	Cell Signaling Technology, #2775
rabbit anti-p62	MBL International, #PM045
mouse anti-ubiquitin (FK2)	Merck Millipore, #04-263
mouse anti-ubiquitin (P4D1)	Cell Signaling Technology, #3936
rabbit anti-ubiquitin K63 specific (Apu3)	Merck Millipore, #05-1308
rabbit anti-ULK1	Cell Signaling Technology, #8054
rabbit anti-UCH-L1	Cell Signaling Technology, #3524
rabbit anti-UCH-L5	Abcam, #ab124931
rabbit anti-USP5	Bethyl Laboratories, #A301-542A
sheep anti-USP9X	provided by the Division of Signal Transduction Therapy, College of Life Sciences, University of Dundee, Scotland
rabbit anti-USP14	Cell Signaling Technology, #8159

General antibodies	
mouse anti-actin (AC-74)	Sigma-Aldrich, #A5316
mouse anti-GAPDH (6C5)	Abcam, #ab8245
mouse anti-GFP	Roche Diagnostics, #11814460001
rabbit anti-HSP90	Cell Signaling Technology, #4874
rabbit anti-Lamin-B1	Abcam, #ab16048
mouse anti-tubulin	Sigma-Aldrich, #T5168

Secondary antibodies

Immunoblotting	
goat anti-mouse IRDye®680LT	LI-COR Biosciences, #926-68020
goat anti-mouse IRDye®800CW	LI-COR Biosciences, #926-32210
goat anti-rabbit IRDye®680LT	LI-COR Biosciences, #926-68021
goat anti-rabbit IRDye®800CW	LI-COR Biosciences, #926-32211
donkey anti-sheep IRDye®800	Rockland Immunochemicals, #613-732-168
Confocal microscopy	
donkey anti-rabbit AlexaFluor®568	Life Technologies, #A10042
donkey anti-mouse AlexaFluor®568	Life Technologies, #A10037
goat anti-rabbit AlexaFluor®594	Life Technologies, #A11037

4.1.5 Enzymes for Molecular Biology

Enzyme	**Supplier and reference number (#)**
FastAP (alkaline phosphatase)	Thermo Scientific, #EF0654
Klenow Fragment	Thermo Scientific, #EP0054
Lambda Protein Phosphatase (λPP)	New England BioLabs, #P0753S
Phusion High-Fidelity DNA Polymerase	Thermo Scientific, #F-530S
Restriction endonucleases	Thermo Scientific
T4 DNA Ligase	Thermo Scientific, #EL0014

4.1.6 Recombinant proteins

GST	Antje Löffler (Düsseldorf, Germany)
GST-ATG13 [human]	Antje Löffler (Düsseldorf, Germany)
GST-MBP [human]	Sigma-Aldrich, #SRP205

GST-ULK1 [human]	Sigma-Aldrich, #SRP5096
His-USP7 [human]	Ubiquigent (Dundee, Scotland), #64-0003-050
GST-USP9X [human]	Ubiquigent (Dundee, Scotland), #64-0017-050

4.1.7 Buffers and Solutions

PBS (1x)	137 mM NaCl; 2.7 mM KCl; 1.4 mM KH_2PO_4; 4.3 mM Na_2HPO_4 7·H2O, pH 7.3
TBS (1x)	150 mM NaCl; 50 mM Tris
TBS-T (Tween® 20)	0.1 % (v/v) Tween® 20 in 1x TBS
Tris/HCl	0.5-1.5 M Tris; adjusted pH to 6.8-8.8 with HCl

4.1.8 Media and supplements for eukaryotic cell cultivation

DMEM (4.5 g/l D-Glucose)	Life Technologies, #41965-039
DMEM (w/o D-Glucose)	Life Technologies, #11966-025
DMEM-GFP medium	Evrogen, #MC102
McCoy's 5A	Life Technologies, #36600-021
RPMI 1640	Life Technologies, #21875-091
EBSS	Life Technologies, #24010-043
DPBS (1x)	Life Technologies, #14190-094
HEPES (1M)	Life Technologies, #15630-080
PBS (10x)	GE Healthcare, #BR100672
Penicillin/Streptomycin 10,000 U/ml / 10,000 µg/ml	Biochrom, Merck Millipore, #A2213
Trypsin/EDTA solution, 0.05%/0.2% (w/v) in PBS	Biochrom, Merck Millipore, #L2143
Fetal Calf Serum (FCS)	PAA, #A15-101
FCS dialyzed	Life Technologies, #26400-044

4.1.9 Compounds

[^{14}C]Valine	PerkinElmer, #NEC291EU050UC
[^{32}P]Adenosine 5'-triphosphate	Hartmann Analytic, #SRP-301
3-methyladenine	Sigma-Aldrich, #M9281
Ac-DEVD-AMC	Biomol, #ABD-13402
bafilomycin A_1	Sigma-Aldrich, #B1793

bortezomib	Merck Millipore, #5.043.140.001
calpeptin	Merck Millipore, #03-34-0051
cathepsin inhibitor III	Merck Millipore, #219419
cycloheximide	Merck Millipore, #239763
cytochrome c	Biovision, #2120-100
doxycycline	Clontech Laboratories, #631311
E-64-D	Enzo Life Sciences, #BML-PI107-0100
epoxomicin	Enzo Life Sciences, # BML-PI127-0100
HBX41108	R&D Tocris, #4285
Hoechst 33342	Life Technologies, #H1399
LDN 57444	LifeSensors, #SI9639
MG132	Merck Millipore, #474790
mitomycin C	AppliChem, #A2190,0002
NEM	Sigma-Aldrich, #E3876
nocodazole	Sigma-Aldrich, #M1404
pepstatin A	Sigma-Aldrich, #77170
PR619	LifeSensors, #SI9619
puromycin	InvivoGen, #ant-pr-1
Q-VD-OPh	Merck Millipore, #551476
saponin	Sigma-Aldrich, #47036-50G-F
spautin-1	Merck Millipore, #567569
staurosporine	Enzo Life Sciences, #BML-EI156-0100
TRAIL [human]	Merck Millipore, #616374
WP1130	Axon Medchem BV, #Axon 1779
WP1130	Merck Millipore, #681685
z-LEVD-FMK	MBL International, #BV-1108-3

4.1.10 Additional Material

Autoradiography Hypercassette	Amersham, GE Healthcare
Colloidal Blue Staining Kit	Life Technologies
dNTPs	Thermo Scientific
EndoFree Plasmid Maxi Kit	Qiagen
FuGENE®6	New England BioLabs
FuGENE®HD	New England BioLabs
Freezing Container, Mr. Frosty™	Thermo Scientific

Gel Filtration Calibration Kit LMW/HMW	GE Healthcare
GeneRuler™ 1 kb DNA ladder	Thermo Scientific
GFP-Trap®	ChromoTek, #gta−200
Intensifying screens BioMax® Transcreen® HE	Kodak
NucleoSpin® Extract II Gel extraction kit	Macherey-Nagel
NucleoSpin® Plasmid purification kit	Macherey-Nagel
Nunc™ Lab-Tek™ Chambered Coverglasses	Thermo Scientific
Mowiol 4-88	Sigma-Aldrich
PAGERuler™ Prestained Protein ladder	Thermo Scientific
Polybrene	Sigma-Aldrich
Protease Inhibitor Cocktail	Sigma-Aldrich
Protein Assay Kit (Bradford)	Bio-Rad
Protein A/G PLUS-Agarose	Santa Cruz
PVDF membranes (HybondP-ECL-Membran)	Amersham Biosciences
Superose 6 column	GE Healthcare
Tissue culture equipment (dishes, pipettes, tubes etc.)	Greiner, Nunc, Falcon
Dounce homogenizer with tight pestle	Wheaton
VECTASHIELD mounting medium with DAPI	Vector Laboratories
X-ray film BioMax® MR	Kodak

4.1.11 Technical equipment

Type and name	**Manufacturer**
bacteria incubator, Certomat BS-1	Sartorius
blotting tank, Trans-Blot cell	Bio-Rad
cell culture bench, HERAsafe®	Thermo Scientific
cell culture incubator, HERAcell® 240 CO_2	Thermo Scientific
centrifuge, Heraeus™ fresco™ 17	Thermo Scientific
centrifuge, Heraeus™ pico™ 17	Thermo Scientific
centrifuge, Megafuge 3.0R	Thermo Scientific
centrifuge, Megafuge 40R	Thermo Scientific
CO_2- and temperature-controlled incubator	Okolab
confocal laser scanning microscope, LSM 710	Zeiss
confocal laser scanning microscope, LSM 780	Zeiss

Deltavision Deconvolution microscope	GE Healthcare
electrophoresis system, Mini-PROTEAN Tetra	Bio-Rad
electrophoresis system, PerfectBlue™ Gelsystem Midi S	PeqLab
electrophoresis system, PerfectBlue™ Gelsystem Mini S	PeqLab
electrophoresis system, SE400	Hoefer
ELISA reader, MR5000	Dynatech
film processing machine, AGFA Curix 60	AGFA Healthcare
flow cytometer, FACSCalibur™	BD Biosciences
flow cytometer, LSRFortessa™ cell analyzer	BD Biosciences
FPLC Äktapurifier	GE Healthcare
gel-drying apparatus, model 583	Bio-Rad
infrared imaging system, Odyssey® I	Li-COR Biosciences
monochromator-based microplate reader, SynergyMX	BioTek
PCR cycler, GeneAmp® PCR System 9700	Applied Biosystems
pH Meter, Calimatic 761	Knick
spectrophotometer, NanoDrop® 1000	Thermo Scientific
super-resolution microscope, Elyra PS	Zeiss
Thermomixer comfort	Eppendorf
ultrasonic bath, Sonorex RK 52 H	Bandelin
ultrasonic homogenizers, Sonoplus HD 2070	Bandelin

4.1.12 Software

Adobe® Photoshop® CS5

CellProfiler analysis software

CorelDraw® X5

FACSDiva analysis software

FinchTV

ImageJ

Microsoft® Office 2010

Odyssey® 3.0 analysis software

Origin® 8.5

pDRAW32

Swiss-PDB Viewer

4.1.13 Internet resources and databases

http://multalin.toulouse.inra.fr/multalin/
http://www.bioinformatics.org/sms/
http://www.blast.ncbi.nlm.nih.gov/Blast.cgi
http://www.ebi.ac.uk/Tools/msa/clustalw2/
http://www.expasy.org
http://www.hprd.org
http://www.ncbi.nlm.nih.gov
http://www.rcsb.org/pdb/home/home.do
http://www.uniprot.org

4.2 Methods

4.2.1 Methods in Molecular Biology

4.2.1.1 Generation of chemically competent *E. coli* bacteria

For the generation of chemically competent *E. coli* bacteria, 5 ml LB medium were inoculated with the *E. coli* bacteria strain DH5α and incubated overnight at 37 °C and 200 rpm in a bacterial shaker. 150 ml LB medium was inoculated with 900 µl overnight culture and was grown at 37 °C and 200 pm until OD_{600} value of 0.45-0.55 was reached. The bacteria suspension was cooled on ice for 10 min and harvested at 3,000 rpm at 4 °C for 10 min. The accrued bacteria pellet was resuspended in 30 ml ice-cold TFB I, incubated for 10 min on ice and harvested as before. Finally, the bacteria pellet was resuspended in 6 ml TFB II and aliquots of 50 µl were transferred to a 1.5 ml reaction tube, frozen in liquid nitrogen and stored at −80 °C.

LB medium	10 g tryptone; 5 g yeast extract; 10 g NaCl ad 1000 ml dH_2O; autoclaved; stored at 4 °C
TFB I	100 mM KCl; 10 mM $CaCl_2 \cdot 2\ H_2O$; 30 mM KOAc, pH 6.0; 15% (v/v) glycerol; adjust to pH 6.1 with HOAc; autoclaved; added 50 mM $MnCl_2 \cdot 4\ H_2O$; sterile filtered; stored at 4 °C
TFB II	75 mM $CaCl_2 \cdot 2\ H_2O$; 10 mM KCl; 10 mM MOPS; 15% (v/v) glycerol; adjust to pH 7.0 with KOH; autoclaved; stored at 4 °C

4.2.1.2 Transformation and selection of *E. coli* bacteria

For transformation, 50 µl chemically competent *E. coli* were thawed on ice and an appropriate amount of plasmid DNA, 5 µl of ligation reaction (see 4.2.1.8), or 5 µl of site-directed mutagenesis reaction (see 4.2.1.9.1) were added to the bacteria and incubated for 15 min on ice. The suspension was heat shocked for 1 min at 42 °C and then incubated on ice for another 2 min. 300 µl LB medium was added and incubated for 1 h at 37 °C and 300 rpm. Subsequently, the transformed bacteria were spread on LB agar plates containing an appropriate antibiotic and incubated overnight at 37 °C. Bacteria transformed with pCRII®- and pCR2.1®-TOPO constructs were spread on LB agar plates containing an appropriate antibiotic and additionally IPTG and X-Gal for blue/white screening. Finally, single colonies were picked with a sterile pipet tip and grown in 5 ml LB medium containing the appropriate antibiotic for plasmid preparation (see 4.2.1.3).

LB agar plates	20 g agar ad 1000 ml LB medium; autoclaved; antibiotics added (temperature of LB agar lower 60 °C); plates stored at 4 °C
LB/IPTG/X-Gal agar plates	LB agar plate supplemented with 80 µg/ml X-Gal and 20 mM IPTG
Ampicillin (Amp)	100 µg/ml final concentration
Kanamycin (Kan)	50 µg/ml final concentration

4.2.1.3 Plasmid DNA preparation and quantification

For plasmid preparation, 5 ml LB medium (containing Amp or Kan for selection) were inoculated with a single colony of transformed bacteria and incubated over night at 37 °C and 200 rpm. The bacteria suspension was harvested at 4 °C and 4,000 rpm for 5 min and plasmid DNA was isolated using Nucleospin® Plasmid Kit (Macherey-Nagel) following the manufacturer's instructions. Larger amounts of plasmid DNA were isolated from 250 ml bacterial suspension using the EndoFree Plasmid Maxi Kit (Qiagen). Isolated plasmid DNA was resuspended in buffer (50 mM Tris/HCl, pH 8.0), quantified via measurement of photometric absorbance and stored at 4 °C. For quantification, the intensity of absorbance at wavelength 260 nm (A_{260}) and 280 nm (A_{280}) was measured using the spectrophotometer NanoDrop® 1000 (Thermo Scientific). The concentration and purity of the DNA sample was determined using the following formulas:

$1\ A_{260}\ \text{unit} \approx 50\ \mu g/ml$ for dsDNA $\qquad A_{260}/A_{280} \approx 1.8$ for pure DNA

4.2.1.4 DNA digestion by restriction endonucleases

For sequence-specific DNA cleavage, DNA molecules were incubated with restriction endonucleases (FastDigest, Thermo Scientific) according to the manufacturer's instructions.

4.2.1.5 Agarose gel electrophoresis of DNA

Enzymatically cleaved DNA was mixed with an appropriate volume of 10x DNA loading buffer, loaded on an agarose gel and separated via gel electrophoresis. The agarose gel contained 0.8% - 1.5% (w/v) agarose, dissolved in TAE buffer which was melted in a microwave. For visualization, ethidium bromide (final concentration 0.5 µg/ml) was added and the solution was poured into a gel casting platform. As reference a DNA molecular weight standard (GeneRuler™ 1 kb DNA ladder, Thermo Scientific) was loaded and the DNA molecules were separated in a gel electrophoresis chamber (PerfectBlue™ Gelsystem Mini/Midi S, PeqLab) filled with TAE buffer at 100 V – 150 V.

TAE buffer (50x)	2 M Tris/AcOH, pH 7.8; 0.5 M NaOAc; 50 mM EDTA, pH 8.0
DNA loading buffer (10x)	66.7% (w/v) sucrose; 0.16% (w/v) SDS; 1.6 mM EDTA; 0.08% bromphenol blue; 0.08% xylene cyanol FF

4.2.1.6 DNA extraction from agarose gel

DNA fragments were extracted from agarose gel using the NucleoSpin® Extract II Gel extraction Kit (Macherey-Nagel) following the manufacturer's instructions. Finally, DNA was eluted in an appropriate volume of 50 mM Tris/HCl, pH 8.0.

4.2.1.7 DNA dephosphorylation

For DNA dephosphorylation, linearized vector DNA was incubated with thermosensitive alkaline phosphatase (FastAP, Thermo Scientific) according to the manufacturer's instructions. With the help of this phosphatase, the removal of 5'- and 3'-phosphate groups of DNA is catalyzed to prevent a re-ligation of vector DNA. The FastAP was directly added after vector DNA digestion by restriction endonucleases (see 4.2.1.6).

4.2.1.8 DNA ligation

For DNA ligation, an appropriate amount of linearized vector DNA (vector) and DNA fragments (insert) of interest were incubated with T4 DNA ligase (Thermo Scientific) following the manufacturer's instructions. The T4 DNA ligase catalyzes the formation of phosphodiester bonds between 5'-P and 3'-OH of dsDNA. The molecular ratio of vector:insert for DNA ligation was calculated as follows:

$$f = \frac{vector\ length\ (bp)}{insert\ length\ (bp)} \times \frac{insert\ intensity}{vevtor\ intensity} \times \frac{1}{3}$$

$$volume\ vector = volume\ insert\ \times f$$

The ligation reaction was directly used for transformation of chemically competent bacteria (see 4.2.1.2).

4.2.1.9 Polymerase chain reaction (PCR)

With the help of PCR, DNA fragments are exponential amplified from donor DNA (template) using short synthetic oligonucleotides (primer) which are complementary to regions of the 5'- (forward primer) and 3'-end (reverse primer) of the DNA region of interest (Saiki et al., 1985; Mullis et al., 1986). The polymerase added to the reaction catalyzes 5'→3' synthesis of DNA, binds to the primer, and elongates it. The PCR consists of three different steps, the denaturation, annealing, and elongation step, which are performed at different temperatures and for an appropriate number of cycles. The method is used for a variety of applications e.g. detection of hereditary disease, detection of virus infections, analysis of genetic fingerprints, cloning genes, and mutagenesis.

4.2.1.9.1 Site-directed mutagenesis

Site-directed mutagenesis of DNA vector sequences containing the insert of interest was carried out by *in vitro* amplification of the dsDNA vector using synthetic oligonucleotides containing the desired mutation. For nucleotide substitution, the desired nucleotide change(s) are incorporated in the center of the forward primer. The changed nucleotide(s) are flanked by at least 15 nucleotides to the 5'- and 3'-site. The last nucleotide at the 3'-end has to be a G or C. The reverse primer is complement to the forward primer. For nucleotide deletion, the primer consists of the nucleotides that flank the region to be deleted, at least 15 nucleotides to the 5'- and 3'end. The last nucleotide at the 3'-end has to be a G or C. The reverse primer is complement to the forward primer. The PCR was carried out using the proof reading Phusion High-Fidelity DNA Polymerase (Thermo Scientific) and the procedure as follows:

PCR reaction for site-directed mutagenesis

5-50 ng	cDNA
10 µl	5x Phusion reaction buffer
1.0 µl	dNTPs (10 mM)
125 ng	primer forward (2 µM)
125 ng	primer reverse (2 µM)

0.5 µl	Phusion High-Fidelity DNA Polymerase (2 U/µl)
ad 50 µl	H_2O

PCR program for site-directed mutagenesis

step	**reaction**	**T [°C]**	**time**
1	initial denaturation	98	30 s
2	denaturation	98	30 s
3	annealing	55	30 s
4	elongation	72	1 min/kb plasmid
5	go to step 2, 17x		
6	final elongation	72	4 min
7	cooling	12	∞

Following the PCR program, the restriction endonuclease *Dnp*I (1 µl) is directly added to the PCR reaction and incubated for 1 h at 37 °C. *Dnp*I digests the non-mutated, dam methylated parental DNA template in the PCR reaction, isolated from dam positive *E. coli* strain DH5α. Finally, chemically competent bacteria are transformed with 5 µl digested PCR reaction mixture that contains the generated plasmid with the mutated insert. To verify the accuracy of the newly formed nucleotide sequence, the plasmid DNA was analyzed via DNA sequencing 4.2.1.10.

4.2.1.10 DNA sequencing

DNA sequencing was realized by GATC biotech using the Sanger DNA sequencing method (Sanger et al., 1977) on an ABI 3730XL sequencer (Life Technology). For sequencing preparation, 5 µl of plasmid DNA (80-100 ng/µl) were mixed with 5 µl primer of interest (5 µM) and send to GATC biotech.

4.2.2 Methods in Cell Biology

4.2.2.1 General aspects of cell culturing

All cell lines used in this thesis were cultivated in humidified atmosphere at 37 °C and 5% CO_2 and were treated under laminar flow cell culture benches to ensure sterile conditions. Complement factors within the fetal calf serum (FCS) and chicken serum (CS) were inactivated by heating the serum to 56 °C for 30 min. The concentration of cells was determined with a Neubauer chamber slide. Cells were harvested with a refrigerated

centrifuge (Megafuge, Heraeus, Thermo Scientific) at 4 °C and 1,200 rpm unless otherwise indicated.

4.2.2.2 Cell lines

Jurkat

The immortalized Jurkat T cell lymphocytes used in this thesis are all derived from 1976 established cells from peripheral blood of a 14-year-old boy with acute lymphoblastic leukemia (Schneider et al., 1977). As wild type cells the subclone 16 of Jurkat T lymphocytes (Jurkat J16) are used (Tepper et al., 1997; Boesen-de Cock et al., 1998). All caspase-9 reconstituted cells are derived from caspase-9 deficient Jurkat cells (Samraj et al., 2007) kindly provided by Klaus Schultze-Osthoff (Interfaculty Institute of Biochemistry, University Tübingen, Germany). For this thesis following Jurkat cell lines were generated by retroviral gene transfer (see 4.2.2.7): Jurkat caspase-9 deficient cell line expressing:

- pMSCVpuro empty vector control
- caspase-9 R13A
- caspase-9 R56A
- caspase-9 C287S
- caspase-9 ΔCARD
- caspase-9-GFP
- caspase-9-GFP R13A
- caspase-9-GFP R56A
- caspase-9-GFP C287S
- caspase-9-GFP C287S R13A
- caspase-9-GFP C287S R56A

Caspase-9 deficient Jurkat cell lines expressing caspase-9 C287S, caspase-9-GFP C287S, caspase-9-GFP R13A, caspase-9-GFP R56A, caspase-9-GFP C287S R13A, and caspase-9-GFP C287S R56A were generated by Quynh Nguyen during her bachelor thesis that was supervised by Stefan Drießen.

DT40

The immature chicken DT40 B lymphocyte cell line is derived from Hyline SC chicken bursal lymphoma induced by an avian leucosis virus (ALV). The original lymphoma was induced by viral infection of a 1 day old chicken with Rous associated virus 1 (RAV-1) (Baba & Humphries, 1984; Baba et al., 1985). DT40 B lymphocytes continue to rearrange their immunoglobulin light chain gene (*IgL*) and exhibit a high frequency of homologous gene

targeting. This makes it very susceptible for targeted to random integration of transfected DNA constructs which enables the convenient generation on knockout cell lines (Sonoda et al., 2001). In this thesis wild type and *ULK1/2*-/- DT40 were used (Alers et al., 2011).

Mouse embryonic fibroblast (MEFs)

Mouse embryonic fibroblasts from *Ulk1/2*-/- mice, as well as genetically matched wild type MEFs were prepared from 13.5 days old post coitus embryos and immortalized by transfection with a plasmid containing SV40 genomic DNA (Cheong et al., 2011). For this thesis wild type and *Ulk1/2*-/- MEFs expressing mCitrine-hLC3B were generated by retroviral gene transfer (see 4.2.2.7).

HCT116

USP9X-/o HCT116 cells were derived from primary human colonic carcinoma, designated HCT116 (Brattain et al., 1981). The endogenous *USP9X* locus was disrupted in HCT116 cells using recombinant adeno-associated virus (rAAV)-based gene targeting methods (Harris et al., 2012). Wild type and *USP9X*-/o HCT116 cells were kindly provided by Fred Bunz (Johns Hopkins Medicine, Baltimore, MD, USA).

HeLa

HeLa cells were established in 1950 from human epithelial cells derived from cervical cancer induced by human papillomavirus 18 (HPV18) infection of a 30 year old woman.

U2OS

U2OS epithelial cells are derived from a moderately differentiated sarcoma of the tibia of a 15 year old girl in 1964 (Ponten & Saksela, 1967).

HEK293

HEK293 epithelial cells were established from human primary embryonic kidney cells transformed by adenovirus type 5 (Ad 5) (Graham et al., 1977).

Platinum E (PlatE)

Platinum E represents a potent retrovirus packaging cell line derived from HEK293T cells via stable transfection with the viral structural genes *gag-pol* and *env* as well as a, through an internal ribosomal entry site (IRES) separated, selectable marker gene, which are both under a potent EF1α promoter (Morita et al., 2000). PlatE is a packaging cell line of third generation which allows the generation of Moloney murine leukemia virus (MMLV)-derived retroviral

particles. PlatE cells were kindly provided by Toshio Kitamura (Institute of Medical Science, University of Tokyo, Japan).

Flp-In™ T-REx™ 293 cells

This cell line is derived from HEK293 cells and stably expresses the Tet repressor from pcDNA6/TR and contains a single, stably integrated Flp Recombination Target (FRT) site from pFRT/lacZeo at a transcriptionally active genomic locus. The cell line is used for generation of stable cell lines that ensure inducible, homogenous expression of the protein of interest. Therefore, Flp-In™ T-REx™ 293 cells were co-transfected with pcDNA5/FRT/TO plasmid containing the gene of interest and pOG44, an expression plasmid coding for the Flp recombinase. The Flp-In™ T-REx™ 293 cells inducibly expressing GFP-ULK1 wt, GFP-ULK1 kd, GFP-ULK2 used in this thesis were described in Löffler et al. (2011).

4.2.2.3 Cell line specific culturing conditions

Jurkat cell lines and derivatives were cultured in RPMI 1640 supplemented with 10% FCS, 10 mM HEPES, 50 U/ml penicillin, and 50 µg/ml streptomycin.

Wild type and *ULK1/2*-/- DT40 cells were cultured in RPMI 1640 supplemented with 10% FCS, 1% chicken serum, 3 mM L-glutamine, 50 µM β-mercaptoethanol, 50 U/ml penicillin, and 50 µg/ml streptomycin.

HEK293 cells and derivatives, MEF, U2OS and HeLa cells were cultured in DMEM (4.5 g/l D-glucose, L-glutamine), supplemented with 10% FCS, 50 U/ml penicillin, and 50 µg/ml streptomycin (full medium). Expression of the respective fusion protein was induced with 0.1 µg/ml doxycycline.

Wild type and *USP9X*-/o HCT116 cells were cultured in McCoy's 5A medium supplemented with 10% FCS, 50 U/ml penicillin, and 50 µg/ml streptomycin.

For amino acid starvation, HEK293 cells and derivatives, and DT40 cells were washed once with PBS and incubated in EBSS for indicated times. For glucose starvation, MEFs were washed once with PBS and incubated for 24 h in glucose-free DMEM supplemented with 10% dialyzed FCS, 50 U/ml penicillin and 50 µg/ml streptomycin.

The adherent cell lines were passaged every 2 – 3 days using PBS and Trypsin/EDTA solution and were diluted 1:3 to 1:25 depending on cell density and division rate. Cell density should not exceed 90% confluence. Suspension cells were splitted 1:5 – 1:50 every 2 – 3 days, cell density should not exceed 1 x 10^6 cells/ml medium.

4.2.2.4 Freezing and thawing of eukaryotic cells

For long time storage of eukaryotic cells in liquid nitrogen, adherent cells were trypsinized, washed once with PBS and after centrifugation resuspended in 1 ml freezing medium (90% (v/v) FCS; 10% (v/v) DMSO). The same was realized with suspension cells except trypsinization. Subsequently, cells were refrigerated to −80 °C at a freezing rate of ~1 °C/min in a freezing container and for long term storage transferred to liquid nitrogen. For thawing, cells were warmed in 37 °C water bath, immediately resuspended in 10 ml full medium and resuspended in full medium again after centrifugation.

4.2.2.5 Transient transfection of HEK293 cells and derivatives via lipofection

For transient transfection, typically 10-cm diameter dishes of GFP-ULK1 Flp-In™ T-REx™ 293 cells or HEK293 cells, were cultured at ~80% confluence. 14 µg of plasmid DNA and 45 µl FuGENE® HD were added to 680 µl DMEM w/o supplements. After 20 min of incubation at RT, the mixture was given dropwise to cells and incubated 18 – 72 h before diverse treatments and analyzes.

4.2.2.6 siRNA mediated knockdown in HEK293 and HCT116 cells

For knockdown of diverse proteins, 1.33 x 10^5 HEK293 cells were seeded in a 24-well plate 24 h before transfection. A volume of 0.625 µl of 20 µM siRNA (diluted in 1x siRNA RNase-free buffer; 25 nM final concentration) was mixed with 49,375 µl serum-free medium and incubated for 5 min at RT. 1 µl DharmaFECT 1 was mixed with 49 µl serum-free medium, both mixtures were combined and applied dropwise to cells, and incubated for 48 – 72 h before being analyzed by immunoblotting.

4.2.2.7 Establishing stable cell line via retroviral gene transfer

4.2.2.7.1 Transfection of PlatE cells for the production of recombinant retroviruses

For the transfection of PlatE cells, confluence was adjusted at ~60% in a 6-cm cell culture dish at day of transfection. Therefore, 7.5 µl FuGENE®6 was mixed with 200 µl serum-free RPMI and incubated for 5 min at RT. 1.9 µg pMSCV based vector DNA and 1.0 µg pVSV-G vector were added and incubated for 15 min at RT. When MEFs were to be transduced, pseudotypisation with VSV-G was not necessary. The PlatE medium was replaced with 3.5 ml full target cell medium and transfection mixture was applied dropwise. Cells were cultivated for 48 h in order to produce recombinant (VSV-G pseudotyped) retroviruses.

4.2.2.7.2 Transduction of target cells with recombinant retroviruses

In case of suspension cells, for transduction of target cells with recombinant retroviruses, 4.5 µl of freshly prepared polybrene (3 mg/ml polybrene in PBS; sterile filtered) was added to 1.5 ml target cell medium and given into a 6-cm dish. For MEFs, 0.25 x 10^5 cells were seeded into a 6-cm dish the day before and medium was exchanged for medium supplemented with freshly prepared polybrene. Retroviral supernatant was then centrifuged at 300 *g* for 4 min at 4 °C. For suspension cells, 1 x 10^6 target cells were resuspended in retroviral supernatant and added to the 6-cm dish with target medium and polybrene. For adherent cells, retroviral supernatant was given to the 6-cm dish supplemented before with target cell medium and polybrene. After 24 h cells were resuspended in fresh medium and seeded into an appropriate cell culture dish or flask. After 24 h, cells were resuspended in selection medium containing 0.5 µg/ml puromycin for suspension cells and 2.5 µg/ml for MEF cells.

4.2.2.8 Confocal laser scanning microscopy and super-resolution microscopy

For confocal laser scanning microscopy and super-resolution microscopy, HEK293 cells or Flp-In™ T-REx™ 293 cells inducibly expressing GFP-ULK1 wt, GFP-ULK1 kd, GFP-ULK2 wt, or GFP-only were seeded on poly-L-lysine coated cover slips. Expression of the respective fusion protein was induced with 0.1 µg/ml doxycycline for 3 or 16 h. Incubation of cells was performed in media and for times as indicated. Cells were fixed with 4% PFA in PBS buffer for 15 min and embedded directly in Mowiol 4-88 containing 1 µg/ml Hoechst 33342 dye for analysis of GFP fusion proteins. For immunofluorescence staining of endogenous LC3, ubiquitin, K63-linked ubiquitin and SQSTM1/p62, HEK293 cells were washed three times with PBS, incubated in 50 mM NH_4Cl for 10 min, and washed in PBS for another 5 min. Cells were permeabilized with 0.05% saponin in PBS for 5 min and incubated for 1 h with corresponding primary antibodies diluted in 0.05% saponin in PBS. After washing the cells three times with 0.05% saponin in PBS, they were incubated for 1 h with appropriate secondary antibodies. Two times washing with 0.05% saponin in PBS followed and once with PBS. Finally, cover slips were embedded in Mowiol 4-88 containing 1 µg/ml Hoechst. For super-resolution microscopy, cover slips were embedded in VECTASHIELD mounting medium with DAPI. DT40 suspension cells were centrifuged on poly-L-lysine coated cover slips for 5 min and at 400 *g*, washed once with PBS, and fixed with 4% PFA in PBS for 5 min. After washing DT40 once with PBS, cells were treated for 10 min with PBSTS (PBS containing 0.1% Tween 20; and 0.02% SDS). Then DT40 cells were incubated for 1 h with LC3 antibody diluted in PBSTS, washed three times with PBSTS, and incubated for 1 h with appropriate secondary antibody. After washing two times with PBSTS and once with PBS, cover slips were

embedded in Mowiol 4-88 containing 1 µg/ml Hoechst 33342 dye. Cells were analyzed on a Zeiss LSM 710, Zeiss LSM 780, or Zeiss Elyra PS. Hoechst, DAPI, GFP, Alexa Fluor® 568 and Alexa Fluor® 594 were excited at 405, 488, 561, and 594 nm, respectively.

4.2.2.9 Live-cell imaging

Flp-In™ T-REx™ 293 GFP-ULK1 cells were seeded overnight on Nunc™ Lab-Tek™ Chambered Coverglasses. After induction of GFP-ULK1 expression with doxycycline for 3 h, medium was replaced with DMEM-GFP medium and treated with 5 µM WP1130 with or without 10 µM nocodazole. Life cell imaging of GFP-ULK1 was performed on a Deltavision Deconvolution microscope equipped with a solid-state light source, a 60x NA 1.42 objective, and a Coolsnap HQ2 CCD camera. The cells were kept at 37 °C and 5% CO_2 using a CO_2- and temperature-controlled incubator.

4.2.2.10 Long-lived protein degradation assay

HEK293, HeLa, and U2OS cells were incubated for 72 h with 0.125 µCi/ml L-[^{14}C]valine-supplemented medium, followed by two washes and a 16 h chase in fresh medium containing 10 mM non-radioactive L-valine to allow degradation of short-lived proteins. Next, cells were washed and treated with indicated medium and inhibitors for 4 h. For each sample, radioactivity of the acid-soluble fraction of the medium and the radioactivity in the cells remaining in the well were measured. Percent degradation was assessed as the acid-soluble radioactivity of the medium divided by the total radioactivity.

4.2.2.11 Flow cytometry

4.2.2.11.1 Analysis of apoptosis

For measurement of apoptosis, Jurkat cells and derivatives (see 4.2.2.2) were stained with propidium iodide and analyzed by flow cytometry. The measurement is based on the fact that during apoptosis DNA is fragmented. Propidium iodide is able to bind DNA stoichiometrically which makes it possible to evaluate cellular DNA content by flow cytometric analysis and identification of hypodiploid (sub G_1) nuclei (Nicoletti et al., 1991). Nuclei were prepared by lysing cells in hypotonic lysis buffer containing propidium iodide, and subsequent analysis by flow cytometry. Nuclei to the left of the G_1 peak are considered as apoptotic. Flow cytometry were carried out on a FACSCalibur™ or LSRFortessa™ cell analyzer using CellQuest or FACSDiva analysis software, respectively.

hypotonic lysis buffer	1% sodium citrate; 0.1% Triton X-100; 50 µg/ml propidium iodide

4.2.2.11.2 Analysis of autophagy

For measurement of autophagy, MEF cells stably expressing mCitrine-hLC3B (see 4.2.2.2) were analyzed by flow cytometry under starvation and medium conditions with indicated inhibitors. Cells were harvested with Trypsin/EDTA solution, washed once with PBS, and finally analyzed on an LSRFortessa™. Reduction of mCitrine-hLC3B compared to medium control indicates autophagy induction.

4.2.3 Methods in Biochemistry

4.2.3.1 Preparation of cleared cell lysates and whole cell lysates

For preparation of cleared cell lysates (CCLs), also called soluble fraction, cells were harvested by centrifugation (300 *g*, 4 min, 4 °C). Adherent cells were trypsinized beforehand. Cell pellets were resuspended in an appropriate volume of ice-cold lysis buffer, with and without NEM depended on the following analysis. Cells were then lysed on ice for 30 min with mixing by vortex every 5 min. Insoluble cell components e.g. aggregated proteins and nuclei, were removed via centrifugation for 10 min at 20.000 *g* and 4 °C. The supernatant called CCL or soluble fraction was transferred to a new reaction tube and an appropriate volume of 6x SDS sample buffer (Laemmli buffer) was added if an immunoblot was carried out. For the preparation of insoluble fraction, the emerged pellet after centrifugation, was resuspended in 2x SDS sample buffer, heated for 5 min at 95 °C, incubated for 15 min at 80 °C in an ultrasound water bath, and finally heated for 5 min at 95 °C to resolve all components for further immunoblot analysis.

For the preparation of whole cell lysates (WCLs), cells were harvested as described before and the formed cell pellet was resuspended in 2x SDS sample buffer and processed as described before for preparation of insoluble fraction.

cell lysis buffer	20 mM Tris/HCl, pH 7.5; 150 mM NaCl; 0.5% (v/v) Triton X-100; 1.0 mM EDTA; 1.0 mM EGTA; 1 mM Na_3VO_4; 50 mM NaF; 1x protease inhibitor cocktail
2x SDS sample buffer	125 mM Tris/HCl; 17.2% (v/v) glycerol; 4.1% (w/v) SDS; 2% (v/v) β-mercaptoethanol; 0.02% (w/v) bromophenol blue
6x SDS sample buffer	375 mM Tris/HCl; 25.8 % (v/v) glycerol; 12.3 % (w/v) SDS; 6% (v/v) β-mercaptoethanol; 0.06% (w/v) bromophenol blue

4.2.3.2 Preparation of S100 cytoplasmic extract

For preparation of S100 cytoplasmic extract, 1 x 10^8 Jurkat cells were harvested and the cell pellet was stored at −80 °C. Jurkat pellet were weighed and three times the volume of Roeder buffer added to the pellet. After 10 min incubation, cell suspension was further lysed with a Dounce homogenizer with tight pestle (10 times). Before centrifugation for 20 min at 20.000 *g* and 4 °C, NaCl concentration was adjusted to 150 mM. The supernatant was transferred into a new reaction tube, protein concentration was determined (see 4.2.3.3), and immunopurification (see 4.2.3.4) was carried out for further mass spectrometric analysis.

Roeder buffer	10 mM KCl; 10 mM HEPES; 1.5 mM $MgCl_2$; 0.5 mM DTT; 1x protease inhibitor cocktail

4.2.3.3 Determination of protein concentration via Bradford protein assay

The Bradford method is a spectroscopic assay for the determination of protein concentration. The dye Coomassie Brilliant Blue G-250 binds to the alkaline amino acids of proteins which causes a shift in absorption maximum of the dye from 465 to 595 nm. The increase in absorption at 595 nm is monitored (Bradford, 1976). The samples were set up in a 96-well plate at duplicates by mixing 10 µl of lysate (diluted from 1:10 to 1:50) with 200 µl Bradford reagent (Protein assay kit dye reagent concentrate, diluted 1:5). The absorbance was measured at 590 nm with a monochromator-based microplate reader and protein content was calculated by comparison to a BSA standard curve (0 – 400 µg/ml BSA in PBS).

4.2.3.4 Immunopurification and affinity purification

For immunopurification and affinity purification, CCLs were made as described in 4.2.3.1. If analysis of ubiquitinated proteins were carried out, 2 mM NEM was added to the lysis buffer. Immunopurification was performed for 16 h at 4 °C with rotation after addition of GFP-Trap® beads. The agarose beads were washed three times with lysis buffer, heated up for 5 min at 95 °C in 2x SDS sample buffer and used for immunoblotting. Affinity purification of ubiquitinated proteins was carried out with Agarose-TUBE2 as described in the user's manual. The lysis buffer was supplemented with 2 mM NEM.

4.2.3.5 Discontinuous SDS-PAGE

Via one-dimensional, discontinuous polyacrylamide gel electrophoresis (PAGE), proteins can be separated according to their molecular weight under denaturing conditions using sodium dodecyl sulphate (SDS) (Weber & Osborn, 1969; Laemmli, 1970). Polyacrylamide gels are

insoluble matrices of acrylamide monomers cross-linked with N,N'-methylene-bisacrylamide in the presence of the free radical initiator APS and the polymerization catalyst TEMED. They consist of two different types of polyacrylamide gels with distinct functions. In the upper stacking gel with 5.1% acrylamide/bisacrylamide concentration, the proteins in the sample are concentrated. In the lower separating gel with 8 – 15% acrylamide/bisacrylamide concentration, the proteins in the sample are separated according to their molecular weight. For better separation of proteins on one gel, gradient gels with acrylamide/bisacrylamide concentration from 8 – 15% were casted. Cleared or whole cell lysates, as well as insoluble portion of cell lysis, were mixed with an appropriate volume of 2x or 6x SDS sample buffer, respectively, and heated for 5 min at 95 °C prior to gel loading. Prestained molecular weight markers (PAGERuler^{TM} Prestained Protein ladder) were used as standards. Proteins were separated at a constant current of 25 – 45 mA per gel and for larger gradient gels up to 800 V/h for at least 4 h. SDS-PAGE was carried out in SDS running buffer using an appropriate electrophoresis system according to the size of gels.

stacking gel	135 mM Tris/HCl, pH 6.8; 5.1% (w/v) acrylamide/bisacrylamide; 0.1% (w/v) SDS; 0.1% (v/v) TEMED; 0.1% (w/v) APS
separating gel	390 mM Tris/HCl, pH 8.8; 8-15% (w/v) acrylamide/bisacrylamide; 0.1% (w/v) SDS; 0.1% (v/v) TEMED; 0.1 % (w/v) APS
SDS running buffer	250 mM Tris; 1.9 M glycine; 0.1% (w/v) SDS

4.2.3.6 Immunoblot analysis

Post SDS-PAGE, separated proteins were transferred electrophoretically onto a polyvinylidene fluoride (PVDF) membrane, to make them accessible for detection with specific antibodies. Blotting was realized in transfer buffer using an appropriate wet transfer blotting tank according to the size of polyacrylamide gel and PVDF membrane. Prior to transfer, the PVDF membrane was activated with MeOH for 1 min. Proteins were transferred at constant voltage of 100 V for 1 h, or constant current of 500 mA for 1.5 h, when transferred to smaller, or larger gel/PVDF-membrane, respectively. Subsequently, the membrane was blocked with blocking buffer for 1 h to reduce unspecific binding of primary antibodies. The PVDF membrane was washed once with TBS-T and incubated with primary antibody diluted 1:200 – 1:5,000 in TBS-T containing NaN_3 for 1 h at RT or at 4 °C over night. The membrane was then washed three times for 5 min with TBS-T following appropriate IRDye®680- or IRDye®800-conjugated secondary antibody incubation (diluted in TBS-T

1:10,000 – 1:20,000) for 1 h at RT. Next, membrane was washed three times with TBS-T for 5 min and dried between blotting paper. Finally, dried immunoblots were analyzed by detection of the infrared fluorescence signal of secondary antibodies using the Odyssey® Infrared Imaging System I (Li-COR Biosciences). Following quantification of immunoblots was realized using the ImageJ analysis software.

transfer buffer	39 mM glycine; 43.58 mM Tris; 20% MeOH
blocking buffer	5% non-fat dried milk in TBS-T
TBS-T (Tween® 20)	0.1 % (v/v) Tween® 20 in 1x TBS

4.2.3.7 *In vitro* apoptosome formation

For *in vitro* apoptosome formation and further analysis of the apoptosome, 5 x 10^7 Jurkat cells were harvested and washed once with ice-cold PBS. Cells were lysed with 1.0 ml cell lysis buffer (20 mM HEPES, 7.5 pH; 50 mM NaCl; 0.3% CHAPS; 10 mM KCl; 1.5 mM $MgCl_2$; 1 mM EDTA; 1 mM EGTA; 1 mM DTT) for 30 min on ice. After centrifugation for 10 min at 4 °C and 20,000 *g*, the supernatant was transferred to a new reaction tube. *In vitro* apoptosome formation was initiated by addition of cytochrome c (final concentration 8.6 µM) and ATP (final concentration 200 mM) and incubation for 15 min at 37 °C (Hill et al., 2004). Cell lysate was diluted with 3 ml cell lysis buffer. Bradford method was carried out (see 4.2.3.3) and 50 µg lysate were transferred to a new reaction tube as CCL control. Remaining cell lysate was incubated with Protein A/G Plus Agarose Beads (~10 µl beads/ml lysate) and caspase-9 antibody (~1.0 µg/ml lysate) for 2 h at 4 °C under permanent rotation. Cell lysate-bead suspension was centrifuged for 5 min at 1,500 rpm and 4 °C and washed with lysis buffer three times. 50 µl 6x SDS sample buffer was added, heated for 5 min at 95 °C and immunoblot of proteins of interest was realized.

4.2.3.8 Gel filtration

To analyze protein complex association of caspase-9 in the presence and absence of STS in Jurkat caspase-9 C287S cells, gel filtration analysis was performed. Therefore, 1 x 10^7 Jurkat cells were harvested and lysed with 2 ml cell lysis buffer containing 1% Triton X-100 (see 4.2.3.1). Cell lysate was filtered with a nylon syringe filter (0.2 µm pores) and applied to a Superose 6 column (GE Healtchcare) separated by FPLC (Äktapurifier). Proteins were eluted with washing buffer (50 mM Tris; 150 mM NaCl) at a constant flow rate of 0.5 ml/min. 0.5 ml fractions were collected and analyzed by immunoblotting. The column was calibrated using the high/low molecular weight calibration standard (GE Healthcare) comprising Blue dextran

2,000 (2 MDa), thyroglobin (669 kDa), ferritin (440 kDa), aldolase (158 kDa), and RNase (14 kDa).

4.2.3.9 Fluorometric determination of caspase-3 activity

For detection of caspase-3-like DEVDase activity, 3 x 10^4 HEK293 cells were seeded in 96-well plates. The cells were incubated overnight and were then treated with indicated inhibitors and times. 5 x 10^4 Jurkat cells were added to 96-well plate and centrifuged. The Jurkat and HEK293 cells were lysed with buffer containing 20 mM HEPES, 84 mM KCl, 10 mM $MgCl_2$, 200 µM EDTA, 200 µM EGTA, 0.5% NP‑40, 1 µg/mL leupeptin, 1 µg/mL pepstatin A, 5 µg/mL aprotinin. Caspase activity was determined by incubation of cell lysates with 70 µM of the fluorogenic substrate Ac-DEVD-AMC (N-acetyl-Asp-Glu-Val-Asp-aminomethyl-coumarin) in 200 µl buffer containing 50 mM HEPES (pH 7.3), 100 mM NaCl, 10% sucrose, 0.1% CHAPS, 2 mM $CaCl_2$ and 13.35 mM DTT. The release of aminomethylcoumarin was measured in a ~1 h kinetic by spectrofluorometry using a monochromator-based microplate reader (SynergyMX, BioTek) with an excitation wavelength of 360 nm and an emission wavelength of 450 nm. The slope of the linear range of the fluorescence curves was considered as corresponding to DEVDase activity and expressed in arbitrary fluorescence units per minute.

4.2.3.10 *In vitro* kinase assay

For *in vitro* phosphorylation, ULK1 was immunopurified (see 4.2.3.4) from Flp-In™ T-REx™ 293 cells expressing GFP-ULK1 wt or GFP-ULK1 kd. Alternatively, GST-ULK1 was used. For *in vitro* reaction of kinase and substrates, immunopurified GFP-ULK1 wt/kd from ~300 µg CCLs was applied or 0.5 µg GST-ULK1. 1-2 µg of (potential) substrate (i.g. GST-ATG13, GST-MBP, 6His-USP7, GST-USP9x) was incubated with purified ULK1 in 50 mM Tris/HCl (pH 7.5), 0.1 mM EGTA, 0.1 mM DTT, 5 mM $Mg(CH_3COO)_2$ and 0.1 mM [^{32}P]ATP. The reaction was stopped by addition of 6x Coomassie staining of the gel (see 4.2.3.11) and autoradiography was performed (see 4.2.3.13).

4.2.3.11 Coomassie staining of polyacrylamide gels

For visualization of proteins after SDS-PAGE, polyacrylamide gels were stained with the Colloidal Blue Staining Kit (Invitrogen) according to the manufacturer's instructions.

4.2.3.12 Drying of polyacrylamide gels

Post in *vitro kinase* assay, SDS-PAGE, and Coomassie staining, polyacrylamide gels were dried to obtain sharper autoradiographic signals when exposed to X-ray films. After destaining, gels were wrapped between two sheets of cellophane and blotting paper, and placed into a gel-drying apparatus (Bio-Rad).

4.2.3.13 Autoradiography of polyacrylamide gels

Dried Coomassie stained polyacrylamide gels were placed into a Amersham Autoradiography Hypercassette (GE Healthcare) with Intensifying screens BioMax® Transcreen® HE (Kodak) exposed to X-ray film BioMax® MR (Kodak) for 1 min to 16 h. For long time exposure, film cassette was stored at −80 °C. X-ray film was developed using an AGFA Curix 60 (AGFA Healthcare).

5 Results

5.1 Apoptosis – Regulation of the initiator caspase-9

In tumor cells, parts of the apoptosis machinery are frequently inactivated which can result in chemo- and radiotherapy resistance. Most common is the disruption of the intrinsic apoptosis pathway, especially with regard to pre-mitochondrial and mitochondrial death processes e.g. mutation of *TP53* gene, pro-, or anti-apoptotic *BCL2* genes (Johnstone et al., 2002).

In previous studies by our group and others it could be demonstrated that staurosporine can induce apoptosis in a dual mode of action (i) on the one hand like anticancer drugs e.g. mitomycin C over the canonical intrinsic apoptosis pathway including cytochrome c release, apoptosome formation and activation of caspase-9 dependent on APAF1 yet independently of external death receptor signaling (ii) and on the other hand via a novel intrinsic apoptosis pathway, which allows the induction of apoptosis in anticancer drug-resistant tumor cells. The alternative intrinsic apoptosis pathway, is characterized by the induction of apoptosis in Bcl-2 and Bcl-xL overexpressing cells as well as the independency of APAF1 and apoptosome formation, and in contrast, the dependency on caspase-9. In other words caspase-9 can be activated independently of the apoptosome formation and APAF1 (Stepczynska et al., 2001; Manns et al., 2011). Consequently, it should be investigated how caspase-9 is activated during this novel intrinsic apoptosis pathway that will help to investigate the possibility of overcoming chemo- and radiotherapy resistance.

A highly suitable cell system for analysis the role of caspase-9 in apoptosis is a caspase-9 deficient Jurkat cell line (Samraj et al., 2007), which can be reconstituted with various caspase-9 mutants. As apoptotic readout systems, we used mainly three different methods (i) fluorometry based effector caspase-3 DEVDase activity assay, (ii) flow cytometry based analysis of DNA fragmentation initiated during apoptosis (Nicoletti assay), (iii) immunoblot based analysis of initiator caspase-9, effector caspase-3, and caspase substrate PARP.

In the following mitomycin C, an anticancer drug, was used as control inducing the intrinsic mitochondrial cytochrome c/APAF1 apoptosis pathway and TRAIL was used as control for the extrinsic death receptor apoptosis pathway predominantly mediated via the initiator caspase-8. Q-VD-OPh a broad-range caspase inhibitor was used as control for caspase activity.

5.1.1 CARD of caspase-9 is indispensable for staurosporine induced apoptosis

During induction of the intrinsic mitochondrial apoptosis pathway, caspase-9 interacts with its caspase activation and recruitment domain (CARD) with the CARD of APAF1 as part of the apoptosome, which results in the autocatalytic activation of caspase-9, subsequent induction of caspase cascade, and finally apoptotic cell death (Li et al., 1997).

Since the CARD region of caspase-9 is essential for APAF1 dependent activation of caspase-9, it was investigated in which extent the CARD is important for STS induced activation of caspase-9.

Therefore, caspase-9 deficient Jurkat cells were reconstituted with a caspase-9 CARD deletion mutant (ΔCARD). Staurosporine had the ability to induce caspase-3 DEVDase activity in Jurkat wt and caspase-9 deficient Jurkat cells reconstituted with caspase-9 wt (C9 rec) with a comparatively fast time course, although, higher caspase-3 activity was obtained in reconstituted cells, possibly due to overexpression. In contrast, staurosporine did not induce caspase-3 activity in caspase-9 deficient vector control and caspase-9 ΔCARD mutant Jurkat cells (**Figure 5-1**, **A**). As to be expected, anticancer drug-induced apoptosis by mitomycin C and processing of caspase-3 and PARP were completely blocked in caspase-9 deficient and caspase-9 ΔCARD mutant Jurkat cells, but not in cells positive for caspase-9. Since death receptor induced apoptosis is predominantly mediated via caspase-8, TRAIL induced apoptosis and caspase activation in caspase-9 deficient and caspase-9 CARD deletion mutant cells. Interestingly, staurosporine-induced apoptosis and processing of caspase-3 was completely abrogated in caspase-9 deficient and caspase-9 ΔCARD mutant Jurkat cells indicating that the CARD region is required for both modes of staurosporine induced activation of caspase-9. Addition of the broad-range caspase inhibitor Q-VD-OPh completely blocked apoptosis induction by staurosporine and processing of caspase-3, -9 and PARP, in caspase-9 deficient Jurkat cells reconstituted with caspase-9 wt, underlining the involvement of caspase activation. (**Figure 5-1, B, C)**. Collectively, these data indicate that the CARD region of caspase-9 is not only required for APAF1 dependent anticancer drug induced caspase-9 activation but moreover for the APAF1 independent alternative activation of caspase-9 via staurosporine.

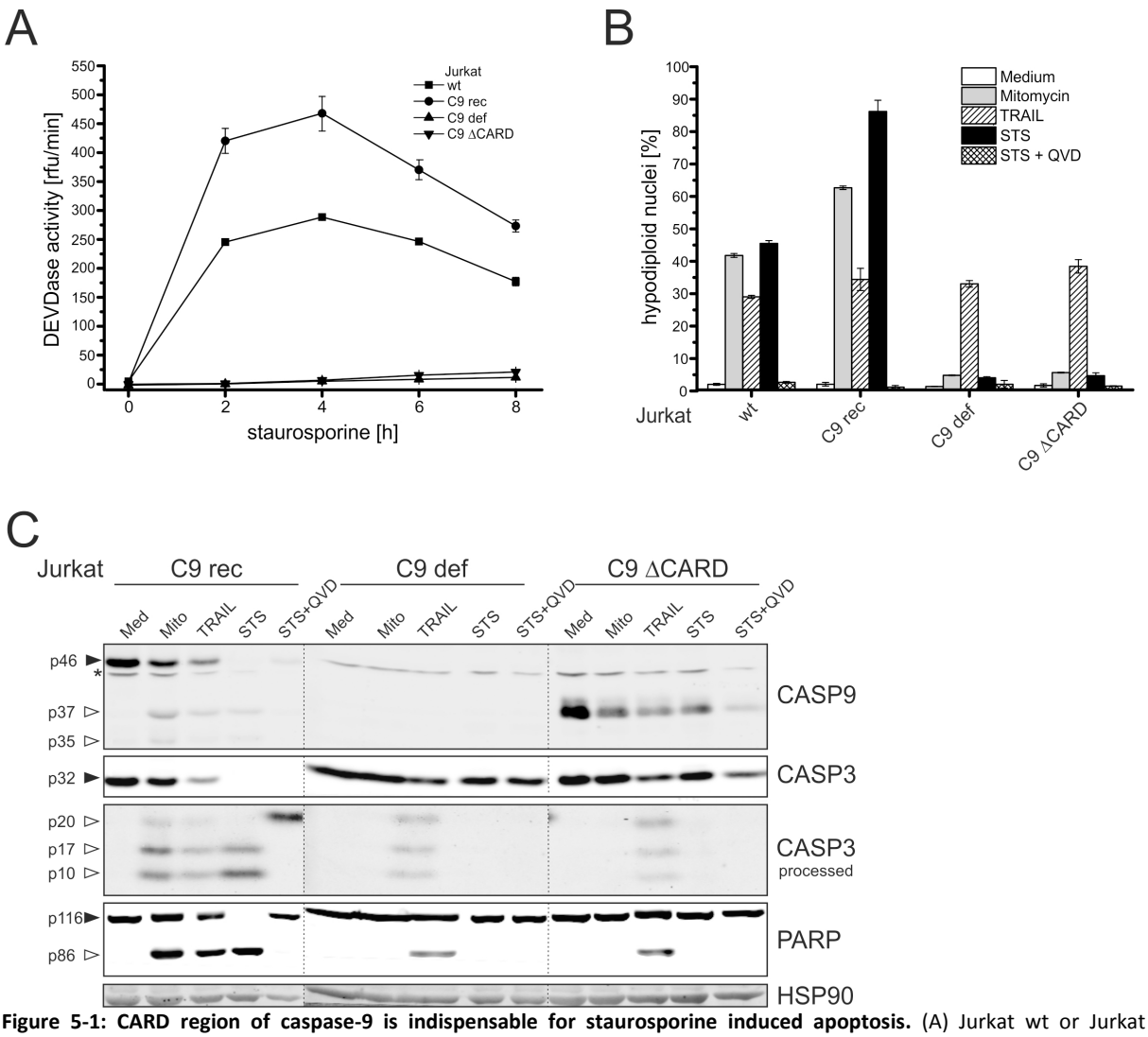

Figure 5-1: CARD region of caspase-9 is indispensable for staurosporine induced apoptosis. (A) Jurkat wt or Jurkat caspase-9 deficient cells reconstituted with caspase-9 wt (C9 rec), pMSCV vector control (C9 def), or caspase-9 ΔCARD mutant (C9 ΔCARD) were treated with 2.5 µM staurosporine for up to 8 h. Cell lysates were prepared and incubated with fluorogenic caspase substrate Ac-DEVD-AMC. DEVDase activity was assessed by the cleavage of Ac-DEVD-AMC and is given in relative fluorescence unit per minute (rfu). Fluorescence (Ex 360 nm, Em 450 nm) was measured at 37 °C over 120 min. The slope of the linear range of the fluorescence curves was considered as correlating to DEVDase activity. Data shown are mean of triplicates ± SD. (B) Cells described in A were treated for 24 h with 25 µg/ml mitomycin C (control inducing the intrinsic apoptosis pathaway), 40 ng/ml TRAIL (control inducing the extrinsic apoptosis pathway), 2.5 µM staurosporine (STS), 2.5 µM staurosporine co-treated with 10 µM Q-VD-OPh (STS + QVD), a broad-range caspase inhibitor, or left untreated (Medium). Apoptosis was analyzed by propidium iodide staining of nuclei and subsequent flow cytometry measurement of hypodiploid nuclei. Data shown are mean of triplicates ± SD. (C) Jurkat caspase-9 deficient cells reconstituted with caspase-9 wt (C9 rec), pMSCV control vector (C9 def), or caspase-9 ΔCARD mutant (C9 ΔCARD), were left untreated (Med) or were treated with 25 µg/ml mitomycin C (Mito), 40 ng/ml TRAIL, 2.5 µM staurosporine (STS), or 2.5 µM staurosporine co-treated with 10 µM Q-VD-OPh (STS + QVD). Mitomycin C treatment was assessed for 10 h; TRAIL, STS, and QVD for 4 h. Cleared cell lysates were prepared and analyzed for caspase-9 (CASP9), caspase-3 (CASP3, CASP3 processed), PARP, or HSP90 by SDS-PAGE and immunoblotting.

5.1.2 Catalytic activity of caspase-9 is indispensable for staurosporine induced apoptosis

Since the catalytic activity of caspase-9 is crucial for APAF1 dependent apoptosis induced by anticancer drugs, the importance of caspase-9 catalytic activity was further characterized

upon staurosporine treatment. Thus, caspase-9 deficient Jurkat cells were reconstituted with a catalytic inactive mutant of caspase-9 (C287S).

Likewise to the Jurkat caspase-9 ΔCARD results, treatment with staurosporine or mitomycin C of caspase-9 deficient and catalytic inactive caspase-9 Jurkat cells did not induce apoptosis and processing of caspase-3 and PARP, whereas apoptosis induction was possible in cells positive for caspase-9. In contrast, as a control for the extrinsic apoptosis pathway, TRAIL was proficient to induce apoptosis in all tested cell lines. Addition of the broad-range caspase inhibitor Q-VD-OPh completely blocked apoptosis induction by staurosporine and processing of caspase-3, -9 and PARP in caspase—9 wt Jurkat cells (C9 rec) (**Figure 5-2, A, B**). Moreover, TRAIL was able to induce the cleavage of catalytic inactive caspase-9 via activation of caspase-3 (p37 fragment of caspase-9). However, the p35 auto-processed form of caspase-9 could not be detected (**Figure 5-2, B**).These results suggest that the catalytic activity is indispensable for staurosporine induced apoptosis.

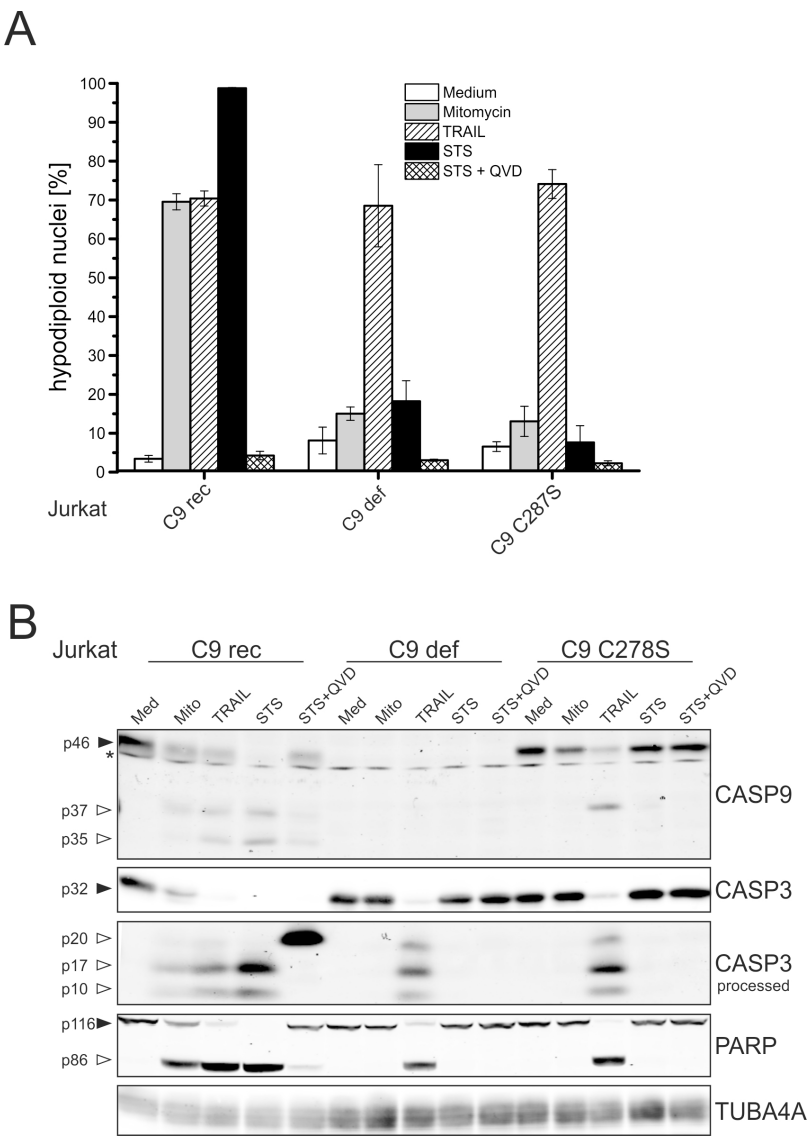

Figure 5-2: Catalytic activity of caspase-9 is indispensable for staurosporine induced apoptosis. (A) Jurkat caspase-9 deficient cells reconstituted with caspase-9 wt (C9 rec), pMSCV control vector (C9 def), or caspase-9 C287S mutant (C9 C287S) were treated for 24 h with 25 µg/ml mitomycin C (control inducing the intrinsic apoptosis pathway), 40 ng/ml TRAIL (control inducing the extrinsic apoptosis pathway), 2.5 µM staurosporine (STS), 2.5 µM staurosporine co-treated with 10 µM Q-VD-OPh (STS + QVD), a broad-range caspase inhibitor, or left untreated (Medium). Apoptosis was analyzed by propidium iodide staining of nuclei and subsequent flow cytometry measurement of hypodiploid nuclei. Data shown are mean of triplicates ± SD. (B) Cells described in (A) were left untreated (Med) or were treated with 25 µg/ml mitomycin C (Mito), 40 ng/ml TRAIL, 2.5 µM staurosporine (STS), or 2.5 µM staurosporine co-treated with 10 µM Q-VD-OPh (STS + QVD). Mitomycin C incubation was assessed for 10 h; TRAIL, STS, and QVD for 4 h. Cleared cell lysates were prepared and analyzed for caspase-9 (CASP9), caspase-3 (CASP3, CASP3 processed), PARP, or alpha-tubulin (TUB4A) by SDS-PAGE and immunoblotting.

5.1.3 Staurosporine induced apoptosis is independent of cathepsins, calpains, or caspase-4

It has previously been reported that caspase-9 is possibly processed by alternative cellular proteases such as cathepsins or calpains (Bitzer et al., 2002). Furthermore, López-Antón et al. discuss the processing and activation of caspase-9 by caspase-4 (Lopez-Anton et al., 2006).

Hence, apoptosis in caspase-9 positive Jurkat cells was induced with staurosporine and co-treated with diverse inhibitors of calpain (calpeptin), cathepsin (cathepsin inhibitor III, pepstatin A), or caspase-4 (z-LEVD-fmk) as well as with the broad-range caspase inhibitor Q-VD-OPh as positive control. Co-treatment with cathepsin inhibitor III, pepstatin A, calpeptin, and z-LEVD-fmk did not hamper staurosporine-induced apoptosis (**Figure 5-3, A, B**), which indicates that no other proteases than caspases are involved in STS-induced apoptosis and activation of caspase-9 is independent of cathepsins, calpains, and caspase-4.

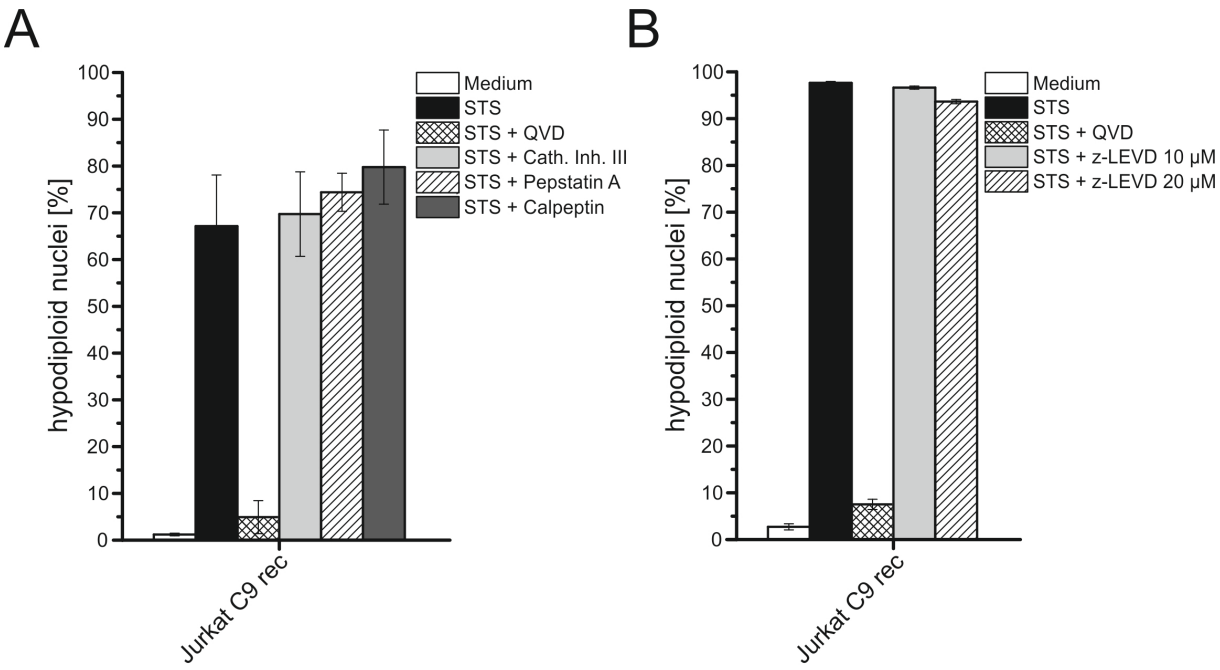

Figure 5-3: Staurosporine induced apoptosis is not affected by inhibition of cathepsins, calpains, or caspase-4. (A) Jurkat caspase-9 deficient cells reconstituted with caspase-9 wt (C9 rec) were left untreated (Medium), were treated with 1.25 µM staurosporine (STS), or were treated with 1.25 µM staurosporine (STS) co-treated with 10 µM Q-VD-OPh (STS + QVD), 10 µM cathepsin inhibitor III (Cath. Inh. III, inhibiting *inter alia* cathepsin B, -L, -S), 10 µM pepstatin A (inhibiting *inter alia* cathepsin D), or 10 µM calpeptin (inhibiting µ-calpains and m-calpains) for 24 h. Apoptosis was analyzed by propidium iodide staining of nuclei and subsequent flow cytometry measurement of hypodiploid nuclei. Data shown are mean of triplicates ± SD. The nicoletti assay was performed by Quynh Nguyen (B) Jurkat caspase-9 deficient cells reconstituted with caspase-9 wt (C9 rec) were left untreated (Medium), were treated with 2.5 µM staurosporine (STS), or were treated with 2.5 µM staurosporine (STS) co-treated with 10 µM Q-VD-OPh (STS + QVD), 10 µM z-LEVD-fmk (inhibiting caspase-4), or 20 µM z-LEVD-fmk. Apoptosis was analyzed as described in (A).

5.1.4 Staurosporine induces apoptosis in caspase-9 CARD R56A mutant but not R13A mutant Jurkat cells

Former studies demonstrated that staurosporine can activate caspase-9 in an apoptosome independent manner (Nagasaka et al., 2010; Manns et al., 2011). Since the CARD of caspase-9 is crucial for STS-induced apoptosis, it appears likely that alternative CARD to CARD interactions function as activation platforms for caspase-9.

First, the interaction between caspase-9 and APAF1 and their impact on staurosporine-induced apoptosis was further characterized. Therefore, caspase-9 deficient Jurkat cells were reconstituted with caspase-9 R13A and R56A CARD mutants, which are unable to interact with the CARD of APAF1 (Qin et al., 1999).

Both mutants were confirmed as not capable of binding APAF1 (**Figure 5-4, A**). Interestingly, while anticancer-drug treatment with mitomycin C could not induce caspase-3 activity in both newly generated cell lines, staurosporine was capable of inducing caspase-3 activity in caspase-9 R56A CARD mutant Jurkat cell, but with delayed kinetics as compared to caspase-9 wt Jurkat cells reaching the highest caspase-3 activity at 6 hours compared to 2 hours. (**Figure 5-4, B**). Accordingly, STS-induced apoptosis and processing of caspases and PARP was abrogated in caspase-9 R13A Jurkat cells, whereas still inducible in caspase-9 R56A Jurkat cells. Compared to caspase-9 positive cells, STS-induced apoptosis and caspase and PARP processing was less potent in caspase-9 R56A Jurkat cells. Anticancer drug treatment with mitomycin C was not capable of inducing apoptosis and processing of caspases and PARP in both mutant cell lines, yet the control for inducing death receptor associated apoptosis TRAIL was capable to induce apoptosis in all tested cell lines. Again, addition of QVD completely blocked apoptosis induction by staurosporine and processing of caspase-3, -9 and PARP (**Figure 5-4, C, D**). Thus, these data indicate that the caspase-9 R56A mutant Jurkat cells are potent to induce solely the alternative intrinsic apoptosis pathway by STS, whereas the caspase-9 R13A mutant cells are not capable. This would explain the reduced apoptosis rate of caspase-9 R56A compared to caspase-9 wt Jurkat cells as well the delayed caspase-3 activity. The APAF1 independent pathway is decelerated and less potent compared to APAF1 dependent pathways, which are both induced by STS, but the induction of apoptosis is still inducible in caspase-9 R56A Jurkat cells in which caspase-9 is insufficient to bind APAF1. Collectively, these results underline the dual mode of staurosporine induced apoptosis induction.

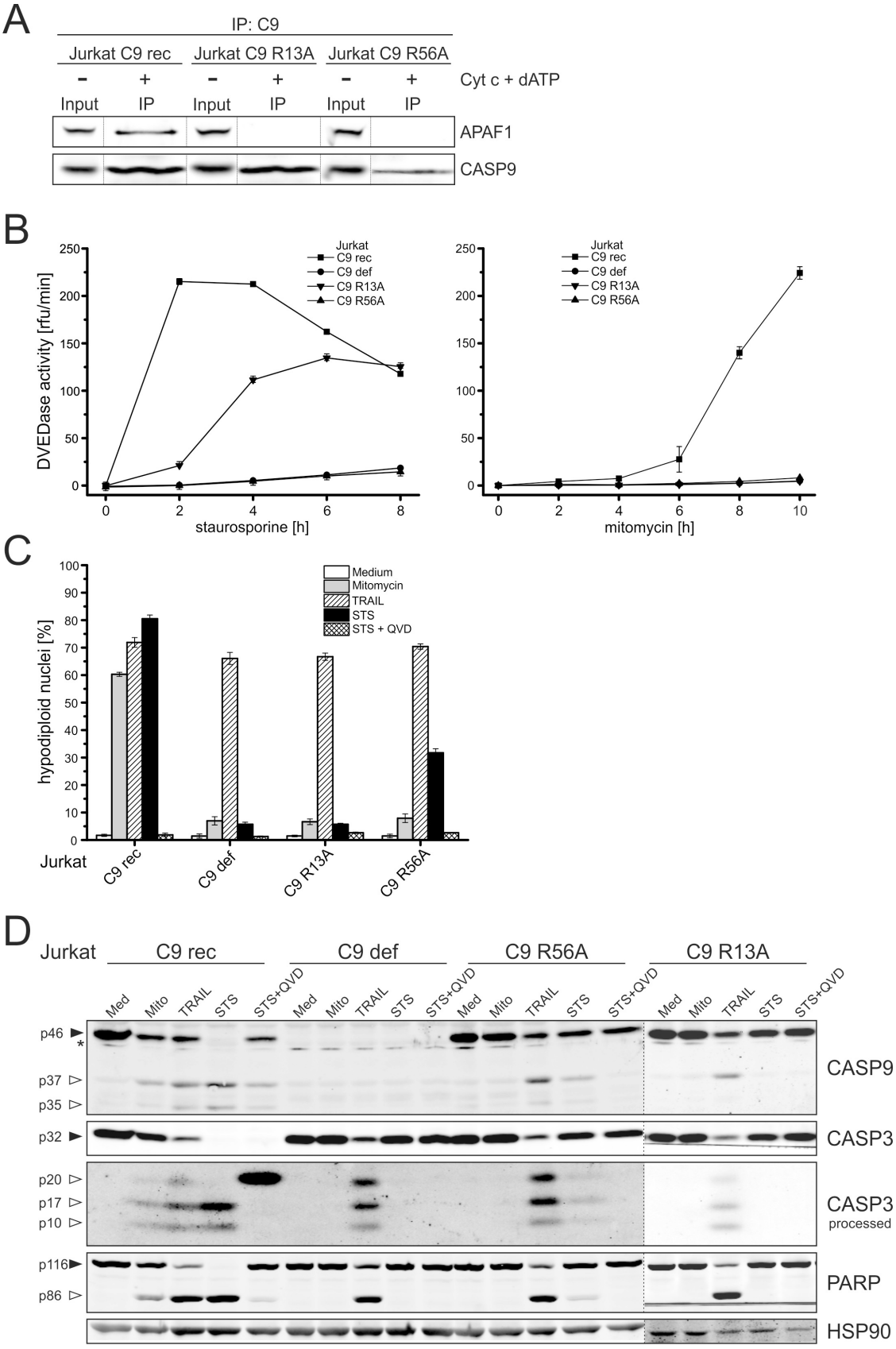

Figure 5-4: Apoptosis by staurosporine can be induced in caspase-9 CARD R56A mutant but not R13A mutant cells which are both deficient for APAF1 binding. (A) After induction of *in vitro* apoptosome formation with 8.6 µM cytochrome c (Cyt c) and 2.4 mM dATP in cleared cell lysates of Jurkat caspase-9 deficient cells reconstituted with caspase-9 wt (C9 rec), caspase-9 R13A mutant (C9 R13A), or caspase-9 R56A mutant (C9 R56A), immunopurification of caspase-9 was assessed. Cleared cell lysates as control (Input) and immunopurified caspase-9 was subjected to SDS-PAGE and immunoblotting of

caspase-9 and APAF1 was carried out. (B) Jurkat caspase-9 deficient cells reconstituted with caspase-9 wt (C9 rec), pMSCV vector control (C9 def), caspase-9 R13A mutant (C9 R13A), or caspase-9 R56A mutant (C9 R56A) were treated with either 2.5 µM staurosporine for up to 8 h, or 25 µg/ml mitomycin C for up to 10 h. DEVDase activity was assessed by cleavage of Ac-DEVD-AMC and is given in relative fluorescence unit per minute (rfu). Fluorescence (Ex 360 nm, Em 450 nm) was measured at 37 °C over the course of 120 min. The slope of the linear range of the fluorescence curves was considered as correlating to DEVDase activity. Data shown are mean of triplicates ± SD. (C) Cells described in (B) were treated for 24 h with 25 µg/ml mitomycin C, 40 ng/ml TRAIL, 2.5 µM staurosporine (STS), 2.5 µM staurosporine co-incubated with 10 µM Q-VD-OPh (STS + QVD), or left untreated (Medium). Apoptosis was analyzed by propidium iodide staining of nuclei and subsequent flow cytometry measurement of hypodiploid nuclei. Data shown are mean of triplicates ±SD. (D) Cells described in (B) were left untreated (Med) or were treated with 25 µg/ml mitomycin C (Mito), 40 ng/ml TRAIL, 2.5 µM staurosporine (STS), or 2.5 µM staurosporine co-treated with 10 µM Q-VD-OPh (STS + QVD). Mitomycin C incubation was assessed for 10 h; TRAIL, STS, and QVD for 4 h. Cleared cell lysates were prepared and analyzed for caspase-9 (CASP9), caspase-3 (CASP3, CASP3 processed), PARP, or HSP90 by SDS-PAGE and immunoblotting.

5.1.5 C-terminal GFP tag at caspase-9 does not impair staurosporine induced apoptosis

Previously we demonstrated that a tag at the N-terminus of caspase-9 derogates its normal functions. A tag linked to the CARD region of caspase-9 obstructs the binding of APAF1. Accordingly, induction of apoptosis by mitomycin C was blocked (Manns et al., 2011). On this account, caspase-9 was tagged at the C-terminus for further analysis of caspase-9 interaction under the influence of staurosporine and the activity of tagged caspase-9 was validated. Therefore, caspase-9 deficient Jurkat cells were reconstituted with C-terminal GFP tagged caspase-9 wt (C9-GFP), catalytically inactive C9-GFP (C9-GFP C287S), R13A and R56A CARD mutants (C9-GFP R13A/R56A), and double mutants of catalytically inactive and APAF-1 binding deficient C9-GFP (C9-GFP R13A/R56A C287S).

STS-induced apoptosis and processing of caspase-3 of C-terminally GFP tagged caspase-9 was similar to untagged caspase-9. Regarding apoptosis induction by staurosporine, mitomycin C, or TRAIL, caspase and PARP processing of all GFP-tagged caspase-9 variants showed similar results compared to their untagged counterpart. Again, TRAIL was proficient to induce apoptosis in all tested cell lines, whereas mitomycin C induced apoptosis solely in caspase-9 wild type and caspase-9 C-terminal GFP tagged Jurkat cells and addition of QVD completely blocked apoptosis induction by staurosporine and processing of caspases and PARP (**Figure 5-5, A, B, C**). Hence, these data indicate that a tag at the C-terminus of caspase-9 has no influence on its activity and according to this on overall apoptosis. Taken together, with the help of GFP-tagged caspase-9 interaction studies are possible, since it phenocopies the untagged caspase-9.

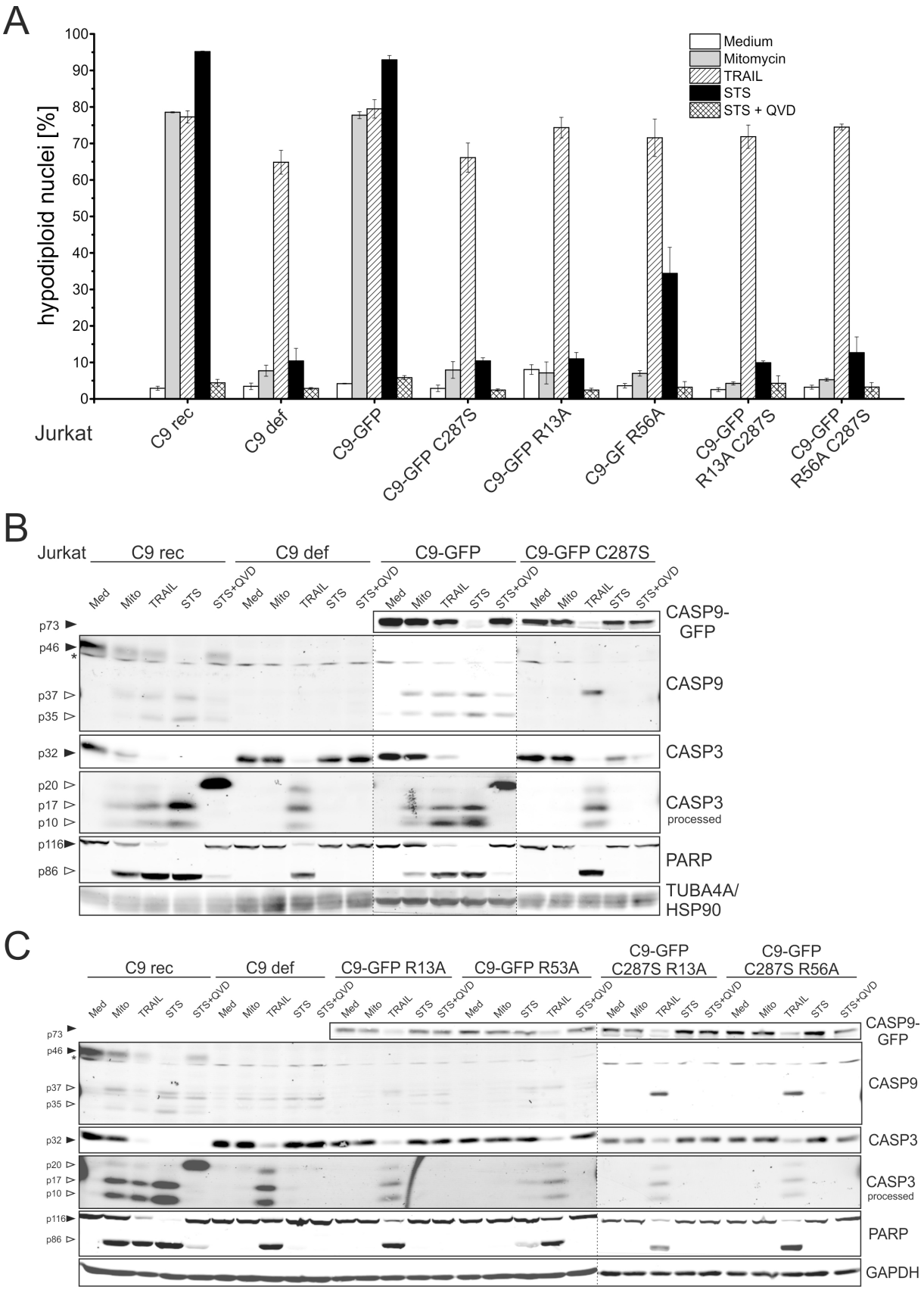

Figure 5-5: GFP tag at C-terminus of caspase-9 does not impair effects of staurosporine-induced apoptosis. (A) Caspase-9 deficient Jurkat cells reconstituted with caspase-9 wt (C9 rec), pMSCV vector control (C9 def), caspase-9 C-terminal tagged with GFP (C9-GFP), C9-GFP tagged C287S mutant (C9-GFP C287S), C9-GFP R13A mutant, C9-GFP R56A mutant, C9-GFP R13A C287S double mutant, or C9-GFP R56A C287S double mutant were treated for 24 h with 25 µg/ml mitomycin C, 40 ng/ml TRAIL, 2.5 µM staurosporine (STS), 2.5 µM staurosporine co-incubated with 10 µM Q-VD-OPh (STS + QVD), or left untreated

(Medium). Apoptosis was assessed by propidium iodide staining of nuclei and subsequent flow cytometry measurement of hypodiploid nuclei. Data shown are mean of triplicates ±SD. (B, C) Cells described in A were left untreated (Med) or were treated with 25 µg/ml mitomycin C (Mito), 40 ng/ml TRAIL, 2.5 µM staurosporine (STS), or 2.5 µM staurosporine co-treated with 10 µM Q-VD-OPh (STS + QVD). Mitomycin C incubation was assessed for 10 h; TRAIL, STS, and QVD for 4 h. Cleared cell lysates were prepared and analyzed for caspase-9 (CASP9), caspase-3 (CASP3, CASP3 processed), PARP, HSP90, alpha-tubulin (TUBA4A), or GAPDH by SDS-PAGE and immunoblotting.

5.1.6 Staurosporine does not alter the phosphorylation status of caspase-9

Previously, it has been reported that caspase-9 is phosphorylated at multiple, mainly inhibitory sites by various protein kinases such as AKT, ERK1/2, CDK1/cyclin B1, PKA, and CK2, which are activated in response to extracellular growth ⁄ survival factors, osmotic stress, or during mitosis (Allan & Clarke, 2009). Since staurosporine is a broad-range kinase inhibitor inhibiting these putative kinases, the phosphorylation status of caspase-9 was investigated under STS-induced apoptosis conditions. The caspase-9 phosphorylation status was analyzed in Jurkat cells expressing caspase-9-GFP by mass spectrometric and 2D-gel fluorescence difference gel electrophoresis (DIGE) analysis carried out by Dr. Anja Stefanski (Molecular Proteomics Laboratory, BMFZ, University of Düsseldorf, Germany). With the help of the DIGE system, up to three different protein samples can be labelled for two-dimensional electrophoresis analysis.

First, during mass spectrometric analysis, a caspase-9 sequence coverage of 69.03% under untreated conditions and 62.98% under staurosporine conditions could be achieved. The peptide KPEVLRPE**T**PRPVDIGSGGFGDVGALESLR was identified as putative phospho-peptide under medium and STS conditions with an ionscore for T125 phosphorylation of 48 and 63, respectively. No significant change in the phosphorylation status under staurosporine-induced apoptosis conditions was detected (**Figure 5-6, A**). For further validation of these data, a 2D-gel analysis was performed. Therefore caspase-9 was immunopurified from Jurkat cells treated with staurosporine or left untreated. Additionally, caspase-9 was immunopurified and treated with lamba phosphatase, which has the ability to dephosphorylate proteins. Those three protein samples were stained with different fluorescent dyes, i.e. Cy2, Cy3, and Cy5, respectively. With 2D-gel analysis it is possible to detect changes in the phosphorylation status of proteins due to the altered isoelectric point. After the 2D-gel electrophoresis the three different fluorescent dyes were detected and the gel was immunoblotted afterwards in order to identify caspase-9. Caspase-9 was detected by immunoblotting in at last three distinct spots (upper panel, right picture). Those spots could also similarly be detected via detection of the fluorescent dyes labelled immunopurified caspase-9 under medium and staurosporine conditions, and upon lambda phosphatase treatment (upper panel left and center picture, lower panel), suggesting that

there was no alteration in caspase-9 proteoforms during treatment with STS (**Figure 5-6, B**). Collectively, these results suggest that the phosphorylation status of caspase-9 is not altered during STS-induced apoptosis.

A

Mass spectrometric PTM analysis of GFP-Caspase-9					
Condition	**Sequence coverage**	**Peptide**	**#PSMs**	**Modification**	**Ionscore**
Med	69.03%	KPEVLRPE**T**PRPVDIGSGGFGDVGALESLR	5	T9(Phospho)	48
STS	62.98%	KPEVLRPE**T**PRPVDIGSGGFGDVGALESLR	7	T9(Phospho)	63

B

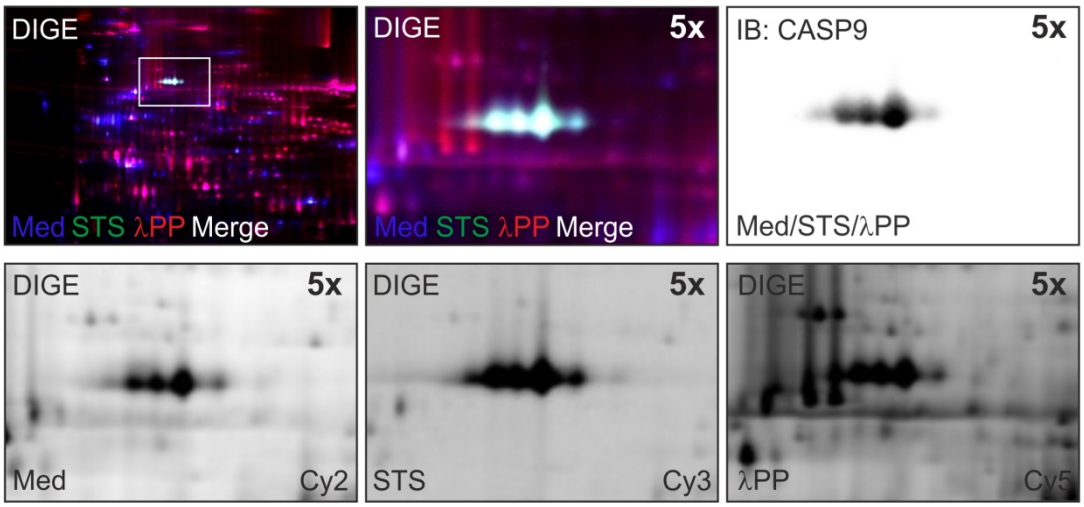

Figure 5-6: Staurosporine does not alter the phosphorylation status of caspase-9. (A) Caspase-9 was immunopurified from caspase-9-GFP C287S Jurkat cells treated with 2.5 µM staurosporine (STS) for 2 h or left untreated (Medium, Med). Immunopurified caspase-9 was analyzed by mass spectrometry. For protein and peptide identification raw files were further processed using the Thermo Proteome Discoverer 1.3 software (Thermo Scientific). Within the software suite, database searches were carried out using the mascot algorithm (Perkins et al., 1999) searching the Swiss-Prot database (24.09.2012; 536789 sequences) considering variable phosphorylation at S, T, and Y. Results were filtered based on peptide confidence threshold ≤ 0.01 and Mascot Ionscore ≥ 20. (B) Caspase-9 was immunopurified from Jurkat caspase-9-GFP C287S cells treated with 2.5 µM staurosporine for 2 h or left untreated (Medium). Additionally, Caspase-9 was immunopurified from untreated cells lysed without phosphatase inhibitors (e.g. Na_3VO_4, NaF, NaPP) and treated with lambda phosphatase (λPP). Immunopurified caspase-9 was incubated in minimal buffer (30 mM Tris/HCl, pH 8.5; 7.0 M Urea, 2.0 M Thiourea, 4% CHAPS), stained with the fluorescent dyes Cy2, Cy3, or Cy5, respectivley and analyzed via 2D-gel electrophoresis and immunoblotting against caspase-9 (CASP9). Cy2 (Med), Cy3 (STS), or Cy5 (λPP) were displayed in blue, green, or red, respectivley in the merged picture. 5 times zoomed in pictures on the CASP9 spots were displayed.

5.1.7 Caspase-9 interactome analysis

Since initiator caspases are activated in macromolecular complexes and caspase-9 can obviously be activated without influence of the apoptosome, it was speculated that caspase-9 interaction partners besides APAF1 could activate the intrinsic apoptosis route independent of the canonical mitochondrial cytochrome c/APAF1 pathway.

Thus, for analyzing putative changes of APAF1, caspase-9, and caspase-3 distribution by molecular weight-depending separation that could indicate the formation of a

macromolecular complex, caspase-9 gel filtration studies were carried out with immunopurified caspase-9-GFP from Jurkat cells treated with or without STS. No significant changes in the absorbance spectra of proteins at 488 nm (blue line) comparing medium and STS treated samples were detected. Interestingly, in contrast to the protein absorbance spectra, the GFP absorbance spectra (red line) visualized a difference between medium and STS treated samples (highlighted with arrow) (**Figure 5-7, A**). This could be a hint for a high molecular caspase-9 activation platform. Unfortunately, no shift of caspase-9 (STS versus medium) into a higher or lower molecular weight complex was observed by immunoblotting of various size exclusion fractions. Also, there was no high molecular complex beyond 2.000 kDa observed (**Figure 5-7, B**).

For analyzing putative caspase-9 interaction partners, which are relevant for caspase-9 activation during the novel intrinsic apoptosis pathways, mass spectrometric analysis were performed of immunopurified caspase-9 wt and R13A/R56A CARD mutants and GFP-only as control under medium and STS conditions. Proteins interacting with GFP-only were excluded. The table in **Figure 5-7**, **C** only comprises proteins, which are differentially enriched under medium (positive *t*-test difference) or under STS conditions (negative *t*-test conditions). Of note, staurosporine induces apoptosis in different ways depending on the expressed caspase-9 variant. In caspase-9 wt expressing cells, STS induces apoptosis in a dual mode, activating the classical mitochondrial apoptosis pathway and an alternative pathway next to the apoptosome. In caspase-9 R56A mutant expressing cells, the activation of the mitochondrial apoptosis pathway is inhibited by mutation of the CARD to CARD interaction of caspase-9 and APAF-1. In those cells solely the apoptosome-independent pathway is activated. Caspase-9 R13A expressing cells are used as negative control, since apoptosis induction by STS is not possible in these cells. Therefore, proteins interacting with the R13A caspase-9 mutant under STS conditions are not relevant for caspase-9 activation. Nevertheless, those proteins were not identified anyways (no negative *t*-test difference).As to be expected in caspase-9 wt expressing cells, APAF1 was identified as caspase-9-interacting protein under STS conditions (*t*-test difference -6.26). In contrast, APAF1 was not detected in R13A and R56A caspase-9 mutant samples, which can be explained by the inability of these mutants to bind APAF1. The caspase-9 R56A interacting proteins comprised only two proteins with increased binding to caspase-9 under STS conditions, i.e. the gamma-glutamyl hydrolase (GGH, *t*-test difference -2.04) and BCL2-associated athanogene 2 (BAG2, *t*-test difference -1.15) (**Figure 5-7, C**). Taken together, the formation of a macromolecular complex upon STS treatment could not be detected under these circumstances. Nevertheless, these results provide indications for an alternative activation platform of caspase-9, and BAG2 as an interaction partner of caspase-9 increasingly associated under

STS-induced apoptosis conditions and potentially essential for activation of caspase-9 independently of APAF1 and apoptosome formation.

A

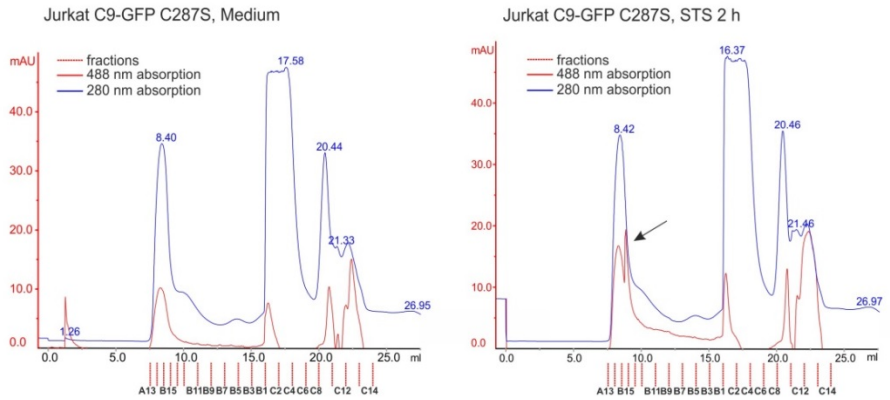

B

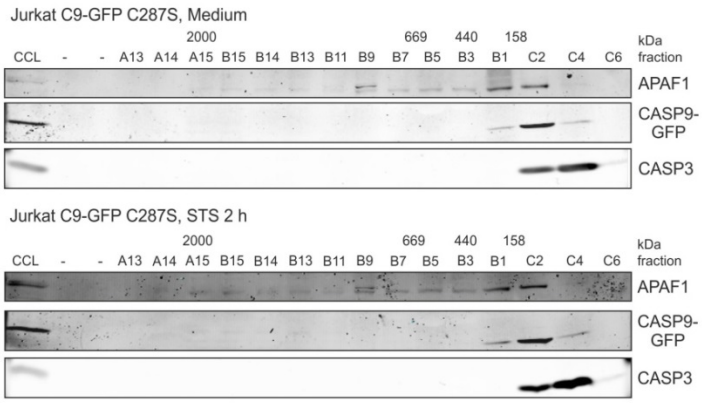

C

Caspase-9 interacting proteins differential enriched under medium (positive value) and STS (negative value) conditions					
C9 WT		**C9 R13A**		**C9 R56A**	
t-test difference	**gene names**	**t-test difference**	**gene names**	**t-test difference**	**gene names**
-0,96095	POLR2B	3,37285	TPD52L2	3,3915	POLDIP3
1,01915	TUBB6	3,60843	KIAA1967	1,87305	VPS26B
3,37915	POLDIP3	2,01473	VPS26B	-1,14565	BAG2
-6,25858	APAF1	0,6798	TCP1	1,02602	IDH3A
2,3505	MAPRE1	3,48203	EIF4A2	1,97608	NUP54
1,9599	ETFB	3,05015	TPD52	2,8643	KIAA1967
3,39022	KIAA1967	3,1767	POLDIP3	3,38303	PYCRL
0,91045	CNOT1	0,818726	CCT2	0,705625	SEH1L
1,8929	TPD52L2	0,529175	HSPA9	-2,03655	GGH
-1,83235	MATR3	1,31335	RIC8A		
-0,577125	RLTPR	1,11897	SEPT1		
-1,62875	DCAF7	0,5754	CCT5		
-1,66345	KIF2A	0,81575	CCT4		
		1,8224	USO1		
		0,920775	CCT6A		
		0,7591	FERMT3		

Figure 5-7: Caspase-9 interaction studies. (A) Jurkat caspase-9-GFP C287S cells treated with 2.5 µM staurosporine for 2 h or left untreated (Medium) were lysed and the CCL analyzed via gel filtration with a superose 6 column. Displayed are absorbance spectra at 280 nm and 488 nm for protein and GFP signal, respectively. (B) The gel filtration fractions from C6 to A13 described in A and CCL as control were analyzed via SDS-PAGE and immunoblotting of APAF1, CASP9 (caspase-9), and CASP3 (caspase-3). (C) Jurkat caspase-9 deficient cells were reconstituted with caspase-9-GFP C287S (C9 WT), caspase-9-GFP R13A C287S (C9 R13A), caspase-9-GFP R56A C287S (C9 R56A), or GFP as negative control. Caspase-9 was immunopurified in the presence and absence of 2 µM staurosporine for 5 h and subjected to mass spectrometric analysis. For protein and peptide identification and quantification raw files were further processed using the MaxQuant software suite version 1.5.0.15 (Max Planck Institute of Biochemistry, Planegg, Germany). Within the software suite database searches were carried out using human protein sequences from the UniProt/SwissProt database including the Trembl part (release 08.2014). To determine true-positive from false-positive binding a *t*-test value ≤ 0.05 was required. *T*-test differences were calculated based on *t*-tests $p < 0.05$ of four independent experiments.

5.2 Autophagy – Regulation of ULK1

In previous mass spectrometric analysis of ULK1-binding proteins, which were performed by Dr. Antje Löffler during her doctoral thesis, two ubiquitin-specific proteases (USPs) were identified, i.e. USP7/HAUSP and USP9X. First, based on these results, GFP-ULK1 interactions with USP7 and USP9X were confirmed and an *in vitro* kinase assay was performed in order to address the question whether USP7 or USP9X represent substrates of the ULK1 kinase and to validate the interaction of ULK1 and these deubiquitinases (DUBs). Next, the influence of DUB inhibition on ULK1 by applying DUB inhibitors, was analyzed, regarding ULK1 ubiquitination status, ULK1 activity, identification of putative ULK1 regulating DUBs, and the overall autophagic flux.

So far, little is known about regulatory post-translational modifications (PTMs) of ULK1 besides phosphorylation. We set our focus on ubiquitination. The aim of this part of the thesis was to characterize the regulation of ULK1 by this post-translational modification.

5.2.1 ULK1 interacts and phosphorylates USP7 and USP9X

Since USP7 and USP9X were identified as ULK1-binding proteins via mass spectrometry, this interaction was further analyzed in co-immunopurification studies. GFP-ULK1 immunopurification was carried out and indeed, USP7 and USP9X were identified as co-purified proteins, whereas the GFP control was negative for USP7 and USP9X (**Figure 5-8, A**). Next, the question was addressed whether ULK1 as a Ser/Thr kinase can phosphorylate USP7 and USP9X. Thus, an *in vitro* kinase assay was performed with GFP-ULK1 wt as kinase of interest and GFP-ULK1 kinase-dead (kd) as negative control that were both immunopurified from Flp-In™ T-REx™ 293 cells. Without substrate incubation strong autophosphorylation was detected by autoradiography in the GFP-ULK1 wt sample, whereas less strong in the GFP-ULK1 kd sample. The high level of GFP-ULK1 wt autophosphorylation would also explain the faster migration in SDS-PAGE compared to GFP-ULK1 kd. With regard to USP7 and USP9X as substrates, both were phosphorylated by GFP-ULK1 wt in contrast to GFP-ULK kd. ATG13 was used as positive control (**Figure 5-8, B**). Since USP7 and USP9X are both deubiquitinases, in the following two USP7 and USP9X DUB inhibitors were analyzed concerning their effect on ULK1 expression: HBX 41108, which inhibits USP7, and WP1130, which inhibits USP9X (Colland et al., 2009; Kapuria et al., 2010). Interestingly, whereas incubation of HEK293 cells with HBX 41108 did not show any effect on ULK1 levels in immunoblot, incubation with WP1130 resulted in decreased levels over time (**Figure 5-8, C**).

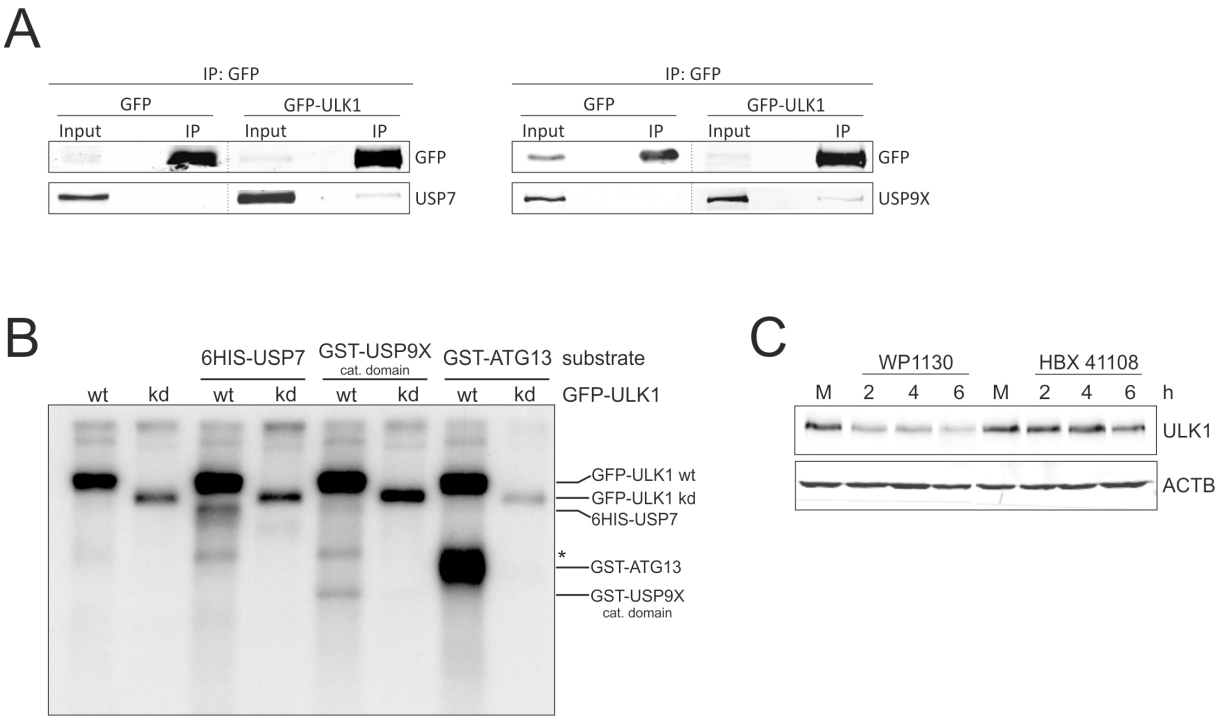

Figure 5-8: ULK1 interacts and phosphorylates USP7 and USP9X. (A) After induction of GFP or GFP-ULK1 expression with doxycycline (Dox) for 16 h, Flp-In™ T-REx™ 293 cells were lysed and GFP-immunopurification was performed. Purified GFP and GFP-ULK1 was analyzed by anti-GFP, anti-USP7, and anti-USP9X immunoblotting. (B) After induction of GFP-ULK1 wt or GFP-ULK1 kd expression with Dox for 16 h, Flp-In™ T-REx™ 293 cells were lysed and GFP-immunopurification was performed. For *in vitro* kinase assay, purified GFP-ULK1 wt or GFP-ULK1 kd was incubated with 1 µg His-USP7, GST-USP9X (catalytic domain), or GST-ATG13 (affinity purified by Dr. Antje Löffler). As negative controls, GFP-ULK1 wt and GFP-ULK1 kd were incubated alone. After SDS-PAGE, autoradiography was performed. Asterisks indicate unspecific background band. (C) HEK293 cells were treated for indicated times with 5 µM WP1130, 10 µM HBX41108, or left untreated (M). Cleared cell lysates/detergent-soluble fractions were subjected to SDS-PAGE followed by immunoblotting of ULK1 and β-actin (ACTB).

5.2.2 WP1130 reduces ULK1 in detergent-soluble fraction independent of proteolytic, proteasomal, and autophagic degradation

Since DUB inhibition can induce K48-linked ubiquitination and subsequent degradation by the proteasome, it was speculated that ULK1 could be degraded by the proteasome system. Accordingly, the effect of two potent proteasome inhibitors was analyzed in how fare they might neutralize the effect of WP1130.

However, treatment with proteasome inhibitors MG132 or bortezomib did not abolish WP1130-induced reduction of ULK1, indicating that the deubiquitinase inhibitor WP1130 reduces ULK1 levels independent of the proteasome system (**Figure 5-9, A**). Furthermore, this effect could not be reversed by co-incubation with various other protease inhibitors, i.e. Q-VD-OPh (QVD, inhibiting caspases), cathepsin inhibitor III (Cath. Inh. III, inhibiting cathepsin B, -L, -S, and papain), pepstatin A (inhibiting cathepsin D), calpeptin (inhibiting µ-calpains and m-calpains), or with bafilomycin A_1, which prevents autophagic degradation through raising the lysosomal pH by blocking the lysosomal proton pump (**Figure 5-9, B**)

(Fass et al., 2006). Taken together, reduced levels of ULK1 after treatment with WP1130 are most likely not initiated by proteolytic, proteasomal, or autophagic degradation processes.

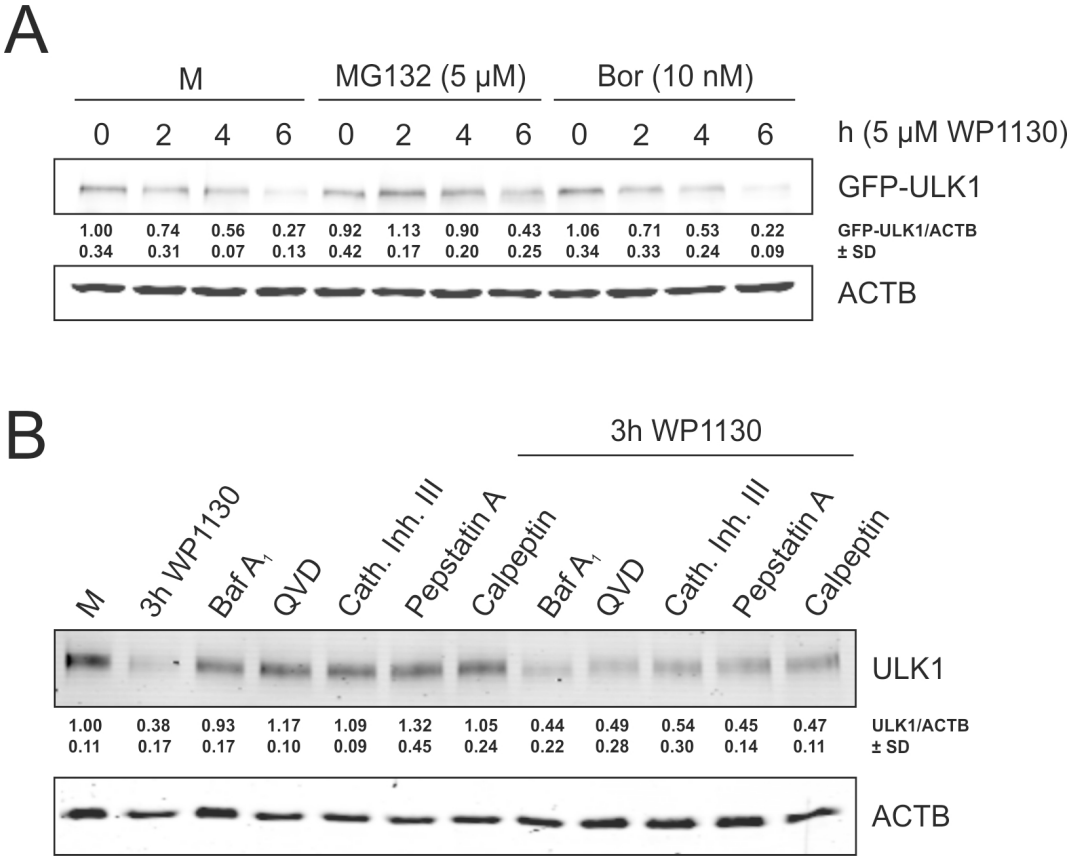

Figure 5-9: WP1130 reduces ULK1 in detergent-soluble fraction independent of degradation through proteasome and autophagosome as well as proteolytic cleavage. (A) After induction of GFP-ULK1 expression with doxycycline for 3 h, Flp-In™ T-REx™ 293 cells were incubated with full medium (M), 5 µM MG132, or 10 nM bortezomib (Bor). After 30 min, cells were either lysed directly (0) or 5 µM WP1130 was added for 2, 4 or 6 h. Subsequently, cells were lysed and cleared cell lysates were separated by SDS-PAGE and analyzed by immunoblotting using antibodies against ULK1 and ACTB/β-actin. (B) HEK293 cells were treated with 10 nM bafilomycin A_1 (Baf A_1), 10 µM Q-VD-OPh (QVD), 10 µM cathepsin inhibitor III (Cath. Inh. III), 10 µM pepstatin A, or 10 µM calpeptin for 4 h in the absence or presence of 5 µM WP1130. Cleared cell lysates were analyzed by anti-ULK1 and anti-ACTB/β-actin immunoblotting. (A and B) Data shown are representative of at least three independent experiments. Fold changes were calculated by dividing each normalized ratio (protein to loading control) by the average of the ratios of the control lane (control lane: fold change = 1.00, n ≥ 3). Results are mean ± SD and are given below the corresponding blots.

5.2.3 WP1130 induces a reversible shift of ULK1 from detergent-soluble to -insoluble fraction

Another explanation for the reduction of ULK1 levels induced by WP1130 could be reduced detergent solubilization caused by aggregation. In order to test this hypothesis, the WP1130-dependent distribution of endogenous ULK1 and GFP-ULK1 in Triton X-100-soluble and -insoluble fractions was analyzed. Notably, WP1130 induced the redistribution of GFP-ULK1 from the soluble to the insoluble fraction, while GFP levels remained unaltered (**Figure 5-10, A**). Previously, it has been reported that overexpression of GFP-ULK1 leads to the formation of cytosolic GFP-positive puncta (Alemu et al., 2012). To exclude that the

aforementioned effect by WP1130 is just an artefact, the distribution of endogenous amounts of ULK1 in HEK293 cells was investigated. Again, WP1130 induced the redistribution of ULK1 from the soluble to the insoluble fraction, whereas the overall level of ULK1, as demonstrated by analysis of the whole cell lysate, remained unaltered (**Figure 5-10**, **B**). This effect could be confirmed by the analysis of ULK1 protein levels in two alternative cell lines, HeLa and U2OS cells (**Figure 5-10, C**). Next, it was analyzed if ULK1 redistribution is a reversible process. For that purpose, HEK293 cells were treated with WP1130 for 3 h, and subsequently the cells were resuspended in WP1130-free medium. We observed that levels of Triton X-100 soluble ULK1 increased again, and that in turn levels of the insoluble fraction decreased (**Figure 5-10, D**). Taken together, WP1130 treatment induces the redistribution of ULK1 levels of various human cell lines from the detergent-soluble fraction to the detergent-insoluble fraction in a reversible manner.

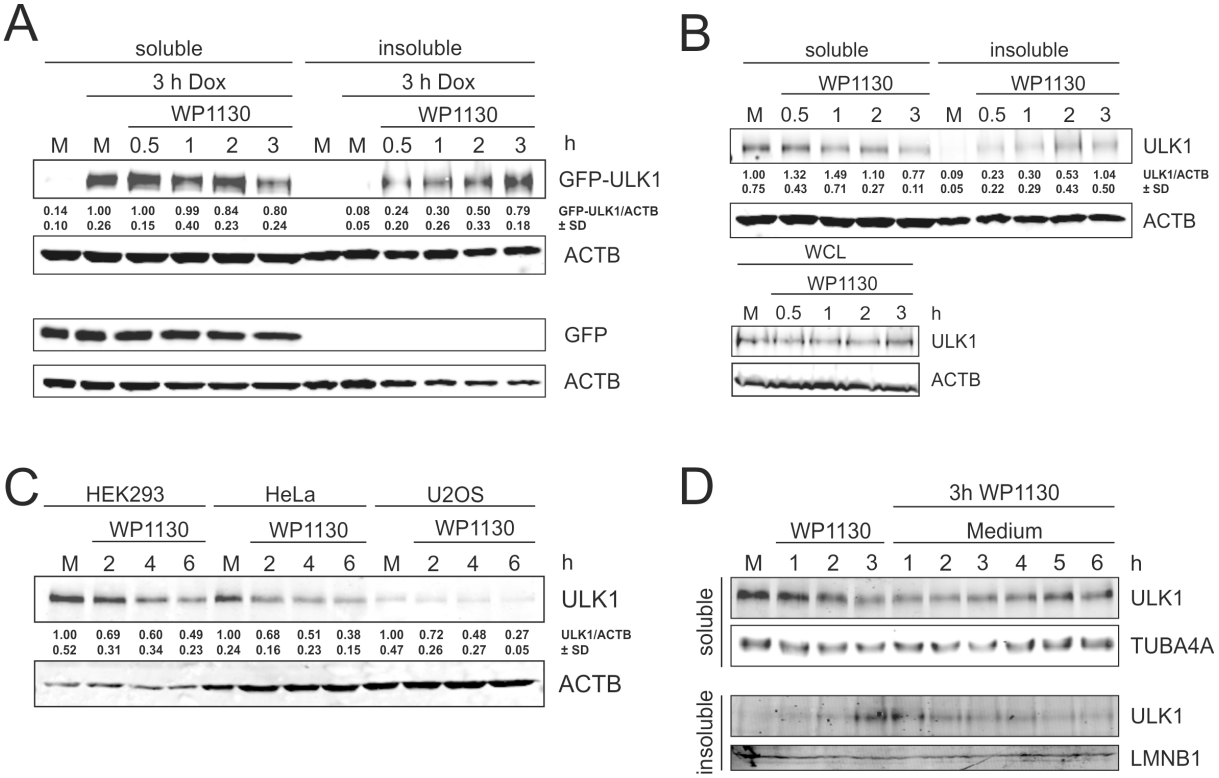

Figure 5-10: WP1130 induces a reversible shift of ULK1 from detergent-soluble to -insoluble-fraction. (A) After induction of GFP-ULK1 or GFP-only expression with doxycycline (Dox) for 3 h, Flp-In™ T-REx™ 293 cells were treated with 5 µM WP1130 for indicated intervals. Following WP1130 treatment, detergent-soluble and -insoluble fractions were prepared and analyzed for ULK1, GFP and β-actin (ACTB) levels by immunoblotting. (B) HEK293 cells were left untreated or were treated with 5 µM WP1130 for indicated times. Then detergent-soluble or -insoluble fractions or whole cell lysates (WCL) were prepared and subjected to anti-ULK1 and anti-ACTB/β-actin immunoblotting. (C) HEK293, HeLa, or U2OS cells were left untreated or were treated with 5 µM WP1130 for 2, 4, or 6 h. Cleared cell lysates/detergent-soluble fractions were subjected to anti-ULK1 and anti-ACTB/β-actin immunoblotting. (D) HEK293 cells were treated for 1, 2, or 3 h with 5 µM WP1130. Alternatively, cells were treated with WP1130 for 3 h, washed once with full medium and then incubated in full medium for 1 to 6 h. Detergent-soluble or -insoluble fractions were prepared and analyzed for ULK1, α-tubulin (TUBA4A), and lamin B1 (LMNB1) via immunoblotting. (A, B and C) Data shown are representative of at least three independent experiments. Fold changes were calculated by dividing each normalized ratio (protein to loading control) by the average of the ratios of the control lane (control lane: fold change = 1.00, n ≥ 3). Results are mean ± SD and are given below the corresponding blots.

5.2.4 WP1130 induces the aggregation of GFP-ULK1/2

Former studies reported that WP1130 induces the formation of perinuclear aggresomes (Kapuria et al., 2010). Accordingly, it was speculated that GFP-ULK1 might be transferred to aggresome-like structures upon WP1130 treatment. Thus, the effect of WP1130 treatment on the localization of GFP-ULK1 was analyzed by confocal microscopy.

The Incubation with WP1130 resulted in the recruitment of GFP-ULK1 to perinuclear punctate structures (**Figure 5-11, A**).This relocalization could also be noticed in experiments using GFP-ULK2 as well as for the kinase-dead variant of GFP-ULK1, which were recruited to aggresomes upon WP1130 treatment. The recruitment of GFP-ULK1 kd to aggresomes indicates that ULK1 activity was not required for the translocation of GFP-ULK1 to perinuclear punctate structures (**Figure 5-11, B**). Further analysis of GFP-ULK1 localization after WP1130 treatment with super-resolution structured illumination microscopy (SR-SIM) pointed out the formation of smaller GFP-ULK1 aggregates and one large aggresome formation within the cell (**Figure 5-11, C**).

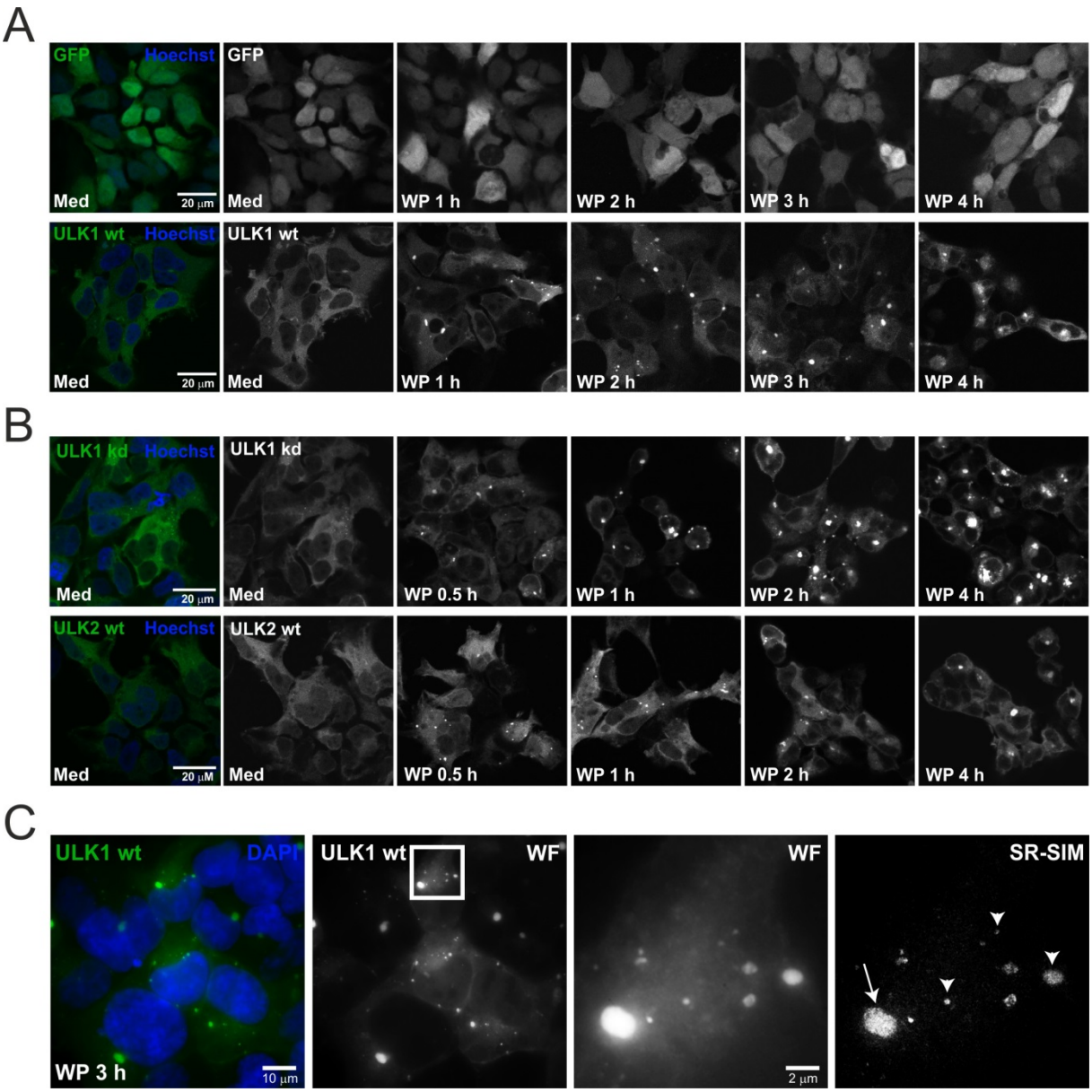

Figure 5-11: WP1130 induces the aggregation of GFP-ULK1 wt/kd and GFP-ULK2. (A) After induction of GFP (upper panels) or GFP-ULK1 (lower panels) expression with doxycycline (Dox) for 3 h, Flp-InTM T-RExTM 293 cells were incubated for indicated intervals with 5 µM WP1130 and were analyzed by confocal laser scanning microscopy. (B) After induction of GFP-ULK1 kd (upper panels) or GFP-ULK2 wt (lower panels) expression with Dox for 3 h, Flp-InTM T-RExTM 293 cells were incubated for indicated times with 5 µM WP1130 and were analyzed by confocal laser scanning microscopy. (C) After induction of GFP-ULK1 expression with Dox for 16 h, Flp InTM T-RExTM 293 cells were treated for 3 h with 5 µM WP1130 and analyzed by widefield (WF) and super-resolution structured illumination microscopy (SR-SIM) displayed as maximum intensity projections. Examples for small GFP-ULK1 aggregates are indicated by white arrowheads, the aggresome is indicated by a white arrow. (A, B, and C) The GFP signal is displayed in green, Hoechst/DAPI in blue in the merged images. For high-contrast pictures, The GFP signal is displayed in greyscale.

5.2.5 Characterization of WP1130 induced aggregate and aggresome structures

For further characterization of WP1130 induced ULK1 aggregation, the distribution GFP-ULK1 was monitored by live cell imaging (**Figure 5-12, A-C**). It could be demonstrated that small GFP-ULK1 aggregates were already formed upon induction of GFP-ULK1 expression

(**Figure 5-12, A**). However, formation of these small peripheral aggregates was considerably enhanced through WP1130 treatment (**Figure 5-12, A)**. In addition, WP1130 induced the translocation of these smaller aggregates to the perinuclear aggresome (**Figure 5-12, A**). Previous studies reported that interference with microtubule polymerisation inhibits aggresome formation (Johnston et al., 1998). Indeed, co-treatment of cells with WP1130 and nocodazole abrogated aggresome formation and led to the formation of GFP-ULK1 aggregates, which are distributed throughout the cell (**Figure 5-12, A**). Furthermore, it has been shown that different proteins are involved in the formation of protein aggregates and the aggresome, e.g. p62/SQSTM1, a polyubiquitin-binding protein, and different ubiquitin-linkages, such as K48- and K63-linked ubiquitin chains (Johnston et al., 1998; Taylor et al., 2003; Pankiv et al., 2007; Kapuria et al., 2010). In fact, WP1130-induced aggresome structures comprised ubiquitin – including K63-linked ubiquitin – and, to a minor extent p62/SQSTM1 (**Figure 5-12, B**). Collectively, these results demonstrated that WP1130 induces the formation of ULK1 aggregates and their transport to the detergent-insoluble aggresome comprising ubiquitin, K63-linked ubiquitin and to a minor extent p62.

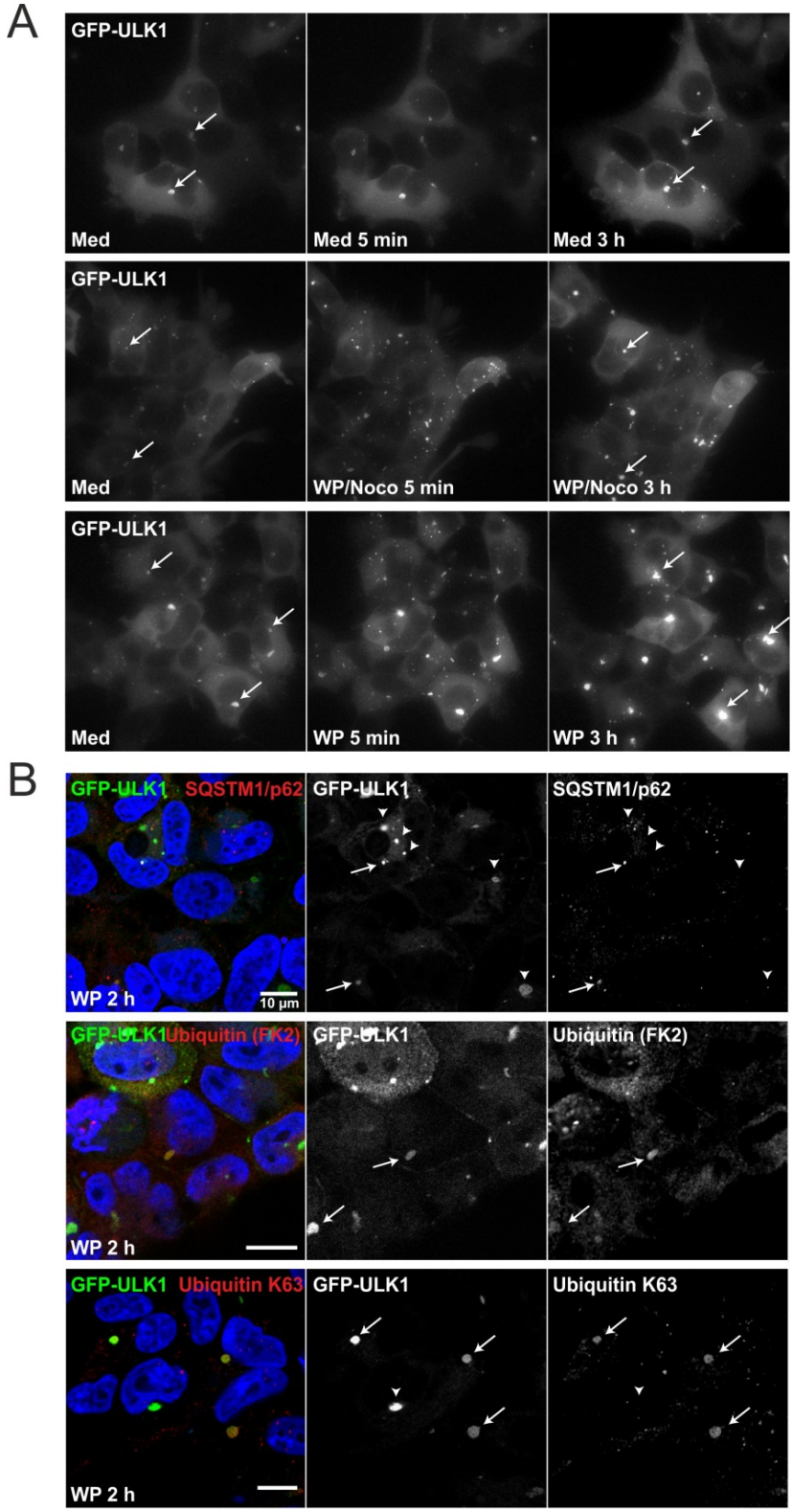

Figure 5-12: Characterization of WP1130 induced aggregate and aggresome structures. (A) After induction of GFP-ULK1 expression with Dox for 3 h, Flp-In™ T-REx™ cells were treated with 5 µM WP1130 with and without 10 µM nocodazole (Noco) over a time period of 4 h. GFP-ULK1 was visualized by live-cell-imaging. Displayed are still-pictures before treatment (Med), 5 min and accordingly 3 h after indicated treatments. For comparison, aggresome structures are indicated by white arrows. (B) After induction of GFP-ULK1 expression with doxycycline (Dox) for 3 h, Flp-In™ T-REx™ 293 were treated with 5 µM WP1130 for 2 h, immunostained for p62, mono/poly-ubiquitin (FK2), and K63-linked ubiquitin; and analyzed by confocal laser scanning microscopy. The GFP-ULK1 signal is displayed in green, the Hoechst signal in blue, and the signals for the immunostained proteins in red in the merged images. Colocalized proteins are indicated by white arrows, non-colocalized proteins are indicated by white arrowheads.

5.2.6 DUB inhibition leads to increased ULK1 ubiquitination

Since WP1130-induced recruitment of ULK1 to aggresomes, which are positive for ubiquitin and K63-linked ubiquitin, was demonstrated, and since recent studies identified WP1130 as a deubiquitinase inhibitor (Kapuria et al., 2010; Kapuria et al., 2011); the question arose whether the ubiquitination status of ULK1 is directly affected by WP1130. In a first approach, GFP-ULK1 was immunopurified under untreated and WP1130-treated conditions and the ubiquitination status of ULK1 was analyzed via anti-mono/poly ubiquitin immunoblotting. Indeed, under WP1130 conditions an increased ubiquitination of GFP-ULK1 was detected, although increased ubiquitination of lower molecular weight proteins was also observed (**Figure 5-13, A**). In a second approach GFP-only as negative control and GFP-ULK1 were immunopurified and analyzed by anti-HA immunoblotting after transfection of Flp-In™ T-REx™ 293 cells with cDNA encoding HA-ubiquitin (HA-Ub) wt and HA-Ub mutant constructs. The HA-Ub mutant constructs were used for dissecting linkage specific ubiquitination. The increased ubiquitination of GFP-ULK1 under WP1130 conditions could be confirmed, whereas GFP-only ubiquitination was not affected. K48 and K63 linkage specific ubiquitination could not be detected after WP1130 treatment, indicating non-K48/non-K63-linked ubiquitination (**Figure 5-13, B**). Thirdly, a vice versa approach was used, in which ubiquitinated proteins were affinity-purified via agarose beads, coated with tandem ubiquitin binding entities (TUBE). Ubiquitin affinity purification and immunoblotting of ULK1 and mono/poly ubiquitin was carried out in HEK293 cells and Flp-In™ T-REx™ 293 GFP-ULK1 expressing cells treated with medium and WP1130 for 0.5 and 1.5 h. In both cell lines, purification of ubiquitinated proteins increased after WP1130 treatment (mono/poly ubiquitin immunoblotting). Notably, increased amounts of endogenous ULK1 as well as GFP-ULK1 could be detected after WP1130 treatment followed by ubiquitin affinity purification. Notably, a ULK1 smear was detected above the molecular weight of ULK1 compared to input. This indicates gaining molecular weights through increased ubiquitination of mono-ubiquitinated and poly-ubiquitinated ULK1. Detection of ULK1 was carried out with a monoclonal ULK1 antibody (Cell Signaling Technology, D8H5), but even better results was reached with a polyclonal ULK1 antibody (Santa Cruz Biotechnology, H-240) (**Figure 5-13, C**). Collectively, these results clearly demonstrate increased ubiquitination of endogenous ULK1 and GFP-ULK1 by WP1130 mainly through non-K48/non-K63-linked ubiquitination.

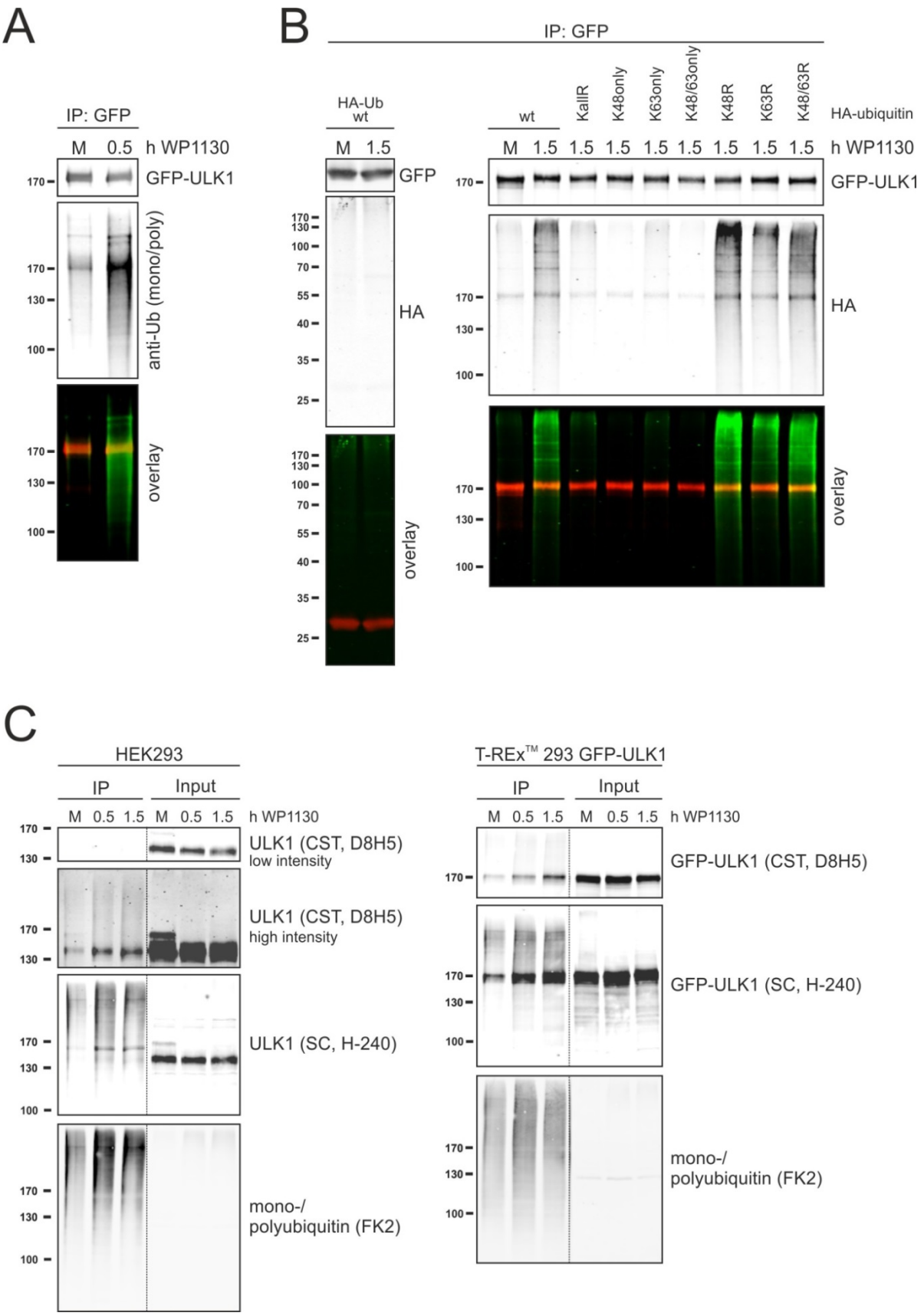

Figure 5-13: DUB inhibition leads to increased ULK1 ubiquitination. (A) After induction of GFP-ULK1 expression with doxycycline (Dox) for 3 h, Flp-In™ T-REx™ 293 cells were incubated in full medium (M) with or without 5 µM WP1130 for 0.5 h. Subsequently, cells were lysed and GFP-immunopurification was performed. Purified GFP-ULK1 was analyzed by anti-ULK1 and anti-ubiquitin (P4D1) immunoblotting. (B) Flp-In™ T-REx™ 293 GFP cells were transiently transfected with cDNA encoding HA-ubiquitin 24 h prior to WP1130 treatment. Flp-In™ T-REx™ 293 GFP-ULK1 cells were transiently transfected

with cDNAs encoding different HA-ubiquitin variants (wt, KallR, K48only, K63only, K48R, K63R) 24 h prior to WP1130 treatment. After induction of GFP or GFP-ULK1 expression with Dox for 3 h, cells were incubated in full medium (M) with or without 5 µM WP1130 for 1.5 h. Subsequently, cells were lysed and GFP-immunopurification was performed. Purified GFP (left panels) and GFP-ULK1 (right panels) were analyzed by anti-GFP, anti-ULK1, and anti-HA immunoblotting. GFP or GFP-ULK1 signal is displayed in red and HA signal is green in the merged images. (C) HEK293 cells or GFP-ULK1-expressing Flp-In™ T-REx™ 293 cells after Dox treatment for 16 h, were left untreated or were treated with 5 µM WP1130 for indicated intervals. Subsequently, cells were lysed and immunopurification of ubiquitinated proteins was performed using agarose-TUBE2. Purified ubiquitinated proteins were analyzed by anti-ULK1 (clone D8H5, Cell Signaling Technology; H-240 antibody, Santa Cruz Biotechnology) or anti-ubiquitin (clone FK2) immunoblotting.

5.2.7 Reported WP1130 targets do not participate in ULK1 aggregation

Recently, it has been reported that WP1130 inhibits different DUBs namely USP5, USP9X, USP14, UCH-L1, and UCH-L5 (Kapuria et al., 2010). Therefore, it was analyzed which DUBs are involved in the regulation of ULK1 aggregation. In a first approach, HEK293 cells were transfected simultaneously with the corresponding siRNAs and endogenous ULK1 expression after 48 and 72 h was analyzed. However, ULK1 levels were not affected (**Figure 5-14, A**). Since previous studies revealed USP9X as one major target of WP1130 (Kapuria et al., 2010; Sun et al., 2011; Peddaboina et al., 2012; Peng et al., 2014; Wang et al., 2014), the effect of WP1130 on ULK1 levels in *USP9X*-/o HCT116 cells was also investigated (Harris et al., 2012). Treatment of *USP9X*+/o and *USP9X*-/o HCT116 cells reduced ULK1 to the same extent, indicating a rather USP9X independent form of ULK1 aggregation by WP1130 (**Figure 5-14, B**). For the purpose of identifying possibly additional DUB(s) targeted by WP1130, a DUB profiling assay was performed using WP1130 as the DUB inhibitor of interest and a library of 35 recombinant DUBs as potential targets. However, none of the tested DUBs was significantly inhibited by 1 or 10 µM WP1130, including the five enzymes recently reported to be inhibited by WP1130 (**Figure 5-14, C**). Collectively, these results could not reveal a WP1130 target that functions solely or in combination in ULK1 aggregation. Other putative DUBs controlling ULK1 ubiquitination could not be identified.

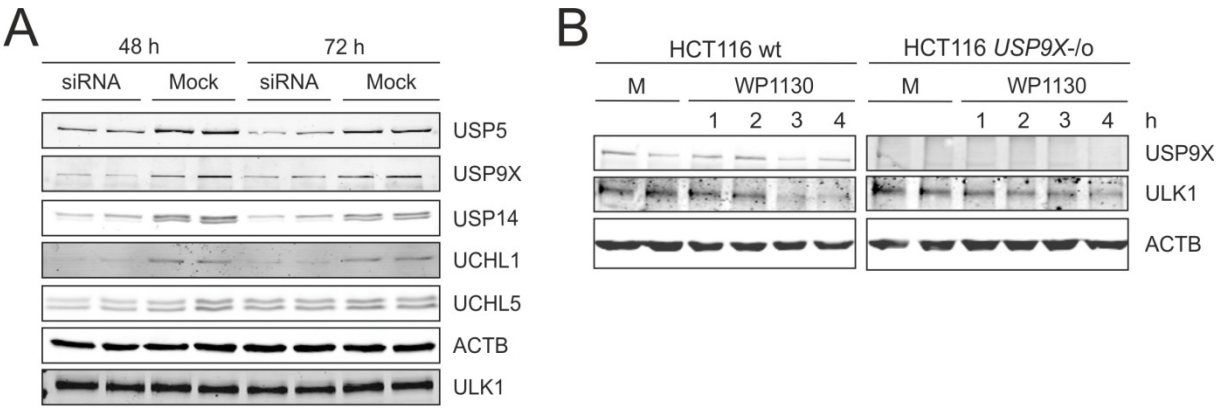

C

DUB$^{profiler™}$ Single Point Screening (Ubiquigent Ltd, Dundee, Scotland, UK) Activity [% Control]*							
	WP1130 concentration [µM]	1	10		WP1130 concentration [µM]	1	10
Compound control	Product Signal Modulation**	-3	-5	Compound control	Product Signal Modulation**	-3	-5
USPs	USP1	91	94	UCHs	UCHL1	99	78
	USP2	100	111		UCHL3	97	88
	USP4	91	95		UCHL5	89	86
	USP5	98	93		BAP1	87	82
	USP6	97	109	OTUs	OTU1	97	99
	USP7	91	96		OTUB2	88	80
	USP9X	93	85		OTUD3	101	102
	USP11	105	98		OTUD6A	88	97
	USP15	99	96		OTUD6B	96	87
	USP19	126	109		Cezanne	89	87
	USP20	91	96	JAMMs	AMSH-LP	96	93
	USP21	88	89		AMSH-LP (+Zinc)	94	99
	USP25	102	92	Josephins	Ataxin3	97	80
	USP28	97	105		Ataxin3L	108	105
	USP30	102	102		JOSD1	126	116
	USP35	105	88		JOSD2	110	93
	USP36	90	96				
	USP45	106	100				
	CYLD	84	91				

* % Control = ((sample - mean no enzyme)/(mean plus enzyme - mean no enzyme))*100

** Product Signal Modulation = ((sample - mean modulator control)/(mean modulator control))*100

Figure 5-14: Knockdown or knockout of various deubiquitinases targeted by WP1130 does not result in aggregation of ULK1. (A) HEK293 cells were simultaneously transfected with 20 nM ON-TARGETplus SMARTpool® siRNA for USP5, USP9X, USP14, UCHL1, and UCHL5. Cells were incubated for 48 or 72 h. Cleared cell lysates were analyzed by immunoblotting for USP5, USP9X, USP14, UCHL1, UCHL5, ACTB/β-actin, and ULK1. (B) HCT116 wt cells and HCT116 USP9X-deficient (*USP9X* -/o) cells were treated with 5 µM WP1130 for indicated times. Cleared cell lysates were subjected to anti-USP9X, anti-ULK1, and anti-ACTB/β-actin immunoblotting. (C) The DUB$^{profiler™}$ Single Point Screening was performed by Ubiquigent Ltd (Dundee, Scotland, UK). WP1130 was tested at two different concentrations (1 or 10 µM) in a ubiquitin-rhodamine(110)-glycine substrate-based assay. Data given represent activity [% control].

5.2.8 The pan-DUB inhibitor PR619 mimics the effect of WP1130 on ULK1

Since none of the WP1130 targeted DUBs are involved in ULK1 ubiquitination and aggregation, the question arose if DUBs at all are involved in regulation of ULK1 aggregation. In order to validate the DUB-dependent effect of WP1130 on ULK1, the influence of the pan-DUB inhibitor PR619 on the amount of ULK1 was characterized in HEK293 cells. Indeed, PR619 induced the reduction of ULK1 to a comparable extent as WP1130, while more specific DUB inhibitors such as LDN 57444 (inhibiting UCH-L1) and spautin-1 (inhibiting USP10 and USP13) could not reduce the amount of ULK1 (**Figure 5-15, A**). Furthermore, treatment of HEK293 cells with PR619 led to the redistribution of ULK1 from the detergent-soluble to the detergent-insoluble fraction (**Figure 5-15, B**). Collectively, these results demonstrate an unambiguous effect of DUB inhibition-dependent ULK1 aggregation.

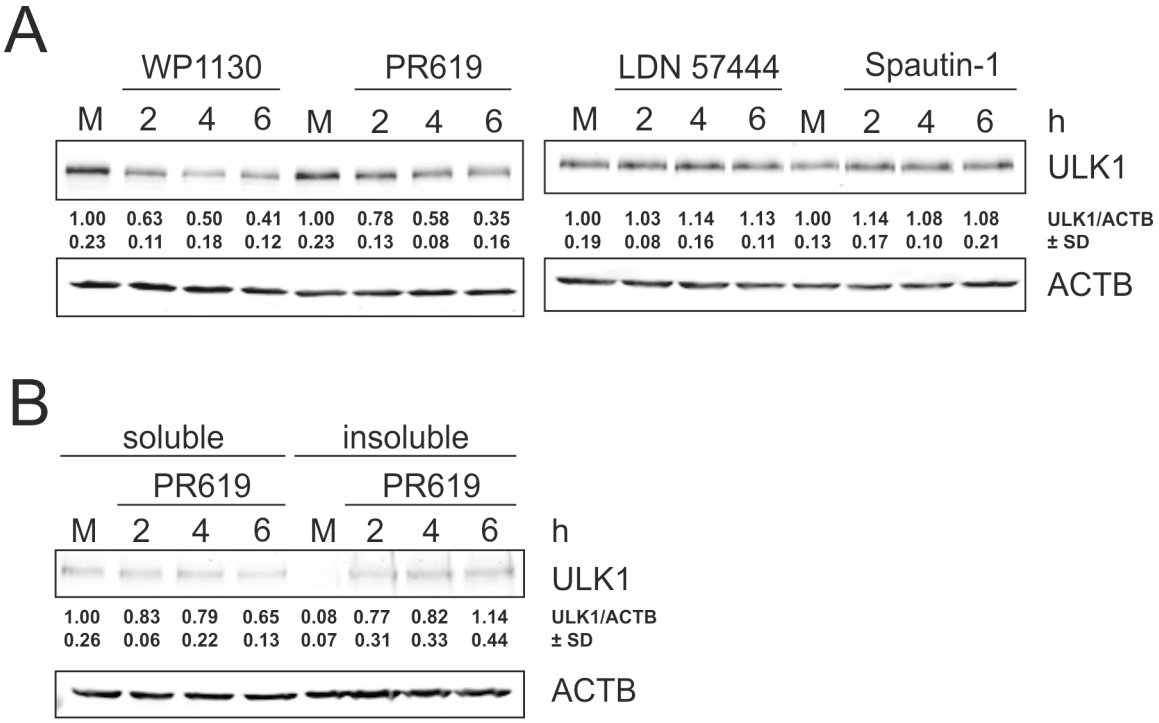

Figure 5-15: The pan-DUB inhibitor PR619 leads to transfer of ULK1 from soluble to insoluble fractions. (A) HEK293 cells were left untreated or were treated with 5 µM WP1130, 20 µM PR619, 25 µM LDN 57444, or 10 µM spautin-1 for 2, 4, or 6 h. Cleared cell lysates were subjected to anti-ULK1 and anti-ACTB/β-actin immunoblotting. (B) HEK293 cells were left untreated or were treated with 20 µM PR619 for indicated intervals. Then detergent-soluble or -insoluble fractions were prepared and analyzed for ULK1 and ACTB/β-actin by immunoblotting. (A and B) Data shown are representative of at least three independent experiments. Fold changes were calculated by dividing each normalized ratio (protein to loading control) by the average of the ratios of the control lane (control lane: fold change = 1.00, n ≥ 3). Results are mean ± SD and are given below the corresponding blots.

5.2.9 WP1130 does not induce aggregation of other components of the ULK1 or the PtdIns3K class III complex

For a better understanding and grading of the following results, it is important to elucidate the influence of WP1130 towards other protein complex components crucial for autophagy induction and regulation. For that, subcellular fractionation was performed and subsequently the distribution of additional autophagy-relevant proteins was analyzed by immunoblotting. Notably, treatment of HEK293 cells with WP1130 induced the redistribution of ULK1 from the detergent-soluble fraction to the detergent-insoluble fraction, but had no influence on the distribution of other ULK1 complex components like FIP200/RB1CC1 or ATG13, as well PIK3C3/VPS34-PIK3R4/VPS15-BECN1-ATG14 class III PtdIns3K complex components such as AMBRA1 or Beclin-1/BECN1 (**Figure 5-16**). This substantiates a rather specific influence of WP1130 on ULK1 aggregation.

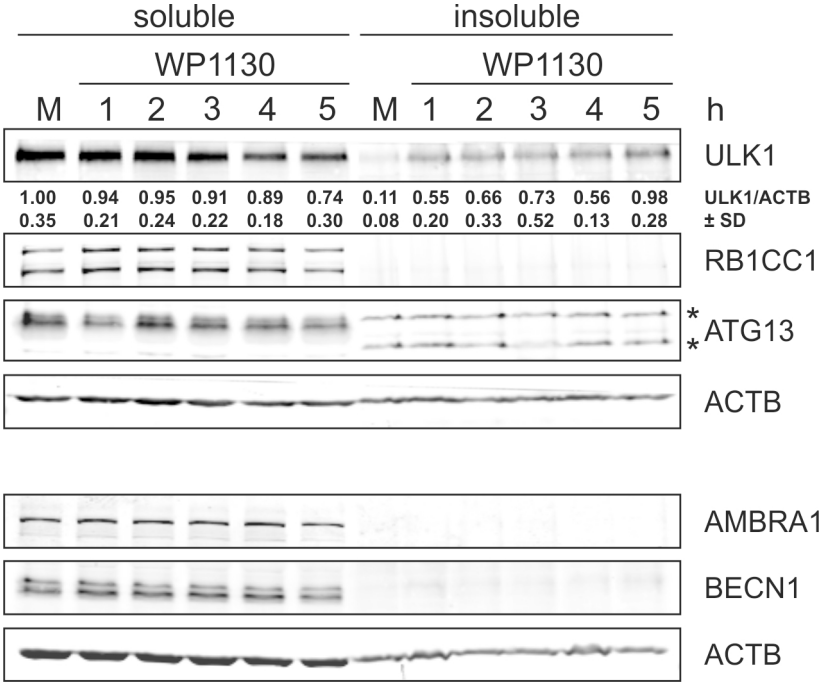

Figure 5-16: WP1130 does not induce aggregation of other components of the ULK1 or PIK3C3/VPS34-PIK3R4/VPS15-BECN1-ATG14 class III PtdIns3K complex. (A) HEK293 cells were left untreated or were treated with 5 µM WP1130 for indicated intervals. Then detergent-soluble or -insoluble fractions were prepared and analyzed for ULK1, RB1CC1, ATG13, AMBRA1, BECN1, and ACTB/β-actin by immunoblotting. Asterisks indicate unspecific background bands. Data shown are representative of at least three independent experiments. Fold changes were calculated by dividing each normalized ratio (protein to loading control) by the average of the ratios of the control lane (control lane: fold change = 1.00, n ≥ 3). Results are mean ± SD and are given below the corresponding blots.

5.2.10 ULK1 activity is inhibited by WP1130

Previously, it has been reported that the tyrosine kinases Bcr-Abl and JAK2 are recruited to aggresomes upon WP1130 treatment, which leads to inhibition of their kinase activity (Kapuria et al., 2011; Sun et al., 2011). Since it could be demonstrated that WP1130 induced the transfer of ULK1 to aggresomes, next, it was analyzed whether this process also affects

ULK1 kinase activity. As a ULK1 activity readout system the phosphorylation status of AMPK-β2, a direct ULK1 substrate, was investigated, as well as the phosphorylation of AMPK-α at T172. The latter is indirectly induced and regulated by ULK1 upon amino acid starvation with EBSS (Löffler et al., 2011). Two different cell systems were used, i.e. the Flp-In™ T-REx™ 293 GFP-ULK1 inducible overexpressing cells and HEK293 cells for determining ULK1 activity on endogenous level (**Figure 5-17, A, B**). For GFP-ULK1, induced overexpression with doxycycline was sufficient to increase ULK1 kinase activity detected by decelerated migration of AMPK-β2 in SDS-PAGE. Further increment of kinase activity was induced by amino acid starvation with EBSS highlighted by phosphorylation of AMPK-α at T172. Interestingly, parallel WP1130 treatment abrogated the effects of ULK1 kinase activity demonstrated by induced faster migration of AMPK-β2 and reduced phosphorylation of AMPK-α at T172 without affecting total AMPK-α levels (**Figure 5-17, A**). Similar results were gained with endogenous ULK1 levels. The decelerated migration of AMPK-β2 in SDS-PAGE and phosphorylation of AMPK-α at T172 was induced by EBSS, whereas additional treatment with WP1130 diminished these effects (**Figure 5-17, B**). In order to exclude a direct inhibition of ULK1 kinase activity through WP1130, an *in vitro* kinase assay with purified ULK1 and MBP as substrate was performed. Indeed, WP1130 could not inhibit phosphorylation of MBP (**Figure 5-17, C**). Taken together, these results clearly demonstrate that WP1130 negatively regulates ULK1 activity indirectly through ULK1 aggregation.

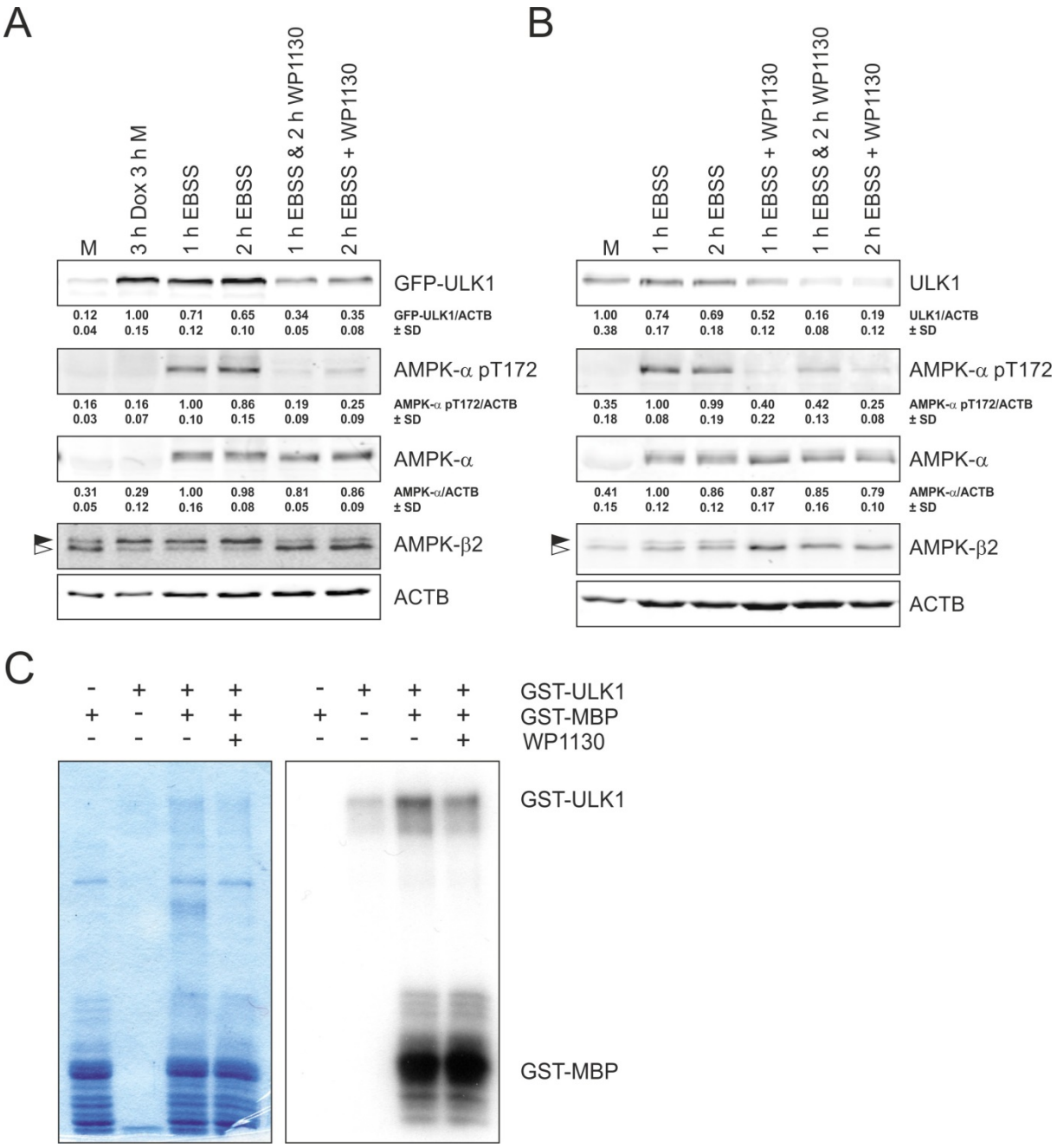

Figure 5-17: WP1130 induces the inhibition of ULK1 activity. (A) After induction of GFP-ULK1 expression with doxycycline for 3 h, Flp-In™ T-REx™ 293 cells were incubated in full medium (M) or starvation medium (EBSS) for 1 or 2 h in the presence or absence of 5 µM WP1130 for indicated times. Subsequently, cells were lysed and cleared cell lysates were separated by SDS-PAGE and analyzed by immunoblotting using antibodies against ULK1, AMPK-α (pT172), AMPK-α, AMPK-β1/2, and ACTB/β-actin. (B) HEK293 cells were treated and analyzed as in (A), except Dox incubation. (C) For the *in vitro* kinase assay, 1 µg GST-myelin basic protein (MBP) was incubated with 0.5 µg GST-ULK1 in the absence or presence of 5 µM WP1130. As controls, GST-MPB or GST-ULK1 was incubated alone. After coomassie staining of the gels (left panel), autoradiography was performed (right panel). (A and B) Solid arrowheads indicate the phosphorylated form of AMPK-β2; open arrowheads indicate the non-phosphorylated form. Data shown are representative of at least three independent experiments. Fold changes were calculated by dividing each normalized ratio (protein to loading control) by the average of the ratios of the control lane (control lane: fold change = 1.00, n ≥ 3). Results are mean ± SD and are given below the corresponding blots.

5.2.11 The autophagic flux is inhibited by WP1130

Recently, it has been speculated that WP1130 might increase autophagy (Kapuria et al., 2010). Due to the fact that a loss of ULK1 kinase activity upon WP1130 treatment was observed, next the effect of WP1130 on autophagy was analyzed. Hence, three different readouts were used. Two of them are based on LC3 lipidation and one detects long-lived protein degradation. First of all, the endogenous LC3 puncta formation was investigated in HEK293 cells under inducing (starvation) and inhibiting conditions of autophagy by confocal microscopy. LC3 puncta indicate the lipidated (LC3-II) form of LC3 that is associated with autophagosomes. Of note, a further increase in autophagosome number analyzed by confocal microscopy or LC3-II amount in immunoblot under lysosomal autophagy inhibiting conditions (bafilomycin A_1, Baf A_1) and parallel autophagy inducing conditions (EBSS starvation) compared to Baf A_1 treatment alone indicates autophagic flux. Ultimately, the differences in the amount of LC3-II between samples in the presence and absence of lysosomal inhibitors represent the amount of LC3 that is delivered to lysosomes, which is equivalent to autophagic flux (Mizushima et al., 2010). The treatment with bafilomycin A_1 resulted in such an increase of LC3 puncta that was further increased by amino acid starvation with EBSS. This phenomenon was completely abrogated by WP1130. All WP1130 treated cells showed similar number of LC3 puncta. The fact that there was no further increase with EBSS, suggests a blockage of autophagy at an early stage of the autophagic signaling pathway (**Figure 5-18, A**). Secondly, the LC3 turnover in HEK293 cells was determined by immunoblotting. This assay substantially confirmed the aforementioned results obtained by LC3 immunofluorescence. Again, treatment with bafilomycin A_1 resulted in an increase of LC3-II/loading control ratio that was further increased by EBSS. When cells were treated with WP1130, similar ratios of LC3-II/loading control were assessed in all samples, independent of EBSS or Baf A_1 treatment (**Figure 5-18, B**). In the last approach a long-lived protein degradation assay in HEK293, HeLa, and U2OS cells was performed by Petter Holland (Institute of Basic Medical Sciences, Faculty of Medicine, University of Oslo, Norway). WP1130 significantly reduced the degradation of long-lived proteins induced by EBSS in all tested cell lines. Besides $BafA_1$, 3-methyladenine (3-MA) was used as a control, which also inhibits autophagy, but in contrast at an initial step of the autophagic machinery by the inhibition of the PtdIns3K class III complex. The induction of long-lived protein degradation and the inhibitory potential of 3-MA, $BafA_1$, and WP1130 differed in the tested cell lines. In HeLa cells the inhibitory effect of WP1130 is similar to that observed for 3-MA, whereas in HEK293 and U2OS, WP1130 induced inhibition of autophagy is similar to $BafA_1$ (**Figure 5-18, C**). This observation might be explained by differences in basal autophagy, differential dependence on various autophagy complexes, and different equipment and

expression levels of deubiquitinases. Collectively, these data strongly suggests an inhibitory effect of WP1130 on autophagy and especially the autophagic flux.

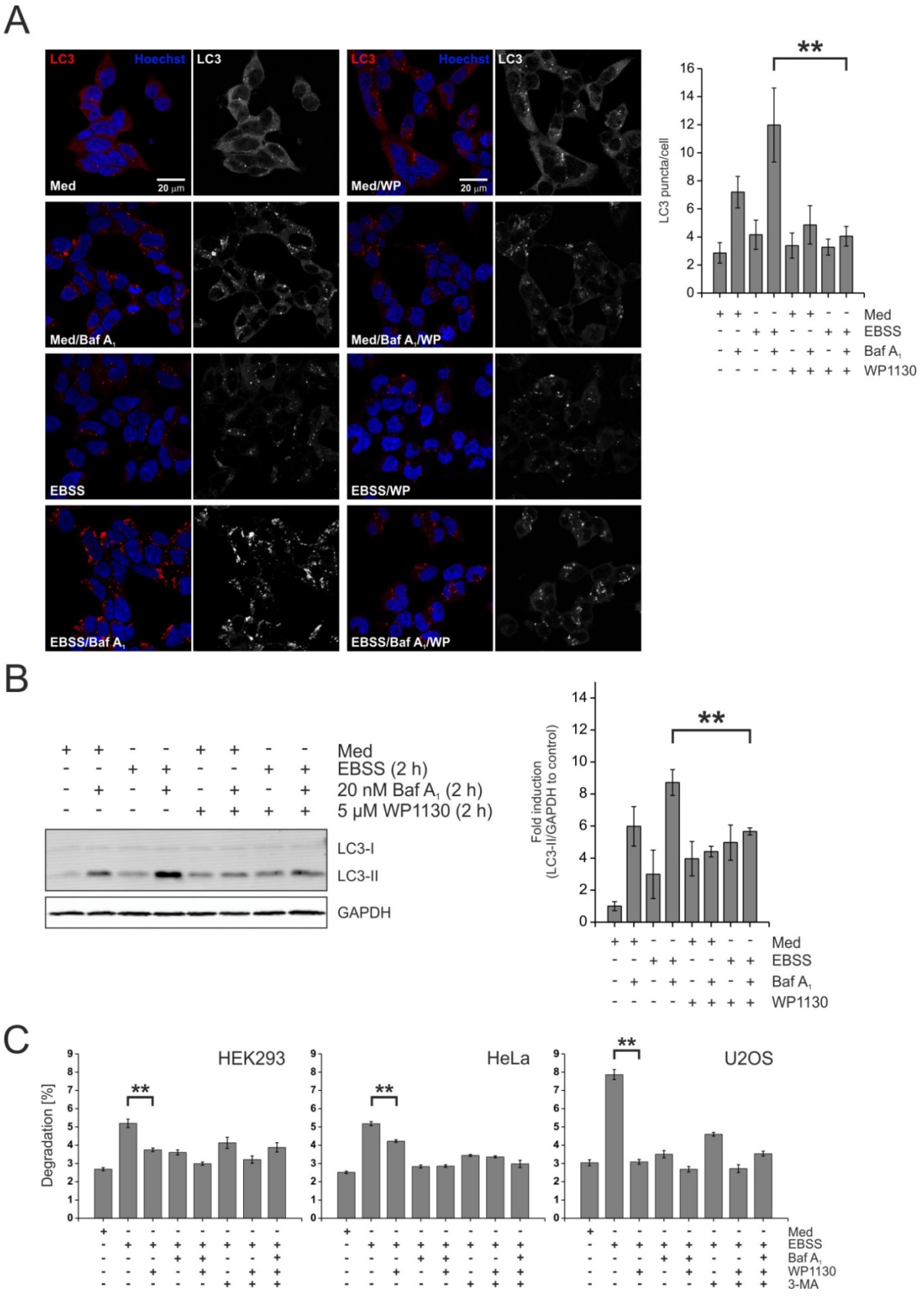

Figure 5-18: WP1130 inhibits the autophagic flux. (A) HEK293 cells were treated with full medium (Med) and/or starvation medium (EBSS) in the presence or absence of 20 nM bafilomycin A_1 and/or 5 µM WP1130 for 2 h. Hereafter, cells were immunostained against LC3 and visualized by confocal laser scanning microscopy. The LC3 signal is displayed in red and the

Hoechst signal in blue in the merged images. For better contrast, LC3 is also displayed in greyscale. At least 168 cells were scored for each condition. The number of LC3 puncta and the number of cells per image were quantified using CellProfiler analysis software. Data represent mean ± SD and are depicted in a bar diagram. (B) HEK293 cells were incubated as described in A. Cleared cell lysates were analyzed for LC3 and GAPDH by immunoblotting. Data shown are representative of at least three independent experiments. Fold changes were calculated by dividing each normalized ratio (protein to loading control) by the average of the ratios of the control lane (control lane: fold change = 1.00, n ≥ 3). Results are mean ± SD and are depicted in a bar diagram. (C) HEK293, HeLa and U2OS cells were labelled with L-[^{14}C] valine. Cells were washed and treated with indicated medium (control or EBSS) and inhibitors (5 μM WP1130, 100 nM bafilomycin A_1, 10 mM 3-methyladenine) for 4 h. For each sample, the radioactivity of the acid-soluble fraction of the medium and the radioactivity in the cells remaining in the well were measured. Percent degradation was assessed as the acid-soluble radioactivity of the medium divided by the total radioactivity. Data shown are mean of triplicates ± SD and depicted in a bar diagram. (A, B, and C) $^{**}p < 0.01$ (Student's *t*-test, two-sample assuming unequal variances).

5.2.12 Autophagy inhibition induced by WP1130 is linked to ULK1/2

Since WP1130 treatment inhibited ULK1/2 kinase activity and moreover inhibited the autophagic flux in various cell lines, it was investigated if the loss of the overall kinase activity is causally linked to inhibition of autophagy. Generally, canonical autophagy pathways largely depend on the ULK1/2 complex, making it difficult to analyze the effect of WP1130 in genetic ULK1/2 knockout cell lines. Hence, the inhibitory effect of WP1130 on ULK1/2 independent autophagic pathways was investigated. Two vertebrate *ULK1/2* knockout cell lines were utilized, in which autophagy induction is possible under certain circumstances, indicating the dispensability of ULK1/2 in these cells. In wild type and *ULK1/2*-/- DT40 cells, autophagy can be induced under amino acid starvation conditions by EBSS (Alers et al., 2011). In contrast, autophagy can be induced in wild type and *Ulk1/2*-/- MEFs through glucose starvation, while amino acid starvation is blocked in *Ulk1/2*-/- MEFs (Cheong et al., 2011).

5.2.12.1 WP1130 does not inhibit starvation-induced autophagy in wild type and ULK1/2-deficient DT40 cells

For the analysis of the ULK1/2 dependency of WP1130 induced autophagy inhibition in DT40 ULK1/2 knockout cells, two different readouts (described in 5.2.11) were used. First, the endogenous LC3 puncta formation was analyzed by confocal microscopy. In contrast to HEK293 (see **Figure 5-18, A**), treatment with WP1130 could not inhibit EBSS induced LC3 puncta formation in wild type and ULK1/2 deficient DT40 cells. The autophagic flux could still be induced, as deduced from the comparison of $BafA_1$ treatment to $BafA_1$/EBSS treatment with and without WP1130 (**Figure 5-19, A**). As a second approach, the LC3 turnover in DT40 cells was investigated by immunoblotting. The LC3 confocal microscopy results were confirmed by the observation that LC3 turnover in this cellular system was not inhibited by WP1130 (**Figure 5-19, B**).

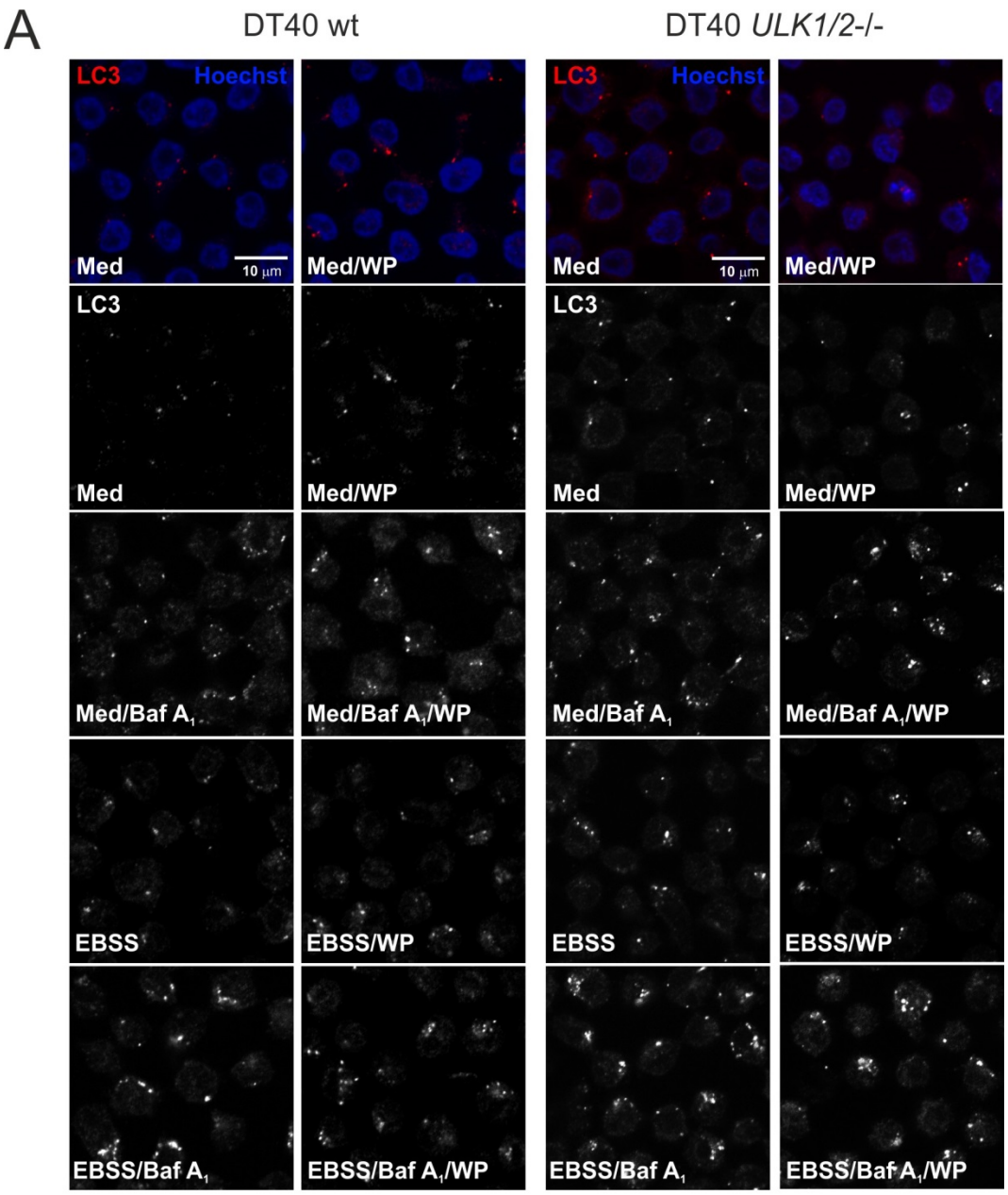
A
DT40 wt
DT40 ULK1/2-/-
LC3
Hoechst
Med
10 µm
Med/WP
Med/Baf A1
Med/Baf A1/WP
EBSS
EBSS/WP
EBSS/Baf A1
EBSS/Baf A1/WP

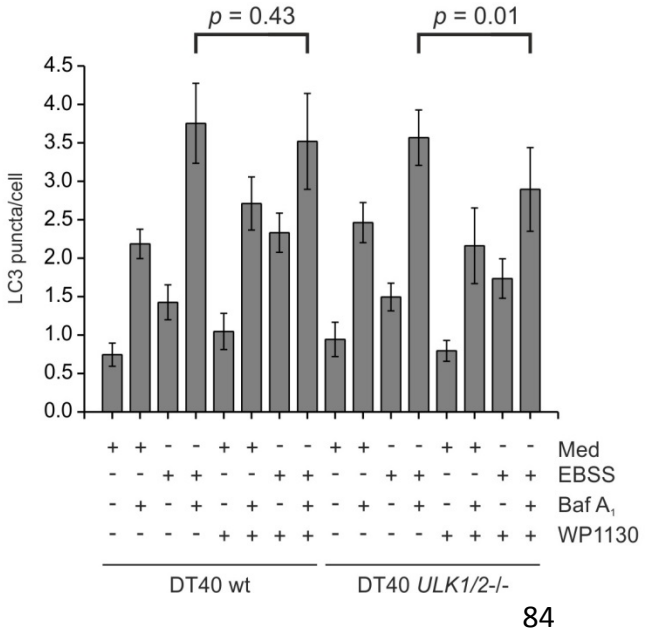
p = 0.43
p = 0.01
LC3 puncta/cell
4.5
4.0
3.5
3.0
2.5
2.0
1.5
1.0
0.5
0.0
Med
EBSS
Baf A1
WP1130
DT40 wt
DT40 ULK1/2-/-

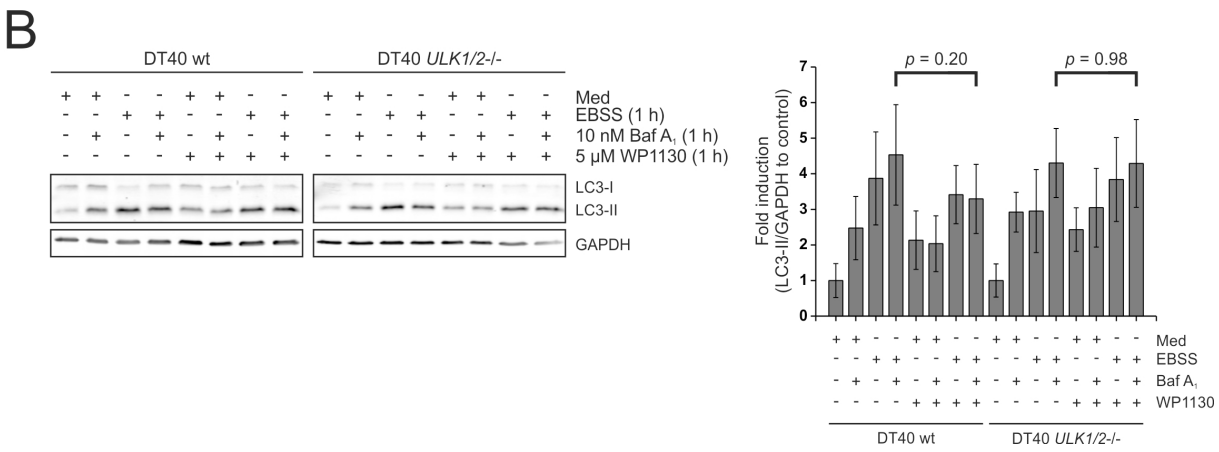

Figure 5-19: WP1130 does not inhibit starvation-induced autophagy in wild type and ULK1/2-deficient DT40 cells. (A) Wild type or ULK1/2-/- DT40 cells were treated with full medium (Med) or starvation medium (EBSS) in the presence or absence of 10 nM bafilomycin A1 and/or 5 µM WP1130 for 1 h. Hereafter, cells were immunostained against LC3 and visualized by confocal laser scanning microscopy. The LC3 signal is displayed in red and the Hoechst signal in blue in the merged images. For better contrast, LC3 is also displayed in greyscale. At least 222 cells were scored for each condition. The number of LC3 puncta and the number of cells per image were quantified using CellProfiler analysis software. Data represent mean ± SD and are depicted in a bar diagram; *p*-values were calculated by Student's *t*-test, two-sample assuming unequal variances. (B) Wild type or ULK1/2-/- DT40 cells were incubated as described in A. Cleared cell lysates were analyzed for LC3 and GAPDH by immunoblotting. Data shown are representative of at least three independent experiments. Fold changes were calculated by dividing each normalized ratio (protein to loading control) by the average of the ratios of the control lane (control lane: fold change = 1.00, n ≥ 3). Results are mean ± SD and are depicted in a bar diagram; *p*-values were calculated by Student's *t*-test, two-sample assuming unequal variances.

5.2.12.2 WP1130 does not inhibit autophagy induced by glucose deprivation in wild type and ULK1/2-deficient MEFs

Next, in order to validate the findings for ULK1/2-deficient DT40 cells, it was analyzed whether WP1130 can inhibit LC3 turnover upon glucose deprivation in ULK1/2 deficient MEFs. For those cells it had previously been reported that autophagy induced by glucose starvation can occur normally (Cheong et al., 2011). Two different readouts were used, the LC3 turnover by immunoblotting and the detection of autophagosomal mCitrine-hLC3B degradation by FACS analysis. Of note, under starvation conditions an increase of LC3-II is observed in immunoblot due to the enrichment of the lipidated form, while by FACS analysis a decrease of mCitrine-hLC3B fluorescence is detected due to the induced lysosomal degradation. First, it could be shown by immunoblotting that LC3 turnover in wild type and ULK1/2 deficient MEFs cells is not inhibited by WP1130 upon glucose starvation (**Figure 5-20, A**). Second, glucose deprivation in wild type and ULK1/2 deficient MEFs induced a reduction of mCitrine-hLC3B fluorescence, which could be inhibited by $BafA_1$. In contrast, treatment with WP1130 could not abrogate this effect (**Figure 5-20, B**). Thus, it was demonstrated in two different ULK1/2-deficient cell systems that the autophagy inhibitory potential mediated by WP1130 largely depends on ULK1/2.

Taken together, it could be shown that the DUB inhibitor WP1130 targets ULK1/2 for ubiquitination, subsequent aggregation/aggresome formation and thereby reduces the

overall ULK1/2 enzymatic activity. Consequently, the WP1130 mediated functional knockdown of ULK1/2 attributed for the reduced autophagic potential.

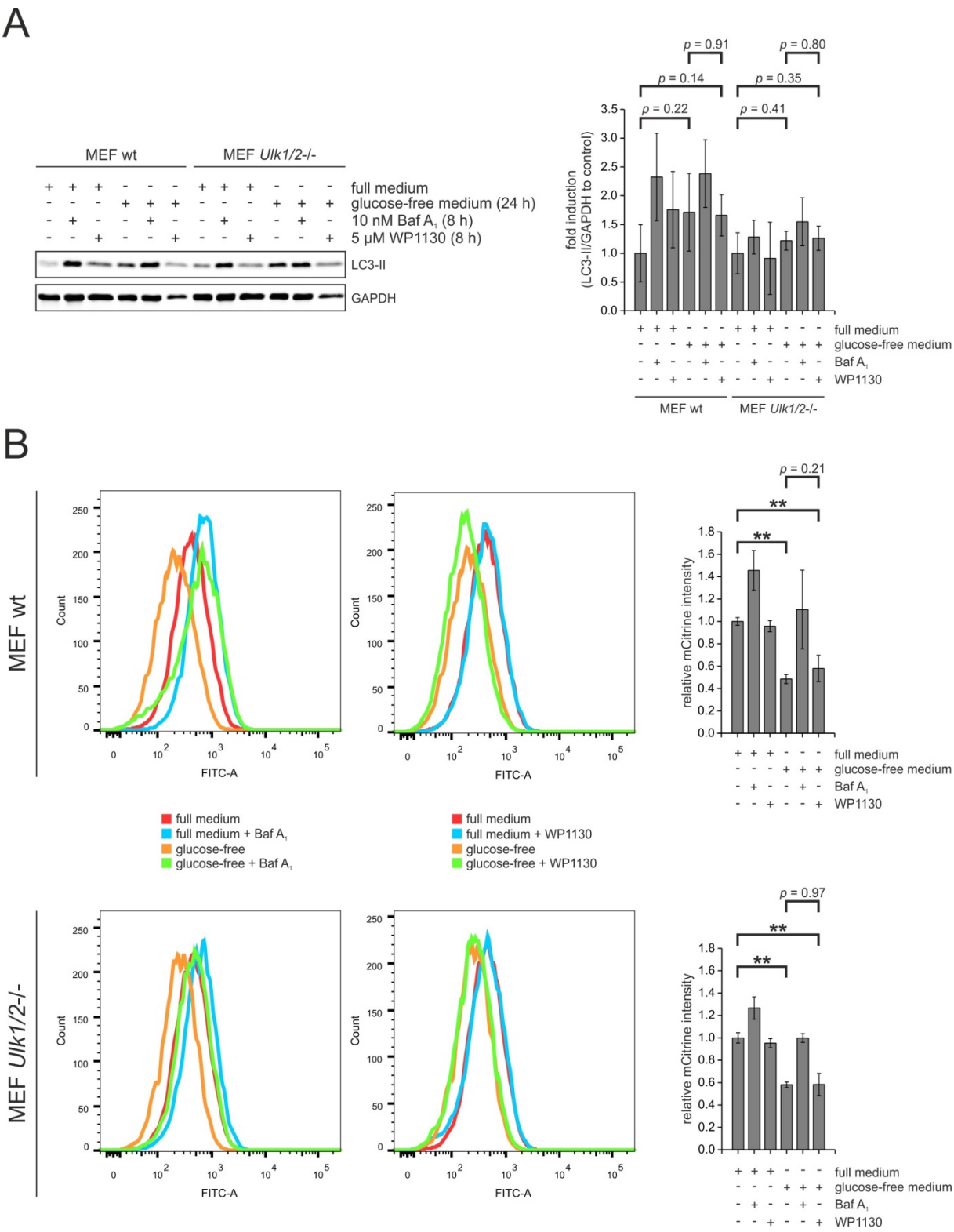

Figure 5-20: WP1130 does not inhibit autophagy induced by glucose deprivation in wild type and ULK1/2-deficient MEFs. (A) Wild type or *Ulk1/2*-/- MEFs were incubated in full medium (Med) or glucose-free medium for 24 h in the presence or absence of 10 nM bafilomycin A_1 (Baf A_1) or 5 µM WP1130 for the last 8 h. Cleared cell lysates were analyzed for LC3 and GAPDH by immunoblotting. Data shown are representative of at least three independent experiments. Fold changes were calculated by dividing each normalized ratio (protein to loading control) by the average of the ratios of the control lane (control lane: fold change = 1.00, n ≥ 3). Results are mean ± SD and are depicted in a bar diagram; *p*-values were calculated

by Student's *t*-test, two-sample assuming unequal variances. (B) Wild type or *Ulk1/2*-/- MEFs stably expressing mCitrine-hLC3B were incubated in full medium or glucose-free medium for 24 h in the absence or presence of 10 nM bafilomycin A_1 (Baf A_1) and/or 5 µM WP1130 for the last 8 h. Then cells were harvested with 0.05% trypsine-EDTA and washed once with PBS. Total cellular mCitrine-hLC3B signals were analyzed by flow cytometry. Representative FACS data from four independent experiments is shown in the panels. Fold changes were calculated by dividing averaged mean values of fluorescence intensity by the average of the means of cells cultured in regular medium (fold change = 1.00). Data represent mean ± SD and are depicted in a bar diagram. $^{**}p < 0.01$ (Student's *t*-test, two-sample assuming unequal variances).

6 Discussion

6.1 Apoptosis – Regulation of the initiator caspase-9

To date, it has been reported that the broad-range kinase inhibitor staurosporine (STS) can induce apoptosis in a dual mode of action, on the one hand like conventional DNA-damaging anticancer drugs through the classical intrinsic mitochondrial cytochrome c/APAF1 pathway independent of external death receptor signaling, and on the other hand by triggering a novel intrinsic apoptosis pathway, which allows the induction of apoptosis in anticancer drug-resistant cancer cells. The alternative intrinsic apoptosis pathway, inducible by STS, is in addition characterized by the induction of apoptosis in Bcl-2 and Bcl-xL overexpressing cells as well as independency of APAF1 and the apoptosome formation, and in contrast, by dependency on caspase-9 (Johnson et al., 1999; Stepczynska et al., 2001; Manns et al., 2011).

The aim of the apoptosis part of the thesis was to further elucidate the alternative induction of intrinsic apoptosis by STS. The focus was set on activation of caspase-9, the common denominator of both modes of STS-induced apoptosis. First, the contribution of the catalytic activity of caspase-9 and its caspase activation and recruitment domain (CARD) in STS-induced apoptosis was investigated. In a second step, the alternative activation of caspase-9 besides the apoptosome was analyzed. In a third approach, the impact of caspase-9 phosphorylation was further dissected. Finally, the identification of additional caspase-9 interaction proteins was assessed that might be important for alternative caspase-9 activation.

Taken together:

- STS-induced apoptosis is dependent on CARD of caspase-9 and its catalytic activity
- STS-induced caspase-9 activation is independent of cathepsins, calpains, and caspase-4
- STS treatment does not alter the phosphorylation status of caspase-9
- STS induces apoptosis in caspase-9 CARD mutant R56A, but not R13A, both unable to interact with APAF1
- STS induces the interaction of caspase-9 R56A with BAG2, but not R13A

6.1.1 CARD of caspase-9 and its catalytic activity are indispensable for staurosporine-induced apoptosis

In previous CARD to CARD interaction and apoptosis assays, performed by Dr. Merle Daubrawa during her doctoral thesis, it was demonstrated that a tag at the N-terminus *ergo*

the CARD region of caspase-9 abolished the interaction of caspase-9 and APAF1 and thus diminished the intrinsic apoptosis induction via mitomycin C. Interestingly, STS-induced apoptosis was not affected.

To clarify whether the CARD of caspase-9 is fundamental for caspase-9 activation during canonical and non-canonical apoptosis induced by STS, apoptosis was monitored in caspase-9 deficient Jurkat cells expressing a ΔCARD caspase-9 mutant. STS treatment led to an increase in caspase activity and apoptosis in wild type Jurkat and caspase-9 wt reconstituted cells, whereas in caspase-9 deficient and ΔCARD caspase-9 mutant cells caspase activity and apoptosis could not be induced. Thus, the CARD of capsase-9 is a prerequisite not only for anticancer drug induced but also for STS-induced apoptosis. However, in contrast to anticancer drug induced apoptosis, STS can also induce apoptosis independent of APAF1 and apoptosome formation

Former caspase-9 catalytic mutant studies demonstrated that expression of catalytic inactive caspase-9 inhibits apoptosis, although interaction with APAF1 was not abrogated and that APAF1 dependent processing of caspase-9 is mediated by its autocatalysis (Li et al., 1997; Hu et al., 1998).

To elucidate if the catalytic center of caspase-9 is crucial for STS-induced canonical and non-canonical apoptosis or if caspase-9 can function as a scaffold CARD interacting protein activating other caspases, caspase activity and apoptosis were analyzed in caspase-9 deficient Jurkat cells expressing a caspase-9 C287S catalytic inactive mutant. STS treatment led to similar results compared with ΔCARD caspase-9 mutant expressing Jurkat cells. STS treatment was not sufficient to induce apoptosis in caspase-9 deficient and caspase-9 C287S mutant Jurkat cells. Hence, the catalytic activity of caspase-9 is crucial for STS-induced apoptosis.

Collectively, by investigation of two Jurkat cell lines expressing caspase-9 mutants, it could be proven that the CARD of caspase-9 is not solely important for the interaction with APAF1 and its subsequent activation, but moreover plays a critical role in STS-induced apoptosis that bypasses the intrinsic mitochondrial apoptosis pathway and the apoptosome. It could also be demonstrated that the catalytic activity is indispensable for STS-induced apoptosis, thus supporting the hypothesis that caspase-9 functions as an initiator caspase also in the alternative apoptosis pathway induced by STS. Since the interaction between the CARD of APAF1 and the CARD of procaspase-9 is essential for the recruitment of procaspase-9 to the apoptosome and its subsequent activation during the intrinsic apoptosis pathway (Bratton et al., 2001; Acehan et al., 2002; Yuan et al., 2010), an analog activation of caspase-9 with other

CARD containing proteins under STS conditions seems likely. This will be further discussed in 6.1.5.

6.1.2 Staurosporine induced apoptosis is independent of cathepsins, calpains, or caspase-4

It has been reported that STS activates caspase-9 in a dual mode of action, on the one hand via the canonical intrinsic mitochondrial cytochrome c/APAF1 pathway, and on the other hand via a novel non-canonical intrinsic apoptosis pathway. This non-canonical pathway has been characterized as being independent of death receptors, cytochrome c release, APAF1, and apoptosome formation, but notably dependent on caspase-9 (Johnson et al., 1999; Stepczynska et al., 2001; Manns et al., 2011). Into accord with this, it has previously been reported that caspase-9 can possibly be activated independent of the apoptosome and mitochondrial apoptosis pathway by cathepsins or calpains (Bitzer et al., 2002), by caspase-4 (Lopez-Anton et al., 2006), or by another multi-protein complex the DRAL-caspase-9 complex (Mille et al., 2009).

To clarify the impact of cathepsins, calpains, or caspase-4 on caspase-9 activation, apoptosis was induced by staurosporine in Jurkat cells expressing caspase-9, which were treated additionally with inhibitors for these proteases. Noteworthy, none of these inhibitors could reduce STS-induced apoptosis. Thus, cathepsins, calpains, or caspase-4 are not able to induce caspase-9 activation.

It has to be mentioned that other studies are conflictive to the findings of this thesis, indicating that STS induces caspase independent apoptosis (Belmokhtar et al., 2001), or that STS induces the cathepsin D dependent release of cytochrome c and thereby activation of caspase-9 (Johansson et al., 2003). As our studies reveal a caspase dependent and cytochrome c independent activation of caspase-9, the studies of Belmokhtar et al. and Johansson et al. are not relevant for the investigation of alternative activation of caspase-9 that bypasses the mitochondrial apoptosis pathway investigated in this thesis.

The results of calpain, cathepsin, and caspase-4 inhibitors in combination with the ΔCARD caspase-9 studies, indicate a rather multi-protein complex dependent activation of caspase-9 upon CARD-to-CARD interaction, e.g. the DRAL-caspase-9 complex, which has to be elucidated (see 6.1.5), rather than direct activation of caspase-9 by other proteases.

6.1.3 Staurosporine induces apoptosis in caspase-9 CARD R56A mutant but not R13A mutant Jurkat cells

The 1:1 stoichiometric binding between the CARD of APAF1 and the CARD of caspase-9 is maintained through electrostatic interaction between the basic surface from one molecule

(APAF1) and the acidic surface of the other (caspase-9). Mutations on the highly charged surfaces of either CARD prevent the interaction of these proteins, such as the mutations D27A and E40A in the APAF1 CARD, and the mutations R13A and R56A in the caspase-9 CARD (Qin et al., 1999).

To further analyze the impact of caspase-9 CARD on STS-induced alternative activation of caspase-9 independently of the apoptosome, caspase activity and apoptosis were monitored in Jurkat cells expressing either caspase-9 R13A mutant or the caspase-9 R56A. Interestingly, STS could not induce caspase activation and apoptosis in R13A mutant cells, just like in caspase-9 deficient cells, whereas induction was still possible in caspase-9 R56A mutant cells. The STS-induced caspase-3 activity was delayed in caspase-9 R56A compared to caspase-9 wt Jurkat cells with a caspase-3 activity maximum after 6 h compared to 2 h in caspase-9 wt cells. The apoptosis rate was also reduced in those cells.

These findings substantiate the possibility of an alternative activation of caspase-9 independent of APAF1 binding and apoptosome formation. The delayed caspase-3 activity by STS in the caspase-9 R56A mutant cells indicates less prominent apoptosis pathway compared to the canonical intrinsic apoptosis pathway induced in the caspase-9 wt cells that takes place under certain specialized conditions. Furthermore, the R13A/R56A caspase-9 Jurkat cells represent the cell system of choice when analyzing apoptosome independent apoptosis. With the help of this cell system, drug libraries can be tested for their ability of inducing apoptosis independent of the canonical intrinsic apoptosis pathway. Drugs that induce cell death in R13A/R56A caspase-9 Jurkat cells are potential drugs for cancer therapies, overcoming chemo- and radiotherapy resistance.

Studies with all caspase-9 variants C-terminally tagged with GFP showed similar results compared to their untagged counterpart. With the help of C-terminally tagged caspase-9 wt, R13A, and R56A mutant cells, interaction studies can be carried out, analyzing the possible interaction molecules, which are crucial for caspase-9 activation under STS bypassing the apoptosome and APAF1. GFP-caspase-9 R13A mutant cells can be used as negative control, since STS is not able to induce apoptosis in these cells. GFP-caspase-9 wt cells are suitable as positive control, since under STS conditions, at least APAF1 should interact with caspase-9. These studies are discussed in section 6.1.5.

6.1.4 Staurosporine does not alter the phosphorylation status of caspase-9

Since STS is a highly promiscuous kinase inhibitor that requires caspase-9 for apoptosis induction, it is conceivable that staurosporine induces apoptosis by changing the phosphorylation status of caspase-9. Accordingly, previous studies reported the

phosphorylation of caspase-9 by multiple kinases, such as AKT, ERK1/2, PKCζ, PKA, cAbl, CDK1/cyclin B1, CK2, and DYRK1A, which inhibits caspase-9 activation in different ways, except for phosphorylation of caspase-9 at Y153 by cAbl, which positively regulates caspase-9 autoprocessing. Interestingly, cAbl is the only tyrosine kinase among the caspase-9 kinases (Cardone et al., 1998; Allan et al., 2003; Brady et al., 2005; Martin et al., 2005; Raina et al., 2005; Allan & Clarke, 2007; McDonnell et al., 2008; Seifert et al., 2008). Notably, inhibition of the known kinases targeting caspase-9 activation, and also of putative caspase-9 kinases, detected via a database search, was not able to induce apoptosis in Jurkat cells overexpressing Bcl-2 or vector control cells (Manns et al., 2011).

To clarify the possible alteration of caspase-9 phosphorylation by STS, caspase-9 was immunopurified from caspase-9-GFP expressing Jurkat cells with and without STS treatment and analyzed via 2D-gel analysis and mass spectrometry. Interestingly, none of these methods identified a change in the phosphorylation status of caspase-9 by staurosporine. Moreover, treatment of lysates with lambda phosphatase did also not affect the phosphorylation status of caspase-9 analyzed in 2D-gel analysis. The peptide from amino acid 117 - 146 was detected as phosphorylated by mass spectrometry analysis, but with no significant difference under medium or STS conditions.

It has to be stressed that most of the published phosphorylation sites were analyzed in a cell-free system and not in intact cells. The phosphorylated peptide comprises the phosphorylation residue T125 which was reported to be phosphorylated by ERK1/2, CDK1/cyclin B1, and DYRK1A in an inhibitory way (Allan et al., 2003; Allan & Clarke, 2007; Seifert et al., 2008). However, this phosphorylation site seems to be not relevant for STS-induced apoptosis. The lack of caspase-9 phosphorylation alteration by STS as well as the lack of apoptosis induction by previously tested kinase inhibitors (Manns et al., 2011) could be explained by the fact that caspase-9 is not a target itself, or that other kinases are targeted by STS. Alternatively, STS might target interaction partners of caspase-9, e.g. XIAP, similar as proposed for APAF1 (Deveraux & Reed, 1999; Martin et al., 2005). Caspase-9 inhibitor proteins such as XIAP or other interaction proteins could be disabled by phosphorylation, losing their ability to bind and inhibit caspase-9, which leads to caspase-9 activation. It is also conceivable that, since STS is a broad-range kinase inhibitor, the inhibition of a single kinase is not sufficient for apoptosis induction, but moreover, the combinative inhibition of more than one kinase is required in order to activate caspase-9 in this pathway. In following studies, it has to be further investigated what role phosphorylation has in alternative caspase-9 activation, e.g. with the help of the caspase-9 R13A/R56A Jurkat cell system and a broad-range kinase inhibitor library testing inhibitors both individually and in combination.

6.1.5 Caspase-9 interaction studies

Since phosphorylation studies failed to elucidate the alternative caspase-9 activation by STS, the focus was set on caspase-9 interaction molecules possibly facilitating the activation of caspase-9, e.g. by induced proximity. To date, several multi-protein complexes are known to participate in initiator caspase activation, e.g. the death inducing signaling complex (DISC) composed of death receptor, FADD, and caspase-8 (Kischkel et al., 1995); the Ripoptosome containing the core complex RIP1, FADD, and caspase-8 (Tenev et al., 2011); the PIDDosome comprising PIDD, RAIDD, and caspase-2 (Tinel & Tschopp, 2004); and the apoptosome containing cytochrome c, APAF1, and caspase-9 (Zou et al., 1999). In addition to the apoptosome activating caspase-9, in the absence of Sonic hedgehog (Shh) the protein receptor Patched (Ptc) recruits a protein complex that includes DRAL, the CARD containing domain proteins TUCAN or NALP1, and caspase-9 (Mille et al., 2009). The recruitment of initiator caspases to these complexes is facilitated through homo-dimerized interaction of the pro-domains of initiator caspases, which contain death domains (DDs; caspase-8) or caspase-activating and recruitment domain (CARD; caspase-2/9), and the corresponding domain of the adaptor protein serving as a scaffold for the complex (McIlwain et al., 2013).
Thus, it is conceivable, that upon staurosporine treatment caspase-9 is recruited via its CARD to another multi-protein complex in order to be activated. It was demonstrated that the R13A and R56A CARD mutant Jurkat cells are a highly suitable system for analyzing intrinsic apoptosis induction bypassing the apoptosome and will be a valuable tool for the dissection of caspase-9 interacting molecules during apoptosis induction (see 6.1.3). Therefore, wild type caspase-9, R13A and R56A CARD mutant caspase-9 were immunopurified under medium and staurosporine conditions and analyzed for interaction proteins via mass spectrometry. Of note, the functionality of this study was verified by the increased interaction of caspase-9 wt with APAF1 under staurosporine conditions (negative *t*-Test difference), whereas, as predicted, R13A and R56A mutant caspase-9 were not able to bind APAF1. Of interest are proteins, which bind the R56A caspase-9 mutant under staurosporine conditions. Proteins binding the R13A caspase-9 mutant are not relevant for the investigation of alternative interaction partners possibly activating caspase-9 since this mutant is resistant to STS-induced apoptosis. Interestingly, the interaction of the R56A caspase-9, which lacks interaction with APAF1 but can still mediate STS-induced apoptosis, with the BAG family molecular chaperone regulator 2 (BAG2) is significantly increased under STS conditions. This increase is not as strong as compared to APAF1 and wild type caspase-9, but the apoptosis efficiency is also reduced in caspase-9 R56A mutant Jurkat cells. Notably, BAG2 seems to have a pro-apoptotic function in death of thyroid cancer cells induced by proteasome inhibition (Wang et al., 2008). However, previously reported CARD containing

proteins interacting and activating caspase-9, or enhancing apoptosis, such as TMS1, DCC, or Nod1 were not detected in this study (Inohara et al., 1999; McConnell & Vertino, 2000; Forcet et al., 2001).

Notwithstanding, the promising role of BAG2 in STS-induced apoptosis has to be further elucidated in caspase-9 interaction studies with caspase-9 wild type, and caspase-9 R13/R56A. With the help of siRNA mediated knockdown of BAG2, the dependency of BAG2 regarding the novel intrinsic apoptosis pathway bypassing the apoptosome can be investigated. Moreover, caspase-9 interaction studies, e.g. after one to six hours STS treatment would help analyzing other possible interaction molecules and the understanding of kinetic discrepancy between caspase activation of the canonical intrinsic apoptosis pathway and the novel intrinsic apoptosis pathway.

6.1.6 Conclusions and future perspectives

The broad-range kinase inhibitor staurosporine (STS) is frequently used as a positive control for apoptosis induction. But how the kinase inhibition of more than 100 kinases leads to apoptosis remains elusive. To date it is reported that STS can induce apoptosis over the classical intrinsic mitochondrial pathway, yet also over a novel intrinsic apoptosis pathway. This novel pathway is characterized by the induction of apoptosis in Bcl-2 and Bcl-xL overexpressing cells, independently of APAF1 and the apoptosome formation (Johnson et al., 1999; Manns et al., 2011). In contrast to the findings of Nagata's group that staurosporine can induce apoptosis in mouse fetal thymus cells deficient for caspase-9 (Imao & Nagata, 2013), in Jurkat T-lymphocytes and DT40 B-lymphocytes caspase-9 is prerequisite for the induction of STS-induced apoptosis.

The findings in this thesis further characterized the importance of caspase-9 in STS-induced apoptosis and especially the novel intrinsic apoptosis pathway. In summary, this thesis could demonstrate that the phosphorylation status of caspase-9 is unaltered under STS conditions and therefore the inhibition of caspase-9 kinases seems to be rather irrelevant. This complements the findings that specific inhibition of the reported caspase-9 kinases does not induce apoptosis in Bcl-2 overexpressing cells (Manns et al., 2011). Nevertheless, additional kinase inhibitors should be tested and possibly in combination with each other, that putatively phenocopies STS-induced apoptosis and reveals the crucial kinase or kinases important for the activation of cspase-9 in the novel intrinsic apoptosis pathway. Furthermore, the catalytic activity of caspase-9 is important for STS-induced apoptosis. Not relevant are other proteases, putatively activating caspase-9 through enzymatic cleavage, i.e. cathepsins, calpains, or caspase-4. Moreover, the caspase activation and recruitment domain (CARD) is also essential for the alternative intrinsic apoptosis pathway, indicating

interaction of caspase-9, which is important for the activation and comparable to the apoptosome formation. The caspase-9 R13A and R56A CARD mutant cells, established in this thesis, is a great tool for analyzing activation of apoptosis bypassing the apoptosome. With the help of these cells the identification of CARD-to-CARD interacting molecules crucial for caspase-9 activation next to APAF1 is suitable. Mass spectrometric analysis using this cell system revealed BAG2 as a putative C9-interacting protein, which appears to inducibly associate with caspase-9 upon STS treatment and thus might contribute to the execution of the novel intrinsic apoptosis pathway.

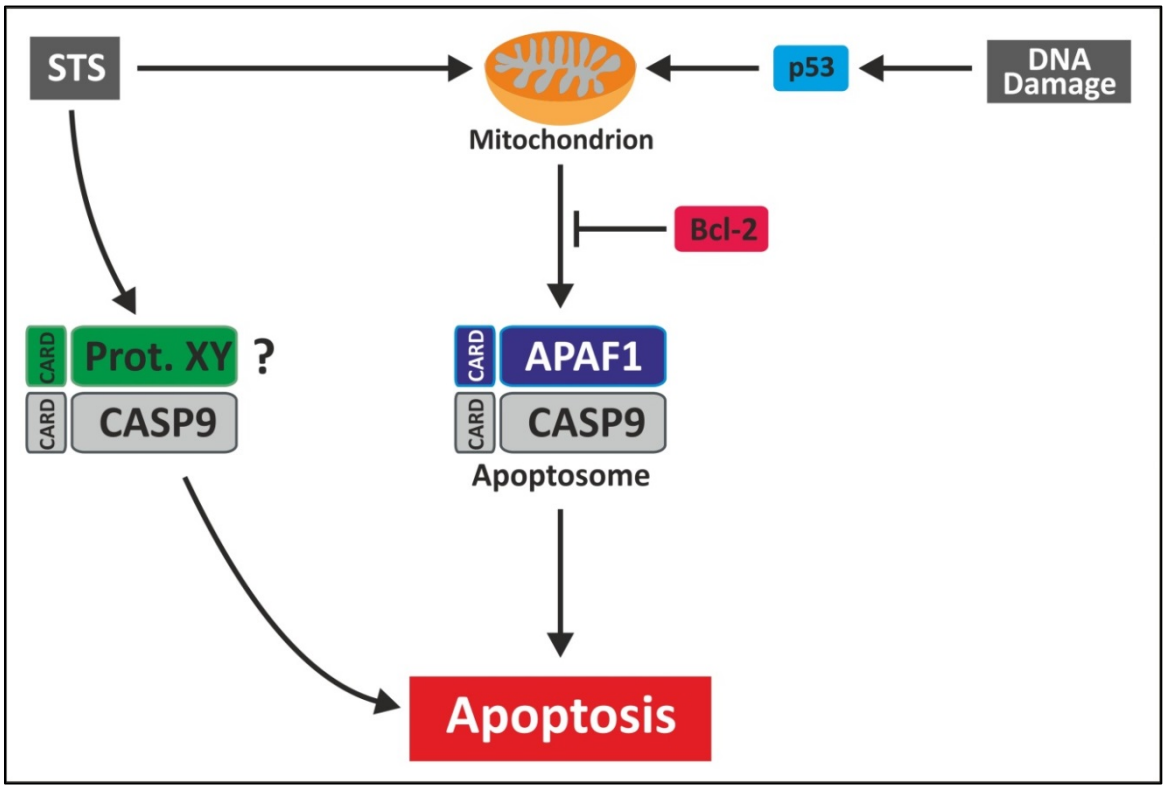

Figure 6-1: Staurosporine induces apoptosis in a dual mode of action. During severe DNA damage, p53 is stabilized and DNA binding capacity is increased which mediates transcriptional activation of apoptotic relevant genes. The canonical intrinsic mitochondrial apoptosis pathway can be induced, mediating the apoptosome formation and activation of the caspase cascade via the initiator caspase-9, which finally leads to apoptosis. Staurosporine (STS) induces apoptosis also via the canonical intrinsic mitochondrial pathway, but, in addition by a novel intrinsic pathway. This pathway bypasses the apoptosome formation and caspase-9 is activated – possibly over a CARD to CARD interaction modus – inducing the caspase cascade and finally apoptosis.

Future studies have to further elucidate the importance of BAG2 for the alternative activation of caspase-9 and the novel intrinsic apoptosis pathway bypassing the apoptosome. With the help of the caspase-9 R13A and R56A CARD mutant cells, drug libraries can be tested, possibly inducing apoptosis independently of the apoptosome. In addition, the characterization of other caspase-9 interacting molecules leading the alternative activation of caspase-9 is of central importance, since every other possibility of inducing apoptosis and the investigation of the mechanism behind this, will increase the chance for overcoming chemo- and radiotherapy resistance in tumor cells.

6.2 Autophagy – Regulation of ULK1

Nowadays, regulation of ULK1 besides phosphorylation is rarely characterized including ubiquitination of ULK1. Nazio et al. previously reported that TRAF6 ubiquitinates ULK1 by K63-Ub linked chains, which stabilizes ULK1.

The aim of the autophagy part of this thesis was to further elucidate the regulation of the ULK1 complex by ubiquitination, setting focus on the role of deubiquitinases (DUBs) in autophagy regulation. First, the interaction of ULK1 with putative DUBs was confirmed and an *in vitro* kinase assay with purified ULK1 and putative interacting DUBs followed. Next, by applying DUB inhibitors, the effect of increased ubiquitination on ULK1 was analyzed, regarding ULK1 ubiquitination status, ULK1 activity, identification of DUBs regulating ULK1 ubiquitination, and the overall autophagic flux.

Taken together:

- DUB inhibition by WP1130 induces the polyubiquitination and aggregation of ULK1/2 and transport to perinuclear aggresome structures
- WP1130 inhibits the overall ULK1/2 kinase activity in the cell, inducing a functional knockdown
- WP1130 inhibits the autophagic flux causally linked to the effect on ULK1/2

6.2.1 ULK1 interacts and phosphorylates USP7 and USP9X

In a previous mass spectrometric analysis of the human autophagy system, ubiquitin-specific protease 10 (USP10) was identified as an interacting DUB of ULK1 (Behrends et al., 2010). Additionally, during mass spectrometric analysis of ULK1-binding proteins, performed by Dr. Antje Löffler, two additional ubiquitin-specific proteases (USPs) – namely USP7/HAUSP and USP9X – were identified.

To further validate the interaction of ULK1 with USP7 and USP9X, co-immunopurification studies and an in *vitro* kinase assay, for analyzing possible phosphorylation of these USPs by ULK1, were carried out. The impact on ULK1 stability was analyzed with the help of two DUB inhibitors, inhibiting USP7 and USP9X.

The co-immunopurification studies verified USP7 and USP9X as ULK1 interacting proteins. This could also be demonstrated in an *in vitro* kinase assay, as ULK1 phosphorylates USP7 and USP9X, identifying those DUBs as potential substrates of ULK1. The inhibition of USP7 by HBX 41108 had no influence on ULK1 stability, whereas inhibition of USP9X by WP1130 (also known as degrasyn) leads to reduced levels of ULK1 in immunoblot analysis of cleared cell lysates (also termed detergent-soluble cell fraction). The partially selective DUB inhibitor

WP1130 inhibiting USP5, USP9X, USP14, UCH-L1, and UCH-L5 was originally identified during a library screen for small molecules that inhibit IL-6-induced phosphorylation of STAT3 (Bartholomeusz et al., 2007; Kapuria et al., 2010; Kapuria et al., 2011). The mechanism how WP1130 leads to reduced ULK1 levels has to be further investigated and also the vice versa influence on USP7 and USP9X by ULK1 phosphorylation remains unclear so far. The influence of ULK1/2 on USP7 and USP9X could be further analyzed in ULK1/2 wt and double-knockout cells comparing the ubiquitination status of reported substrates in these cells, i.e. p53 and Mcl-1 ubiquitination (Li et al., 2002; Schwickart et al., 2010). Yet another DUB activity readout may be carried out in for instance HEK293 cells, silenced for ULK1/2 and the subsequent incubation of the respective USP with Ub-AMC followed by a fluorometric analysis.

6.2.2 WP1130 reduces ULK1 in detergent-soluble fraction independent of proteolytic, proteasomal, and autophagic degradation

One explanation for the reduced levels of ULK1 upon WP1130 treatment detected by immunoblot analysis is that DUB inhibition leads to increased K48-linked ubiquitination of ULK1, which is reported to tag proteins for proteasomal degradation (Hershko & Ciechanover, 1992). Another possibility is the increased degradation of ULK1 by autophagic processes, or through various proteases like caspases, calpains, or cathepsins.

To further analyze the WP1130 induced reduction of ULK1 levels, GFP-ULK1 expressing Flp-In™ T-REx™ 293 cells and HEK293 cells were treated with WP1130 and co-treated with proteasome, autophagy, caspase, calpain, and cathepsin inhibitors, respectively. None of these inhibitors reversed the ULK1 reduction upon WP1130 treatment, suggesting a WP1130 function independent of proteasomal, autophagic, and proteolytic activity regarding caspases, calpains, and cathepsins. The reduction of ULK1 levels in detergent-soluble fraction induced by WP1130 remained unclear.

6.2.3 WP1130 induces a reversible shift of ULK1 from detergent-soluble to -insoluble fraction by aggregation and transfer to aggresomes

Former studies demonstrated that WP1130 triggers the loss of JAK2 from the detergent-soluble cell fraction and a corresponding increase of JAK2 within the detergent-insoluble fraction with no decline of total JAK2 protein levels from whole cell lysates, and the formation of an aggresome within the cells (Kapuria et al., 2010; Kapuria et al., 2011).

This effect is also conceivable regarding ULK1, as this would explain the reduced levels of ULK1 in cleared cell lysates. Thus, GFP-ULK1/2 expressing Flp-In™ T-REx™ 293 cells, Hek293, U2O2, and HeLa cells were treated with WP1130 and the detergent-soluble and -insoluble cell fractions were analyzed by immunoblotting and confocal microscopy.

Indeed, the results reflect the former studies regarding JAK2 (Kapuria et al., 2010; Kapuria et al., 2011). WP1130 treatment triggers the shift of GFP-ULK1 and endogenous ULK1 from the detergent-soluble to the -insoluble fractions in GFP-ULK1 expressing Flp-In™ T-REx™ 293 cells and various human ULK1 wild type expressing cell lines. This reduction is induced in a reversible manner and overall ULK1 levels were not affected. Furthermore, aggregation of and aggresome formation was induced in GFP-ULK1 as well in GFP-ULK2 expressing Flp-In™ T-REx™ 293 cells. The observed effect of aggregation and aggresome formation upon WP1130 treatment might be caused by proteasomal overload due to the accumulation of ubiquitinated proteins and ULK1 in particular (Johnston et al., 1998). Aggregated proteins cannot properly be unfolded to pass the proteolytic barrel of the proteasome and can in fact inhibit the proteasome activity (Snyder et al., 2003). Consequently, the aggresome pathway can be activated and ULK1 aggregates are transported to the microtubule organizing center (MTOC), where aggresomes are formed (Johnston et al., 1998). The aggresome formation is considered as a cyto-protective response, enabling the sequestration of potentially toxic misfolded proteins and the subsequent clearance by autophagy (Chin et al., 2010). Another possibility could be that ULK1 is indeed regulated by a specific ubiquitin conjugation-deconjugation cycle that is disrupted by WP1130 treatment. The reversible effect of WP1130 substantiates a possible physiological role of ULK1 aggregation, since irreversible effects would harm the cell.

6.2.4 Characterization of WP1130 induced aggregate and aggresome structures

In the case of aggresome pathway activation, polyubiquitinated protein aggregates are transported via microtubule tracts to the MTOC forming aggresome. The histone deacetylase 6 (HDAC6) plays a key role in this mechanism by binding polyubiquitinated aggregates and dynactin, a component of the dynein motor complex, hence bridging the ubiquitinated proteins to the dynein motor complex (Kawaguchi et al., 2003; Dompierre et al., 2007). Accordingly, it has been demonstrated that interference with microtubule polymerisation inhibits aggresome formation e.g. inhibition with nocodazole (Johnston et al., 1998). It has also been shown that multiple proteins are involved in the formation of protein aggregates and the aggresome e.g. different types of ubiquitin and SQSTM1/p62, a polyubiquitin-binding protein.

To further clarify the formation of aggregates and aggresomes and their constitution, GFP-ULK1 expressing cells were treated with WP1130 with and without nocodazole and analyzed via live cell imaging. Cells treated with WP1130 were immunostained for ubiquitin, K63-linked ubiquitin, and SQSTM1 and analyzed via confocal microscopy.

WP1130 treatment led to the formation of aggregates and one aggresome per cell, which is positive for ubiquitin, K63-linked ubiquitin, and partly SQSTM1. The aggresome formation is abolished by inhibition of the microtubule transportation machinery. These results strongly indicate that WP1130 induces the formation of ULK1 aggregates, which are subsequently transported to the MTOC to form an aggresome. The detection of ubiquitin within the aggresome was conceivable since WP1130 induces DUB inhibition and therefore polyubiquitinated proteins accumulate in the cell and thus the aggresome pathway is induced. The finding that those aggresomes are strongly positive for K63-linked ubiquitin is interesting, since ULK1 seems to be ubiquitinated by TRAF6 under autophagy inducing conditions in a K63-linked polyubiquitin manner (Nazio et al., 2013). Also the involvement of SQSTM1 as a polyubiquitin binding protein seems plausible. The role of SQSTM1 in ULK1 aggregation and aggresome transport has to be further investigated as well as the ubiquitination of ULK1 in detail. The influence of SQSTM1 could be performed in SQSTM1 knockdown cells, comparing the formation GFP-ULK1 aggregates upon WP1130 treatment to control cells.

6.2.5 DUB inhibition leads to increased ULK1 ubiquitination

Upon WP1130 treatment, aggresomes are formed which are positive for GFP-ULK1, ubiquitin, and K63-linked ubiquitin. However, the conclusion that WP1130 triggers increased ULK1 ubiquitination is not stringent so far. Recently, it has been reported that WP1130 treatment leads to the accumulation of JAK2 containing K63-linked ubiquitin chains and generally to the accumulation of cellular proteins containing both K48- and K63-linked polyubiquitin chains (Kapuria et al., 2010; Kapuria et al., 2011).

To further elucidate the ubiquitination status of ULK1 after WP1130 treatment, GFP-ULK1 was immunopurified with and without WP1130 incubation and analyzed for different types of ubiquitination with the help of transfection of various types of cDNAs encoding HA-tagged ubiquitin prior to immunoblot analysis against HA, ubiquitin, and ULK1. A vice versa approach, by which ubiquitinated proteins were affinity purified, was also performed.

WP1130 induced the ubiquitination of GFP-ULK1 and endogenous ULK1. Immunopurified GFP-ULK1 apparently contains non-K48/non-K63-linked ubiquitin chains. That K63-linked ubiquitin chains were not detected can be due to the fact that detergent-soluble cell fractions were analyzed and not whole cell lysates. The above mentioned detection of K63-

linked ubiquitin of the aggresome by immunostaining, could not be investigated by immunopurification assay of detergent-soluble cell fraction due to the resistance of aggregates and aggresomes to these conditions. During the trafficking from the soluble to the insoluble fraction potentially the “ubiquitin barcode” of ULK1 might vary. Collectively, these results demonstrate an increase of ULK1 ubiquitination, which is a strong indication that WP1130 inhibits DUBs which under normal conditions deubiquitinate ULK1. The loss of DUB activity leads to polyubiquitination of ULK1, aggregation, and aggresome formation. In combination with the confocal microscopy results, ULK1 within the aggresome structures seems to be ubiquitinated in a K63-linked polyubiquitin manner. Further studies have to elucidate the specific ubiquitination sites of ULK1 and the prominent subtypes of ubiquitin linkage in ULK1 soluble and insoluble cell fraction. This could be performed via mass spectrometric analysis of immunopurified GFP-ULK1 under WP1130 conditions regarding post-translational modification by ubiquitin. If lysines within the ULK1 protein are identified as ubiquitinated, they can be mutated and ectopically expressed in cells followed by WP1130 treatment and morphological investigation of ULK1 aggregation. This will help analyzing the physiological role of ULK1 ubiquitination and regulation.

6.2.6 Reported WP1130 targets do not participate in ULK1 aggregation

To date it is reported that ULK1 is K63-linkage specific ubiquitinated by TRAF6, a E3 ubiquitin ligase, under the control of mTOR, which has a positive influence on the stabilization of ULK1 (Nazio et al., 2013). Next to TRAF6, it has been reported that the COP1 E3 ligase interacts with RB1CC1 of the ULK1 complex. In contrast, the authors did not observe any alterations of ULK1 stabilization upon ectopic expression of COP1 (Kobayashi et al., 2013). It is likely that additional E3 ligases targeting the ULK1 complex will be identified in the future. The regulation of protein ubiquitination is often performed by an enzymatic counterpart, the DUBs, e.g. the ubiquitination of p53 by Mdm2 and its deubiquitination and stabilization by USP7 (Li et al., 2002). Furthermore, since DUB inhibition leads to increased ULK1 ubiquitination and USP7, USP9X, and USP10 were detected in mass spectrometry analysis of ULK1-binding proteins, it is conceivable that DUB(s) target ULK1 by cleaving ubiquitin-chains enzymatically from ubiquitinated residues.

Next, it was investigated which DUB(s) regulate ULK1 ubiquitination. Therefore, knockdown of known WP1130 targets was performed and ULK1 levels were analyzed via immunoblot for a possible imitation of the WP1130 effect. The same was performed in USP9X knockout cells, since USP9X is the main target of WP1130 (Kapuria et al., 2010; Sun et al., 2011; Peddaboina

et al., 2012; Peng et al., 2014; Wang et al., 2014). In the last approach, the inhibitory potential of WP1130 was tested in a DUB*profiler™* Single Point Screen including 35 DUBs.

Neither the knockdown of WP1130 targets nor the USP9X knockout cells could mimic the results obtained after WP1130 treatment, since the ULK1 levels in the soluble fraction remained unaltered. None of the tested DUBs, including the five enzymes recently reported to be inhibited by WP1130, was significantly inhibited by 1 or 10 µM WP1130. Apparently, the reported WP1130 targets are not or at least only partially involved in the regulation of ULK1. Additionally, inhibition of the published ULK1 interacting deubiquitinase USP10 with spautin-1 (**Figure 5-15, A**) and the inhibition of USP-7 by HBX 41108 (**Figure 5-8, C**) did not reduce ULK1 levels in the soluble cell fraction (Behrends et al., 2010). Taken together, it is well conceivable that additional DUBs or a combination of several DUBs mediate the effect of WP1130 on ULK1, since the human genome encodes 79 DUBs, subdivided into five subfamilies, which are predicted to be catalytically active (Komander et al., 2009). It is of tremendous interest to find the DUB(s) regulating ULK1 ubiquitination, which would be a central issue for the understanding of ULK1 regulation. This could be analyzed via immunopurification of polyubiquitinated ULK1 under WP1130 conditions and its subsequent incubation with certain DUBs followed by immunoblotting of ULK1 to detect a possible change of the ubiquitination status.

6.2.7 The pan-DUB inhibitor PR619 mimics the effect of WP1130 on ULK1

Since the inhibitory potential of WP1130 could not be confirmed in the DUB*profiler™* Single Point Screen of 35 DUBs, it has to be validated that the effect of WP1130 on ULK1 is truly dependent on DUB inhibition.

To clarify the DUB dependency of the WP1130 effect, HEK293 cells were treated with the pan-DUB inhibitor PR619, which is reported to inhibit all of the putative DUBs targeted by WP1130 and others (Altun et al., 2011), and the two more specific DUB inhibitors LDN 57444 inhibiting UCH-L1 (Liu et al., 2003), and spautin-1 inhibiting USP10 and USP13 (Liu et al., 2011) followed by immunoblotting for ULK1.

The more specific inhibitors spautin-1 and LDN 57444 were not able to mimic the effect of WP1130 in case of reduction of ULK1 levels in the detergent-soluble cell fraction, whereas PR619 could mimic the reduction of ULK1 levels by WP1130. A shift of ULK1 from the detergent-soluble to the -insoluble fraction could also be detected upon PR619 treatment. These results strongly indicate a DUB dependent effect of WP1130 on ULK1.

6.2.8 WP1130 does not induce aggregation of other components of the ULK1 or the PtdIns3K class III complex

To date it has been reported that WP1130 induced USP9X inhibition triggers the destabilization or aggregation of the kinases JAK2 and Bcr-Abl, the anti-apoptotic Bcl-2 protein Mcl-1, and the transcription factor ERG (Kapuria et al., 2010; Kapuria et al., 2011; Sun et al., 2011; Wang et al., 2014). Since several proteins are affected by WP1130, it is questionable whether WP1130 has also an effect on other components of the ULK1 complex and further ATG proteins e.g. components of the PtdIns3K class III complex.

Hence, the protein levels of ULK1, RB1CC1, ATG13, AMBRA1, and BECN1 in the detergent-soluble and -insoluble fraction were analyzed via immunoblotting after WP1130 treatment.

Notably, ULK1 was the only ATG protein, shifting from the soluble to the insoluble fraction. All other tested ATG protein levels in the soluble fraction remained unaltered. Apparently, the WP1130 effect on ULK1 is rather exclusive regarding other ATG proteins. This conclusion is essential for the following investigation concerning the functionality of ULK1 upon WP1130 treatment and the impact on autophagy since a potential effect on autophagy induced by WP1130 could not be linked to ULK1 if other components of the autophagy machinery are affected.

6.2.9 ULK1 activity is inhibited by WP1130

Previously, it has been reported that WP1130 induced JAK2 K63-linked ubiquitination resulting in trafficking by HDAC6 to perinuclear aggresomes. The kinase activity is lost during the process of aggresome formation (Kapuria et al., 2011). Thus, it is likely that WP1130 induced aggregation and subsequent aggresome formation of ULK1 also results in a loss of ULK1 kinase activity.

To clarify the putative WP1130 dependent inhibition of ULK1 activity, GFP-ULK1 expressing Flp-In™ T-REx™ 293 and HEK293 cells were treated with WP1130 and analyzed for ULK1 activity by immunoblotting of ULK1 substrates or indirect regulated proteins.

Indeed, ULK1 activity was reduced in GFP-ULK1 overexpressing cells and on endogenous level upon WP1130 treatment. To further exclude a direct inhibition of WP1130 on ULK1 e.g. by binding of the ULK1 catalytic center, an *in vitro* kinase assay was carried out, which demonstrated that WP1130 had no direct effect on ULK1 kinase activity. These results clearly reveal the inhibition of ULK1 overall kinase activity via a functional knockdown by WP1130. Accordingly, in the following part the impact of WP1130 dependent inactivation of ULK1 on autophagy was characterized.

6.2.10 The autophagic flux is inhibited by WP1130

Since the ULK1 complex and ULK1 in particular is important for autophagy initiation, it has to be clarified which impact the WP1130 induced inhibition of ULK1 activity has on autophagy and the autophagic flux. Therefore, HEK293 cells were analyzed regarding the autophagic flux by LC3 lipidation assay and subsequent immunoblotting or confocal microscopy, and in addition in HEK293, HeLa, and U2OS cells a long-lived protein degradation assay was performed.

WP1130 treatment led to the inhibition of autophagic flux in HEK293 cells and the long-lived protein degradation assay showed also an inhibition of autophagy induced by amino-acid starvation in HEK293, HeLa, and U2OS cells under WP1130 conditions. Since WP1130 inhibits both ULK1 activity and also autophagy the question arose, if there is a causal context between the loss of ULK1 activity and the inhibition of autophagy. Moreover, the stage at which WP1130 inhibits autophagy has to be further elucidated. This could be carried out by electron microscopy analysis of WP1130 treated cells and morphological characterization of autophagosomes compared with early and late inhibition of autophagy, i.e. with 3-MA and $BafA_1$, respectively, or several ATG knockout cells.

6.2.11 Autophagy inhibition induced by WP1130 is linked to ULK1/2

To date three ULK1/2-deficient vertebrate cell systems have been reported, the *ULK1/2*-/- chicken DT40 cell line and two separately generated *Ulk1/2*-/- murine embryonic fibroblasts (MEFs) (Alers et al., 2011; Cheong et al., 2011; McAlpine et al., 2013). In two cell lines autophagy induction independently of ULK1/2 has been described (Alers et al., 2011; Cheong et al., 2011). Autophagy can be induced upon amino acid starvation with EBSS in ULK1/2 deficient DT40 cells and upon glucose starvation in ULK1/2 deficient MEFs. In contrast to the DT40 ULK1/2 deficient cells, in ULK1/2 deficient MEFs amino acid starvation cannot induce autophagy. In theory, if WP1130 induced inhibition of autophagy is causally associated with loss of ULK1 kinase activity, autophagy should occur normally upon WP1130 treatment in wild type and *ULK1/2*-/- DT40 cells treated with EBSS and in wild type and *Ulk1/2*-/- MEFs under glucose starvation.

To clarify the causal context between the loss of ULK1 activity and autophagy inhibition upon WP1130 treatment, autophagy was induced in ULK1/2 deficient DT40 cells and MEFs and their corresponding wild type cell lines, in the presence and absence of WP1130. As autophagy readout in DT40 cells, LC3 lipidation was analyzed by immunoblot and confocal microscopy. LC3 lipidation was also assessed by immunoblot in MEFs, and furthermore the degradation of mCitrine-LC3 was measured by flow cytometry.

In both cell lines, autophagy and the autophagic flux occurred normally under the influence of WP1130 in wild type and also ULK1/2 deficient cells. WP1130 treatment was not able to inhibit autophagy induction by EBSS or glucose deprivation, respectively. Taken together, these results demonstrate that WP1130 inhibits autophagy, which is causally connected to the loss of ULK1 kinase activity. A functional knockdown of ULK1/2 induced by DUB inhibition through WP1130 results in the inhibition of autophagy.

6.2.12 Conclusions and future perspectives

In summary, this thesis could demonstrate, in addition to prior studies showing the binding of ULK1 and USP10 (Behrends et al., 2010), that ULK1 interacts with two other deubiquitinases USP7 and USP9X, and phosphorylates these DUBs. However, USP7, USP9X, and USP10 had no influence on ULK1 stability when inhibited each alone or down regulated by siRNA knockdown, respectively. Notably, DUB inhibition by WP1130 influences ULK1 stability, which leads to the shift of ULK1 from the detergent-soluble cell fraction to the detergent-insoluble fraction, caused by aggregation of ULK1. These aggregates are transported via the microtubule network to the MTOC to form an aggresome in the cell. During this DUB inhibition, ULK1 gets polyubiquitinated. In the detergent-soluble cell fraction, ULK1 contains non-K48/non-K63-linked ubiquitin chains. Apparently, insoluble ULK1 stored in the aggresome seems to be K63-linkage specific ubiquitinated. This indicates that DUB(s) inhibited by WP1130 regulates ULK1 ubiquitination and maybe K63-linked ubiquitination of the reported E3 ubiquitin ligase TRAF6 regulating ULK1 stabilization (Nazio et al., 2013). Notably, WP1130 induces the inhibition of ULK1 activity, since aggregated ULK1 is not able to fulfil its normal function. Moreover, WP1130 also inhibits autophagy and the autophagic flux in human cell lines, in which ULK1/2 is indispensable for autophagy induction, whereas under ULK1/2 independent autophagy conditions, WP1130 cannot execute its inhibitory potential. This suggests a ULK1/2 dependent inhibition of autophagy by WP1130.

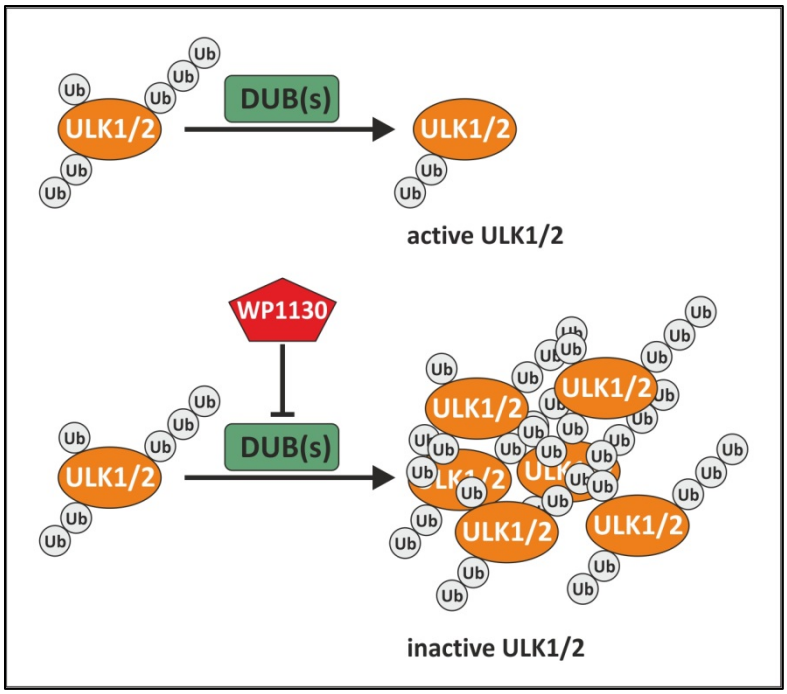

Figure 6-2: DUB inhibition leads to ULK1/2 aggregation, loss of ULK1/2 activity and autophagy inhibition. Deubiquitinases (DUBs) regulate the ubiquitination status of ULK1 and function as a counterpart to ULK1 E3 ubiquitin ligases e.g. TRAF6. Upon DUB inhibition by WP1130, ULK1 polyubiquitination is increased. This results in ULK1 aggregation, inactivation of ULK1 kinase activity, and finally inhibition of autophagy.

Future studies have to address the question which DUB(s) in particular regulate ULK1 ubiquitination and *vice versa* what impact has ULK1 on DUBs, i.e. USP7 and USP9X. The ULK1 ubiquitination pattern, in detail which lysine residues are ubiquitinated under certain conditions has to be analyzed. Moreover, the linkage specificity is of tremendous importance, since various linkages have various functional relevance.

Collectively, DUB inhibition by WP1130 represents an efficient tool to inhibit autophagy in general and to modulate ULK1 activity in particular. Next to the direct inhibition of ULK1 kinase activity (Petherick et al., 2015), the regulation of ULK1 ubiquitination might be an effective approach to modulate the autophagic response. It has been proposed that anticancer drugs induce cyto-protective autophagy, leading to impaired efficacy of these compounds (Wong et al., 2013). Therefore, combinatorial therapies of these anticancer agents and in parallel the ULK1 inhibition might represent a promising anticancer strategy.

7 References

Acehan D, Jiang X, Morgan DG, Heuser JE, Wang X, Akey CW (2002). Three-dimensional structure of the apoptosome: implications for assembly, procaspase-9 binding, and activation. *Mol Cell* **9**: 423-432

Al Rawi S, Louvet-Vallee S, Djeddi A, Sachse M, Culetto E, Hajjar C, . . . Galy V (2012). Allophagy: a macroautophagic process degrading spermatozoid-inherited organelles. *Autophagy* **8**: 421-423

Alemu EA, Lamark T, Torgersen KM, Birgisdottir AB, Larsen KB, Jain A, . . . Johansen T (2012). ATG8 family proteins act as scaffolds for assembly of the ULK complex: sequence requirements for LC3-interacting region (LIR) motifs. *J Biol Chem* **287**: 39275-39290

Alers S, Löffler AS, Paasch F, Dieterle AM, Keppeler H, Lauber K, . . . Stork B (2011). Atg13 and FIP200 act independently of Ulk1 and Ulk2 in autophagy induction. *Autophagy* **7**: 1423-1433

Alers S, Löffler AS, Wesselborg S, Stork B (2012). The incredible ULKs. *Cell communication and signaling : CCS* **10**: 7

Allan LA, Clarke PR (2007). Phosphorylation of caspase-9 by CDK1/cyclin B1 protects mitotic cells against apoptosis. *Mol Cell* **26**: 301-310

Allan LA, Clarke PR (2009). Apoptosis and autophagy: Regulation of caspase-9 by phosphorylation. *FEBS J* **276**: 6063-6073

Allan LA, Morrice N, Brady S, Magee G, Pathak S, Clarke PR (2003). Inhibition of caspase-9 through phosphorylation at Thr 125 by ERK MAPK. *Nat Cell Biol* **5**: 647-654

Altun M, Kramer HB, Willems LI, McDermott JL, Leach CA, Goldenberg SJ, . . . Kessler BM (2011). Activity-based chemical proteomics accelerates inhibitor development for deubiquitylating enzymes. *Chem Biol* **18**: 1401-1412

Araki Y, Ku WC, Akioka M, May AI, Hayashi Y, Arisaka F, . . . Ohsumi Y (2013). Atg38 is required for autophagy-specific phosphatidylinositol 3-kinase complex integrity. *J Cell Biol* **203**: 299-313

Ashkenazi A, Pai RC, Fong S, Leung S, Lawrence DA, Marsters SA, . . . Schwall RH (1999). Safety and antitumor activity of recombinant soluble Apo2 ligand. *The Journal of clinical investigation* **104**: 155-162

Axe EL, Walker SA, Manifava M, Chandra P, Roderick HL, Habermann A, . . . Ktistakis NT (2008). Autophagosome formation from membrane compartments enriched in phosphatidylinositol 3-phosphate and dynamically connected to the endoplasmic reticulum. *J Cell Biol* **182**: 685-701

Baba TW, Giroir BP, Humphries EH (1985). Cell lines derived from avian lymphomas exhibit two distinct phenotypes. *Virology* **144**: 139-151

Baba TW, Humphries EH (1984). Differential response to avian leukosis virus infection exhibited by two chicken lines. *Virology* **135**: 181-188

Bain J, Plater L, Elliott M, Shpiro N, Hastie CJ, McLauchlan H, . . . Cohen P (2007). The selectivity of protein kinase inhibitors: a further update. *Biochem J* **408**: 297-315

Bartholomeusz GA, Talpaz M, Kapuria V, Kong LY, Wang S, Estrov Z, . . . Donato NJ (2007). Activation of a novel Bcr/Abl destruction pathway by WP1130 induces apoptosis of chronic myelogenous leukemia cells. *Blood* **109**: 3470-3478

Behrends C, Sowa ME, Gygi SP, Harper JW (2010). Network organization of the human autophagy system. *Nature* **466**: 68-76

Belmokhtar CA, Hillion J, Segal-Bendirdjian E (2001). Staurosporine induces apoptosis through both caspase-dependent and caspase-independent mechanisms. *Oncogene* **20**: 3354-3362

Bharate SB, Sawant SD, Singh PP, Vishwakarma RA (2013). Kinase inhibitors of marine origin. *Chem Rev* **113**: 6761-6815

Billard C (2012). Design of novel BH3 mimetics for the treatment of chronic lymphocytic leukemia. *Leukemia* **26**: 2032-2038

Bitzer M, Armeanu S, Prinz F, Ungerechts G, Wybranietz W, Spiegel M, . . . Lauer UM (2002). Caspase-8 and Apaf-1-independent caspase-9 activation in Sendai virus-infected cells. *J Biol Chem* **277**: 29817-29824

Boatright KM, Renatus M, Scott FL, Sperandio S, Shin H, Pedersen IM, . . . Salvesen GS (2003). A unified model for apical caspase activation. *Mol Cell* **11**: 529-541

Boesen-de Cock JG, de Vries E, Williams GT, Borst J (1998). The anti-cancer drug etoposide can induce caspase-8 processing and apoptosis in the absence of CD95 receptor-ligand interaction. *Apoptosis* **3**: 17-25

Boise LH, Gonzalez-Garcia M, Postema CE, Ding L, Lindsten T, Turka LA, . . . Thompson CB (1993). bcl-x, a bcl-2-related gene that functions as a dominant regulator of apoptotic cell death. *Cell* **74**: 597-608

Bradford MM (1976). A rapid and sensitive method for the quantitation of microgram quantities of protein utilizing the principle of protein-dye binding. *Anal Biochem* **72**: 248-254

Brady SC, Allan LA, Clarke PR (2005). Regulation of caspase 9 through phosphorylation by protein kinase C zeta in response to hyperosmotic stress. *Mol Cell Biol* **25**: 10543-10555

Brattain MG, Fine WD, Khaled FM, Thompson J, Brattain DE (1981). Heterogeneity of malignant cells from a human colonic carcinoma. *Cancer Res* **41**: 1751-1756

Bratton SB, Walker G, Srinivasula SM, Sun XM, Butterworth M, Alnemri ES, Cohen GM (2001). Recruitment, activation and retention of caspases-9 and -3 by Apaf-1 apoptosome and associated XIAP complexes. *EMBO J* **20**: 998-1009

Brill A, Torchinsky A, Carp H, Toder V (1999). The role of apoptosis in normal and abnormal embryonic development. *J Assist Reprod Genet* **16**: 512-519

Brugarolas J, Lei K, Hurley RL, Manning BD, Reiling JH, Hafen E, . . . Kaelin WG, Jr. (2004). Regulation of mTOR function in response to hypoxia by REDD1 and the TSC1/TSC2 tumor suppressor complex. *Genes Dev* **18**: 2893-2904

Budanov AV, Karin M (2008). p53 target genes sestrin1 and sestrin2 connect genotoxic stress and mTOR signaling. *Cell* **134**: 451-460

Cabal-Hierro L, Lazo PS (2012). Signal transduction by tumor necrosis factor receptors. *Cell Signal* **24**: 1297-1305

Cardone MH, Roy N, Stennicke HR, Salvesen GS, Franke TF, Stanbridge E, . . . Reed JC (1998). Regulation of cell death protease caspase-9 by phosphorylation. *Science* **282**: 1318-1321

Chan EY, Kir S, Tooze SA (2007). siRNA screening of the kinome identifies ULK1 as a multidomain modulator of autophagy. *J Biol Chem* **282**: 25464-25474

Chan EY, Longatti A, McKnight NC, Tooze SA (2009). Kinase-inactivated ULK proteins inhibit autophagy via their conserved C-terminal domains using an Atg13-independent mechanism. *Mol Cell Biol* **29**: 157-171

Chan EY, Tooze SA (2009). Evolution of Atg1 function and regulation. *Autophagy* **5**: 758-765

Chao Y, Shiozaki EN, Srinivasula SM, Rigotti DJ, Fairman R, Shi Y (2005). Engineering a dimeric caspase-9: a re-evaluation of the induced proximity model for caspase activation. *PLoS biology* **3**: e183

Chen DJ, Huerta S (2009). Smac mimetics as new cancer therapeutics. *Anticancer Drugs* **20**: 646-658

Cheong H, Lindsten T, Wu J, Lu C, Thompson CB (2011). Ammonia-induced autophagy is independent of ULK1/ULK2 kinases. *Proc Natl Acad Sci U S A* **108**: 11121-11126

Chin LS, Olzmann JA, Li L (2010). Parkin-mediated ubiquitin signalling in aggresome formation and autophagy. *Biochem Soc Trans* **38**: 144-149

Choi SS, Park IC, Yun JW, Sung YC, Hong SI, Shin HS (1995). A novel Bcl-2 related gene, Bfl-1, is overexpressed in stomach cancer and preferentially expressed in bone marrow. *Oncogene* **11**: 1693-1698

Chowdhury I, Tharakan B, Bhat GK (2008). Caspases - an update. *Comp Biochem Physiol B Biochem Mol Biol* **151**: 10-27

Clague MJ, Coulson JM, Urbe S (2012). Cellular functions of the DUBs. *J Cell Sci* **125**: 277-286

Colland F, Formstecher E, Jacq X, Reverdy C, Planquette C, Conrath S, . . . Daviet L (2009). Small-molecule inhibitor of USP7/HAUSP ubiquitin protease stabilizes and activates p53 in cells. *Mol Cancer Ther* **8**: 2286-2295

Crawford ED, Wells JA (2011). Caspase substrates and cellular remodeling. *Annu Rev Biochem* **80**: 1055-1087

Czabotar PE, Lessene G, Strasser A, Adams JM (2014). Control of apoptosis by the BCL-2 protein family: implications for physiology and therapy. *Nat Rev Mol Cell Biol* **15**: 49-63

Davies SP, Reddy H, Caivano M, Cohen P (2000). Specificity and mechanism of action of some commonly used protein kinase inhibitors. *Biochem J* **351**: 95-105

de Almagro MC, Vucic D (2012). The inhibitor of apoptosis (IAP) proteins are critical regulators of signaling pathways and targets for anti-cancer therapy. *Exp Oncol* **34**: 200-211

Declercq W, Vanden Berghe T, Vandenabeele P (2009). RIP kinases at the crossroads of cell death and survival. *Cell* **138**: 229-232

Deter RL, Baudhuin P, De Duve C (1967). Participation of lysosomes in cellular autophagy induced in rat liver by glucagon. *The Journal of cell biology* **35**: C11-16

Deveraux QL, Reed JC (1999). IAP family proteins--suppressors of apoptosis. *Genes Dev* **13**: 239-252

DeYoung MP, Horak P, Sofer A, Sgroi D, Ellisen LW (2008). Hypoxia regulates TSC1/2-mTOR signaling and tumor suppression through REDD1-mediated 14-3-3 shuttling. *Genes Dev* **22**: 239-251

Di Bartolomeo S, Corazzari M, Nazio F, Oliverio S, Lisi G, Antonioli M, . . . Fimia GM (2010). The dynamic interaction of AMBRA1 with the dynein motor complex regulates mammalian autophagy. *J Cell Biol* **191**: 155-168

Dimberg LY, Anderson CK, Camidge R, Behbakht K, Thorburn A, Ford HL (2013). On the TRAIL to successful cancer therapy? Predicting and counteracting resistance against TRAIL-based therapeutics. *Oncogene* **32**: 1341-1350

Dompierre JP, Godin JD, Charrin BC, Cordelieres FP, King SJ, Humbert S, Saudou F (2007). Histone deacetylase 6 inhibition compensates for the transport deficit in Huntington's disease by increasing tubulin acetylation. *J Neurosci* **27**: 3571-3583

Egan DF, Shackelford DB, Mihaylova MM, Gelino S, Kohnz RA, Mair W, . . . Shaw RJ (2011). Phosphorylation of ULK1 (hATG1) by AMP-activated protein kinase connects energy sensing to mitophagy. *Science* **331**: 456-461

Elmore S (2007). Apoptosis: a review of programmed cell death. *Toxicol Pathol* **35**: 495-516

Fabian MA, Biggs WH, 3rd, Treiber DK, Atteridge CE, Azimioara MD, Benedetti MG, . . . Lockhart DJ (2005). A small molecule-kinase interaction map for clinical kinase inhibitors. *Nat Biotechnol* **23**: 329-336

Fadok VA, Voelker DR, Campbell PA, Cohen JJ, Bratton DL, Henson PM (1992). Exposure of phosphatidylserine on the surface of apoptotic lymphocytes triggers specific recognition and removal by macrophages. *Journal of immunology* **148**: 2207-2216

Fass E, Shvets E, Degani I, Hirschberg K, Elazar Z (2006). Microtubules support production of starvation-induced autophagosomes but not their targeting and fusion with lysosomes. *J Biol Chem* **281**: 36303-36316

Feng Y, He D, Yao Z, Klionsky DJ (2014). The machinery of macroautophagy. *Cell Res* **24**: 24-41

Fimia GM, Di Bartolomeo S, Piacentini M, Cecconi F (2011). Unleashing the Ambra1-Beclin 1 complex from dynein chains: Ulk1 sets Ambra1 free to induce autophagy. *Autophagy* **7**: 115-117

Fimia GM, Kroemer G, Piacentini M (2013). Molecular mechanisms of selective autophagy. *Cell Death Differ* **20**: 1-2

Fischer T, Stone RM, Deangelo DJ, Galinsky I, Estey E, Lanza C, . . . Giles FJ (2010). Phase IIB trial of oral Midostaurin (PKC412), the FMS-like tyrosine kinase 3 receptor (FLT3) and multi-targeted kinase inhibitor, in patients with acute myeloid leukemia and high-risk myelodysplastic syndrome with either wild-type or mutated FLT3. *J Clin Oncol* **28**: 4339-4345

Fischer U, Janicke RU, Schulze-Osthoff K (2003). Many cuts to ruin: a comprehensive update of caspase substrates. *Cell Death Differ* **10**: 76-100

Flygare JA, Beresini M, Budha N, Chan H, Chan IT, Cheeti S, . . . Fairbrother WJ (2012). Discovery of a potent small-molecule antagonist of inhibitor of apoptosis (IAP) proteins and clinical candidate for the treatment of cancer (GDC-0152). *J Med Chem* **55**: 4101-4113

Forcet C, Ye X, Granger L, Corset V, Shin H, Bredesen DE, Mehlen P (2001). The dependence receptor DCC (deleted in colorectal cancer) defines an alternative mechanism for caspase activation. *Proc Natl Acad Sci U S A* **98**: 3416-3421

Fulda S, Vucic D (2012). Targeting IAP proteins for therapeutic intervention in cancer. *Nat Rev Drug Discov* **11**: 109-124

Funderburk SF, Wang QJ, Yue Z (2010). The Beclin 1-VPS34 complex--at the crossroads of autophagy and beyond. *Trends Cell Biol* **20**: 355-362

Fuse E, Kuwabara T, Sparreboom A, Sausville EA, Figg WD (2005). Review of UCN-01 development: a lesson in the importance of clinical pharmacology. *J Clin Pharmacol* **45**: 394-403

Ganley IG, Lam du H, Wang J, Ding X, Chen S, Jiang X (2009). ULK1.ATG13.FIP200 complex mediates mTOR signaling and is essential for autophagy. *J Biol Chem* **284**: 12297-12305

Garami A, Zwartkruis FJ, Nobukuni T, Joaquin M, Roccio M, Stocker H, . . . Thomas G (2003). Insulin activation of Rheb, a mediator of mTOR/S6K/4E-BP signaling, is inhibited by TSC1 and 2. *Mol Cell* **11**: 1457-1466

Geng J, Klionsky DJ (2008). The Atg8 and Atg12 ubiquitin-like conjugation systems in macroautophagy. 'Protein modifications: beyond the usual suspects' review series. *EMBO Rep* **9**: 859-864

Gescher A (2000). Staurosporine analogues - pharmacological toys or useful antitumour agents? *Crit Rev Oncol Hematol* **34**: 127-135

Gibson L, Holmgreen SP, Huang DC, Bernard O, Copeland NG, Jenkins NA, . . . Cory S (1996). bcl-w, a novel member of the bcl-2 family, promotes cell survival. *Oncogene* **13**: 665-675

Graham FL, Smiley J, Russell WC, Nairn R (1977). Characteristics of a human cell line transformed by DNA from human adenovirus type 5. *J Gen Virol* **36**: 59-74

Grasso D, Ropolo A, Lo Re A, Boggio V, Molejon MI, Iovanna JL, . . . Vaccaro MI (2011). Zymophagy, a novel selective autophagy pathway mediated by VMP1-USP9x-p62, prevents pancreatic cell death. *J Biol Chem* **286**: 8308-8324

Gwinn DM, Shackelford DB, Egan DF, Mihaylova MM, Mery A, Vasquez DS, . . . Shaw RJ (2008). AMPK phosphorylation of raptor mediates a metabolic checkpoint. *Mol Cell* **30**: 214-226

Hailey DW, Rambold AS, Satpute-Krishnan P, Mitra K, Sougrat R, Kim PK, Lippincott-Schwartz J (2010). Mitochondria supply membranes for autophagosome biogenesis during starvation. *Cell* **141**: 656-667

Hamasaki M, Furuta N, Matsuda A, Nezu A, Yamamoto A, Fujita N, . . . Yoshimori T (2013). Autophagosomes form at ER-mitochondria contact sites. *Nature* **495**: 389-393

Hanada T, Noda NN, Satomi Y, Ichimura Y, Fujioka Y, Takao T, . . . Ohsumi Y (2007). The Atg12-Atg5 conjugate has a novel E3-like activity for protein lipidation in autophagy. *J Biol Chem* **282**: 37298-37302

Hanahan D, Weinberg RA (2011). Hallmarks of cancer: the next generation. *Cell* **144**: 646-674

Happo L, Strasser A, Cory S (2012). BH3-only proteins in apoptosis at a glance. *J Cell Sci* **125**: 1081-1087

Hara K, Maruki Y, Long X, Yoshino K, Oshiro N, Hidayat S, . . . Yonezawa K (2002). Raptor, a binding partner of target of rapamycin (TOR), mediates TOR action. *Cell* **110**: 177-189

Harkin ST, Cohen GM, Gescher A (1998). Modulation of apoptosis in rat thymocytes by analogs of staurosporine: lack of direct association with inhibition of protein kinase C. *Mol Pharmacol* **54**: 663-670

Harris DR, Mims A, Bunz F (2012). Genetic disruption of USP9X sensitizes colorectal cancer cells to 5-fluorouracil. *Cancer Biol Ther* **13**: 1319-1324

Hayashi-Nishino M, Fujita N, Noda T, Yamaguchi A, Yoshimori T, Yamamoto A (2009). A subdomain of the endoplasmic reticulum forms a cradle for autophagosome formation. *Nat Cell Biol* **11**: 1433-1437

He C, Baba M, Cao Y, Klionsky DJ (2008). Self-interaction is critical for Atg9 transport and function at the phagophore assembly site during autophagy. *Mol Biol Cell* **19**: 5506-5516

He C, Klionsky DJ (2009). Regulation mechanisms and signaling pathways of autophagy. *Annu Rev Genet* **43**: 67-93

Herrero-Martin G, Hoyer-Hansen M, Garcia-Garcia C, Fumarola C, Farkas T, Lopez-Rivas A, Jaattela M (2009). TAK1 activates AMPK-dependent cytoprotective autophagy in TRAIL-treated epithelial cells. *EMBO J* **28**: 677-685

Hershko A, Ciechanover A (1992). The ubiquitin system for protein degradation. *Annu Rev Biochem* **61**: 761-807

Hill MM, Adrain C, Duriez PJ, Creagh EM, Martin SJ (2004). Analysis of the composition, assembly kinetics and activity of native Apaf-1 apoptosomes. *EMBO J* **23**: 2134-2145

Hinds MG, Norton RS, Vaux DL, Day CL (1999). Solution structure of a baculoviral inhibitor of apoptosis (IAP) repeat. *Nat Struct Biol* **6**: 648-651

Hosokawa N, Hara T, Kaizuka T, Kishi C, Takamura A, Miura Y, . . . Mizushima N (2009). Nutrient-dependent mTORC1 association with the ULK1-Atg13-FIP200 complex required for autophagy. *Mol Biol Cell* **20**: 1981-1991

Hoyer-Hansen M, Bastholm L, Szyniarowski P, Campanella M, Szabadkai G, Farkas T, . . . Jaattela M (2007). Control of macroautophagy by calcium, calmodulin-dependent kinase kinase-beta, and Bcl-2. *Mol Cell* **25**: 193-205

Hu Y, Ding L, Spencer DM, Nunez G (1998). WD-40 repeat region regulates Apaf-1 self-association and procaspase-9 activation. *J Biol Chem* **273**: 33489-33494

Huang J, Manning BD (2009). A complex interplay between Akt, TSC2 and the two mTOR complexes. *Biochem Soc Trans* **37**: 217-222

Ikeda F, Dikic I (2008). Atypical ubiquitin chains: new molecular signals. 'Protein Modifications: Beyond the Usual Suspects' review series. *EMBO Rep* **9**: 536-542

Imao T, Nagata S (2013). Apaf-1- and Caspase-8-independent apoptosis. *Cell Death Differ* **20**: 343-352

Inohara N, Koseki T, del Peso L, Hu Y, Yee C, Chen S, . . . Nunez G (1999). Nod1, an Apaf-1-like activator of caspase-9 and nuclear factor-kappaB. *J Biol Chem* **274**: 14560-14567

Inoki K, Ouyang H, Zhu T, Lindvall C, Wang Y, Zhang X, . . . Guan KL (2006). TSC2 integrates Wnt and energy signals via a coordinated phosphorylation by AMPK and GSK3 to regulate cell growth. *Cell* **126**: 955-968

Itakura E, Kishi-Itakura C, Mizushima N (2012). The hairpin-type tail-anchored SNARE syntaxin 17 targets to autophagosomes for fusion with endosomes/lysosomes. *Cell* **151**: 1256-1269

Janssens S, Tinel A (2012). The PIDDosome, DNA-damage-induced apoptosis and beyond. *Cell Death Differ* **19**: 13-20

Johansson AC, Steen H, Ollinger K, Roberg K (2003). Cathepsin D mediates cytochrome c release and caspase activation in human fibroblast apoptosis induced by staurosporine. *Cell Death Differ* **10**: 1253-1259

Johnson VL, Cooper IR, Jenkins JR, Chow SC (1999). Effects of differential overexpression of Bcl-2 on apoptosis, proliferation, and telomerase activity in Jurkat T cells. *Exp Cell Res* **251**: 175-184

Johnston JA, Ward CL, Kopito RR (1998). Aggresomes: a cellular response to misfolded proteins. *J Cell Biol* **143**: 1883-1898

Johnstone RW, Ruefli AA, Lowe SW (2002). Apoptosis: a link between cancer genetics and chemotherapy. *Cell* **108**: 153-164

Jung CH, Jun CB, Ro SH, Kim YM, Otto NM, Cao J, . . . Kim DH (2009). ULK-Atg13-FIP200 complexes mediate mTOR signaling to the autophagy machinery. *Mol Biol Cell* **20**: 1992-2003

Kabeya Y, Mizushima N, Yamamoto A, Oshitani-Okamoto S, Ohsumi Y, Yoshimori T (2004). LC3, GABARAP and GATE16 localize to autophagosomal membrane depending on form-II formation. *J Cell Sci* **117**: 2805-2812

Kaczmarek A, Vandenabeele P, Krysko DV (2013). Necroptosis: the release of damage-associated molecular patterns and its physiological relevance. *Immunity* **38**: 209-223

Kang R, Zeh HJ, Lotze MT, Tang D (2011). The Beclin 1 network regulates autophagy and apoptosis. *Cell Death Differ* **18**: 571-580

Kantari C, Walczak H (2011). Caspase-8 and bid: caught in the act between death receptors and mitochondria. *Biochim Biophys Acta* **1813**: 558-563

Kapuria V, Levitzki A, Bornmann WG, Maxwell D, Priebe W, Sorenson RJ, . . . Donato NJ (2011). A novel small molecule deubiquitinase inhibitor blocks Jak2 signaling through Jak2 ubiquitination. *Cell Signal* **23**: 2076-2085

Kapuria V, Peterson LF, Fang D, Bornmann WG, Talpaz M, Donato NJ (2010). Deubiquitinase inhibition by small-molecule WP1130 triggers aggresome formation and tumor cell apoptosis. *Cancer Res* **70**: 9265-9276

Kaufmann T, Tai L, Ekert PG, Huang DC, Norris F, Lindemann RK, . . . Strasser A (2007). The BH3-only protein bid is dispensable for DNA damage- and replicative stress-induced apoptosis or cell-cycle arrest. *Cell* **129**: 423-433

Kawaguchi Y, Kovacs JJ, McLaurin A, Vance JM, Ito A, Yao TP (2003). The deacetylase HDAC6 regulates aggresome formation and cell viability in response to misfolded protein stress. *Cell* **115**: 727-738

Kerr JF, Wyllie AH, Currie AR (1972). Apoptosis: a basic biological phenomenon with wide-ranging implications in tissue kinetics. *Br J Cancer* **26**: 239-257

Khaw SL, Huang DC, Roberts AW (2011). Overcoming blocks in apoptosis with BH3-mimetic therapy in haematological malignancies. *Pathology* **43**: 525-535

Kim DH, Sarbassov DD, Ali SM, Latek RR, Guntur KV, Erdjument-Bromage H, . . . Sabatini DM (2003). GbetaL, a positive regulator of the rapamycin-sensitive pathway required for the nutrient-sensitive interaction between raptor and mTOR. *Mol Cell* **11**: 895-904

Kim J, Kundu M, Viollet B, Guan KL (2011). AMPK and mTOR regulate autophagy through direct phosphorylation of Ulk1. *Nat Cell Biol* **13**: 132-141

Kischkel FC, Hellbardt S, Behrmann I, Germer M, Pawlita M, Krammer PH, Peter ME (1995). Cytotoxicity-dependent APO-1 (Fas/CD95)-associated proteins form a death-inducing signaling complex (DISC) with the receptor. *EMBO J* **14**: 5579-5588

Klionsky DJ (2008). Autophagy revisited: a conversation with Christian de Duve. *Autophagy* **4**: 740-743

Klionsky DJ, Abdalla FC, Abeliovich H, Abraham RT, Acevedo-Arozena A, Adeli K, . . . Zuckerbraun B (2012). Guidelines for the use and interpretation of assays for monitoring autophagy. *Autophagy* **8**: 445-544

Kobayashi S, Yoneda-Kato N, Itahara N, Yoshida A, Kato JY (2013). The COP1 E3-ligase interacts with FIP200, a key regulator of mammalian autophagy. *BMC Biochem* **14**: 1

Komander D, Clague MJ, Urbe S (2009). Breaking the chains: structure and function of the deubiquitinases. *Nature reviews Molecular cell biology* **10**: 550-563

Kozopas KM, Yang T, Buchan HL, Zhou P, Craig RW (1993). MCL1, a gene expressed in programmed myeloid cell differentiation, has sequence similarity to BCL2. *Proc Natl Acad Sci U S A* **90**: 3516-3520

Kulikov AV, Shilov ES, Mufazalov IA, Gogvadze V, Nedospasov SA, Zhivotovsky B (2012). Cytochrome c: the Achilles' heel in apoptosis. *Cell Mol Life Sci* **69**: 1787-1797

Kundu M, Lindsten T, Yang CY, Wu J, Zhao F, Zhang J, . . . Thompson CB (2008). Ulk1 plays a critical role in the autophagic clearance of mitochondria and ribosomes during reticulocyte maturation. *Blood* **112**: 1493-1502

Laemmli UK (1970). Cleavage of structural proteins during the assembly of the head of bacteriophage T4. *Nature* **227**: 680-685

Lamkanfi M, Kalai M, Vandenabeele P (2004). Caspase-12: an overview. *Cell Death Differ* **11**: 365-368

Laplante M, Sabatini DM (2012). mTOR signaling in growth control and disease. *Cell* **149**: 274-293

Lauber K, Bohn E, Krober SM, Xiao YJ, Blumenthal SG, Lindemann RK, . . . Wesselborg S (2003). Apoptotic cells induce migration of phagocytes via caspase-3-mediated release of a lipid attraction signal. *Cell* **113**: 717-730

Lavrik I, Golks A, Krammer PH (2005). Death receptor signaling. *J Cell Sci* **118**: 265-267

Lavrik IN, Krammer PH (2012). Regulation of CD95/Fas signaling at the DISC. *Cell Death Differ* **19**: 36-41

Li H, Zhu H, Xu CJ, Yuan J (1998). Cleavage of BID by caspase 8 mediates the mitochondrial damage in the Fas pathway of apoptosis. *Cell* **94**: 491-501

Li M, Chen D, Shiloh A, Luo J, Nikolaev AY, Qin J, Gu W (2002). Deubiquitination of p53 by HAUSP is an important pathway for p53 stabilization. *Nature* **416**: 648-653

Li P, Nijhawan D, Budihardjo I, Srinivasula SM, Ahmad M, Alnemri ES, Wang X (1997). Cytochrome c and dATP-dependent formation of Apaf-1/caspase-9 complex initiates an apoptotic protease cascade. *Cell* **91**: 479-489

Lin EY, Orlofsky A, Berger MS, Prystowsky MB (1993). Characterization of A1, a novel hemopoietic-specific early-response gene with sequence similarity to bcl-2. *Journal of immunology* **151**: 1979-1988

Lin SY, Li TY, Liu Q, Zhang C, Li X, Chen Y, . . . Lin SC (2012). GSK3-TIP60-ULK1 signaling pathway links growth factor deprivation to autophagy. *Science* **336**: 477-481

Liu J, Xia H, Kim M, Xu L, Li Y, Zhang L, . . . Yuan J (2011). Beclin1 controls the levels of p53 by regulating the deubiquitination activity of USP10 and USP13. *Cell* **147**: 223-234

Liu X, Kim CN, Yang J, Jemmerson R, Wang X (1996). Induction of apoptotic program in cell-free extracts: requirement for dATP and cytochrome c. *Cell* **86**: 147-157

Liu Y, Lashuel HA, Choi S, Xing X, Case A, Ni J, . . . Lansbury PT, Jr. (2003). Discovery of inhibitors that elucidate the role of UCH-L1 activity in the H1299 lung cancer cell line. *Chem Biol* **10**: 837-846

Llambi F, Moldoveanu T, Tait SW, Bouchier-Hayes L, Temirov J, McCormick LL, . . . Green DR (2011). A unified model of mammalian BCL-2 protein family interactions at the mitochondria. *Mol Cell* **44**: 517-531

Löffler AS, Alers S, Dieterle AM, Keppeler H, Franz-Wachtel M, Kundu M, . . . Stork B (2011). Ulk1-mediated phosphorylation of AMPK constitutes a negative regulatory feedback loop. *Autophagy* **7**: 696-706

Lomonosova E, Chinnadurai G (2008). BH3-only proteins in apoptosis and beyond: an overview. *Oncogene* **27 Suppl 1**: S2-19

Lopez-Anton N, Rudy A, Barth N, Schmitz ML, Pettit GR, Schulze-Osthoff K, . . . Vollmar AM (2006). The marine product cephalostatin 1 activates an endoplasmic reticulum stress-specific and apoptosome-independent apoptotic signaling pathway. *J Biol Chem* **281**: 33078-33086

Ly JD, Grubb DR, Lawen A (2003). The mitochondrial membrane potential (deltapsi(m)) in apoptosis; an update. *Apoptosis* **8**: 115-128

Mack HI, Zheng B, Asara JM, Thomas SM (2012). AMPK-dependent phosphorylation of ULK1 regulates ATG9 localization. *Autophagy* **8**: 1197-1214

Madeo F, Frohlich E, Frohlich KU (1997). A yeast mutant showing diagnostic markers of early and late apoptosis. *J Cell Biol* **139**: 729-734

Manns J, Daubrawa M, Driessen S, Paasch F, Hoffmann N, Löffler A, . . . Wesselborg S (2011). Triggering of a novel intrinsic apoptosis pathway by the kinase inhibitor staurosporine: activation of caspase-9 in the absence of Apaf-1. *FASEB J* **25**: 3250-3261

Marino G, Uria JA, Puente XS, Quesada V, Bordallo J, Lopez-Otin C (2003). Human autophagins, a family of cysteine proteinases potentially implicated in cell degradation by autophagy. *J Biol Chem* **278**: 3671-3678

Martin MC, Allan LA, Lickrish M, Sampson C, Morrice N, Clarke PR (2005). Protein kinase A regulates caspase-9 activation by Apaf-1 downstream of cytochrome c. *J Biol Chem* **280**: 15449-15455

McAlpine F, Williamson LE, Tooze SA, Chan EY (2013). Regulation of nutrient-sensitive autophagy by uncoordinated 51-like kinases 1 and 2. *Autophagy* **9**: 361-373

McConnell BB, Vertino PM (2000). Activation of a caspase-9-mediated apoptotic pathway by subcellular redistribution of the novel caspase recruitment domain protein TMS1. *Cancer Res* **60**: 6243-6247

McDonnell MA, Abedin MJ, Melendez M, Platikanova TN, Ecklund JR, Ahmed K, Kelekar A (2008). Phosphorylation of murine caspase-9 by the protein kinase casein kinase 2 regulates its cleavage by caspase-8. *J Biol Chem* **283**: 20149-20158

McIlwain DR, Berger T, Mak TW (2013). Caspase functions in cell death and disease. *Cold Spring Harb Perspect Med* **3**: a008656

Meijer WH, van der Klei IJ, Veenhuis M, Kiel JA (2007). ATG genes involved in non-selective autophagy are conserved from yeast to man, but the selective Cvt and pexophagy pathways also require organism-specific genes. *Autophagy* **3**: 106-116

Meley D, Bauvy C, Houben-Weerts JH, Dubbelhuis PF, Helmond MT, Codogno P, Meijer AJ (2006). AMP-activated protein kinase and the regulation of autophagic proteolysis. *J Biol Chem* **281**: 34870-34879

Mille F, Thibert C, Fombonne J, Rama N, Guix C, Hayashi H, . . . Mehlen P (2009). The Patched dependence receptor triggers apoptosis through a DRAL-caspase-9 complex. *Nat Cell Biol* **11**: 739-746

Mizushima N (2010). The role of the Atg1/ULK1 complex in autophagy regulation. *Curr Opin Cell Biol* **22**: 132-139

Mizushima N, Kuma A, Kobayashi Y, Yamamoto A, Matsubae M, Takao T, . . . Yoshimori T (2003). Mouse Apg16L, a novel WD-repeat protein, targets to the autophagic isolation membrane with the Apg12-Apg5 conjugate. *J Cell Sci* **116**: 1679-1688

Mizushima N, Levine B (2010). Autophagy in mammalian development and differentiation. *Nat Cell Biol* **12**: 823-830

Mizushima N, Noda T, Ohsumi Y (1999). Apg16p is required for the function of the Apg12p-Apg5p conjugate in the yeast autophagy pathway. *EMBO J* **18**: 3888-3896

Mizushima N, Noda T, Yoshimori T, Tanaka Y, Ishii T, George MD, . . . Ohsumi Y (1998). A protein conjugation system essential for autophagy. *Nature* **395**: 395-398

Mizushima N, Yoshimori T, Levine B (2010). Methods in mammalian autophagy research. *Cell* **140**: 313-326

Mizushima N, Yoshimori T, Ohsumi Y (2011). The role of Atg proteins in autophagosome formation. *Annu Rev Cell Dev Biol* **27**: 107-132

Moldoveanu T, Follis AV, Kriwacki RW, Green DR (2014). Many players in BCL-2 family affairs. *Trends Biochem Sci* **39**: 101-111

Morita S, Kojima T, Kitamura T (2000). Plat-E: an efficient and stable system for transient packaging of retroviruses. *Gene Ther* **7**: 1063-1066

Mullis K, Faloona F, Scharf S, Saiki R, Horn G, Erlich H (1986). Specific enzymatic amplification of DNA in vitro: the polymerase chain reaction. *Cold Spring Harb Symp Quant Biol* **51 Pt 1**: 263-273

Nagasaka A, Kawane K, Yoshida H, Nagata S (2010). Apaf-1-independent programmed cell death in mouse development. *Cell Death Differ* **17**: 931-941

Nagata S, Hanayama R, Kawane K (2010). Autoimmunity and the clearance of dead cells. *Cell* **140**: 619-630

Nakano K, Vousden KH (2001). PUMA, a novel proapoptotic gene, is induced by p53. *Mol Cell* **7**: 683-694

Nazio F, Strappazzon F, Antonioli M, Bielli P, Cianfanelli V, Bordi M, . . . Cecconi F (2013). mTOR inhibits autophagy by controlling ULK1 ubiquitylation, self-association and function through AMBRA1 and TRAF6. *Nat Cell Biol* **15**: 406-416

Nicoletti I, Migliorati G, Pagliacci MC, Grignani F, Riccardi C (1991). A rapid and simple method for measuring thymocyte apoptosis by propidium iodide staining and flow cytometry. *J Immunol Methods* **139**: 271-279

Nijman SM, Luna-Vargas MP, Velds A, Brummelkamp TR, Dirac AM, Sixma TK, Bernards R (2005). A genomic and functional inventory of deubiquitinating enzymes. *Cell* **123**: 773-786

Nilsson C, Johansson U, Johansson AC, Kagedal K, Ollinger K (2006). Cytosolic acidification and lysosomal alkalinization during TNF-alpha induced apoptosis in U937 cells. *Apoptosis* **11**: 1149-1159

Oda E, Ohki R, Murasawa H, Nemoto J, Shibue T, Yamashita T, . . . Tanaka N (2000). Noxa, a BH3-only member of the Bcl-2 family and candidate mediator of p53-induced apoptosis. *Science* **288**: 1053-1058

Oltersdorf T, Elmore SW, Shoemaker AR, Armstrong RC, Augeri DJ, Belli BA, . . . Rosenberg SH (2005). An inhibitor of Bcl-2 family proteins induces regression of solid tumours. *Nature* **435**: 677-681

Omura S, Iwai Y, Hirano A, Nakagawa A, Awaya J, Tsuchya H, . . . Masuma R (1977). A new alkaloid AM-2282 OF Streptomyces origin. Taxonomy, fermentation, isolation and preliminary characterization. *J Antibiot (Tokyo)* **30**: 275-282

Pan B, Yi J, Song H (2013). MicroRNA-mediated autophagic signaling networks and cancer chemoresistance. *Cancer Biother Radiopharm* **28**: 573-578

Pankiv S, Clausen TH, Lamark T, Brech A, Bruun JA, Outzen H, . . . Johansen T (2007). p62/SQSTM1 binds directly to Atg8/LC3 to facilitate degradation of ubiquitinated protein aggregates by autophagy. *J Biol Chem* **282**: 24131-24145

Peddaboina C, Jupiter D, Fletcher S, Yap JL, Rai A, Tobin RP, . . . Cao X (2012). The downregulation of Mcl-1 via USP9X inhibition sensitizes solid tumors to Bcl-xl inhibition. *BMC Cancer* **12**: 541

Peng Z, Maxwell DS, Sun D, Bhanu Prasad BA, Schuber PT, Jr., Pal A, . . . Bornmann WG (2014). Degrasyn-like symmetrical compounds: Possible therapeutic agents for multiple myeloma (MM-I). *Bioorg Med Chem* **22**: 1450-1458

Perez RP, Lewis LD, Beelen AP, Olszanski AJ, Johnston N, Rhodes CH, . . . Eastman A (2006). Modulation of cell cycle progression in human tumors: a pharmacokinetic and tumor

molecular pharmacodynamic study of cisplatin plus the Chk1 inhibitor UCN-01 (NSC 638850). *Clinical cancer research : an official journal of the American Association for Cancer Research* **12**: 7079-7085

Perkins DN, Pappin DJ, Creasy DM, Cottrell JS (1999). Probability-based protein identification by searching sequence databases using mass spectrometry data. *Electrophoresis* **20**: 3551-3567

Peter ME, Krammer PH (2003). The CD95(APO-1/Fas) DISC and beyond. *Cell Death Differ* **10**: 26-35

Petherick KJ, Conway OJ, Mpamhanga C, Osborne SA, Kamal A, Saxty B, Ganley IG (2015). Pharmacological Inhibition of ULK1 Blocks mTOR-Dependent Autophagy. *J Biol Chem*

Petiot A, Ogier-Denis E, Blommaart EF, Meijer AJ, Codogno P (2000). Distinct classes of phosphatidylinositol 3'-kinases are involved in signaling pathways that control macroautophagy in HT-29 cells. *J Biol Chem* **275**: 992-998

Polson HE, de Lartigue J, Rigden DJ, Reedijk M, Urbe S, Clague MJ, Tooze SA (2010). Mammalian Atg18 (WIPI2) localizes to omegasome-anchored phagophores and positively regulates LC3 lipidation. *Autophagy* **6**: 506-522

Ponten J, Saksela E (1967). Two established in vitro cell lines from human mesenchymal tumours. *International journal of cancer Journal international du cancer* **2**: 434-447

Pop C, Salvesen GS (2009). Human caspases: activation, specificity, and regulation. *J Biol Chem* **284**: 21777-21781

Pop C, Timmer J, Sperandio S, Salvesen GS (2006). The apoptosome activates caspase-9 by dimerization. *Mol Cell* **22**: 269-275

Proikas-Cezanne T, Waddell S, Gaugel A, Frickey T, Lupas A, Nordheim A (2004). WIPI-1alpha (WIPI49), a member of the novel 7-bladed WIPI protein family, is aberrantly expressed in human cancer and is linked to starvation-induced autophagy. *Oncogene* **23**: 9314-9325

Qin H, Srinivasula SM, Wu G, Fernandes-Alnemri T, Alnemri ES, Shi Y (1999). Structural basis of procaspase-9 recruitment by the apoptotic protease-activating factor 1. *Nature* **399**: 549-557

Raina D, Pandey P, Ahmad R, Bharti A, Ren J, Kharbanda S, . . . Kufe D (2005). c-Abl tyrosine kinase regulates caspase-9 autocleavage in the apoptotic response to DNA damage. *J Biol Chem* **280**: 11147-11151

Ravichandran KS (2011). Beginnings of a good apoptotic meal: the find-me and eat-me signaling pathways. *Immunity* **35**: 445-455

Reggiori F, Komatsu M, Finley K, Simonsen A (2012). Selective types of autophagy. *Int J Cell Biol* **2012**: 156272

Reiling JH, Hafen E (2004). The hypoxia-induced paralogs Scylla and Charybdis inhibit growth by down-regulating S6K activity upstream of TSC in Drosophila. *Genes Dev* **18**: 2879-2892

Renatus M, Stennicke HR, Scott FL, Liddington RC, Salvesen GS (2001). Dimer formation drives the activation of the cell death protease caspase 9. *Proc Natl Acad Sci U S A* **98**: 14250-14255

Renehan AG, Booth C, Potten CS (2001). What is apoptosis, and why is it important? *BMJ* **322**: 1536-1538

Reubold TF, Eschenburg S (2012). A molecular view on signal transduction by the apoptosome. *Cell Signal* **24**: 1420-1425

Riedl SJ, Salvesen GS (2007). The apoptosome: signalling platform of cell death. *Nat Rev Mol Cell Biol* **8**: 405-413

Rodriguez J, Lazebnik Y (1999). Caspase-9 and APAF-1 form an active holoenzyme. *Genes Dev* **13**: 3179-3184

Russell RC, Tian Y, Yuan H, Park HW, Chang YY, Kim J, . . . Guan KL (2013). ULK1 induces autophagy by phosphorylating Beclin-1 and activating VPS34 lipid kinase. *Nat Cell Biol* **15**: 741-750

Saiki RK, Scharf S, Faloona F, Mullis KB, Horn GT, Erlich HA, Arnheim N (1985). Enzymatic amplification of beta-globin genomic sequences and restriction site analysis for diagnosis of sickle cell anemia. *Science* **230**: 1350-1354

Saleh A, Srinivasula SM, Acharya S, Fishel R, Alnemri ES (1999). Cytochrome c and dATP-mediated oligomerization of Apaf-1 is a prerequisite for procaspase-9 activation. *J Biol Chem* **274**: 17941-17945

Salvesen GS, Dixit VM (1999). Caspase activation: the induced-proximity model. *Proc Natl Acad Sci U S A* **96**: 10964-10967

Samraj AK, Sohn D, Schulze-Osthoff K, Schmitz I (2007). Loss of caspase-9 reveals its essential role for caspase-2 activation and mitochondrial membrane depolarization. *Mol Biol Cell* **18**: 84-93

Sancak Y, Peterson TR, Shaul YD, Lindquist RA, Thoreen CC, Bar-Peled L, Sabatini DM (2008). The Rag GTPases bind raptor and mediate amino acid signaling to mTORC1. *Science* **320**: 1496-1501

Sancak Y, Thoreen CC, Peterson TR, Lindquist RA, Kang SA, Spooner E, . . . Sabatini DM (2007). PRAS40 is an insulin-regulated inhibitor of the mTORC1 protein kinase. *Mol Cell* **25**: 903-915

Sanger F, Nicklen S, Coulson AR (1977). DNA sequencing with chain-terminating inhibitors. *Proc Natl Acad Sci U S A* **74**: 5463-5467

Satoo K, Noda NN, Kumeta H, Fujioka Y, Mizushima N, Ohsumi Y, Inagaki F (2009). The structure of Atg4B-LC3 complex reveals the mechanism of LC3 processing and delipidation during autophagy. *EMBO J* **28**: 1341-1350

Scaffidi C, Fulda S, Srinivasan A, Friesen C, Li F, Tomaselli KJ, . . . Peter ME (1998). Two CD95 (APO-1/Fas) signaling pathways. *EMBO J* **17**: 1675-1687

Schneider U, Schwenk HU, Bornkamm G (1977). Characterization of EBV-genome negative "null" and "T" cell lines derived from children with acute lymphoblastic leukemia and leukemic transformed non-Hodgkin lymphoma. *International journal of cancer Journal international du cancer* **19**: 621-626

Schwickart M, Huang X, Lill JR, Liu J, Ferrando R, French DM, . . . Dixit VM (2010). Deubiquitinase USP9X stabilizes MCL1 and promotes tumour cell survival. *Nature* **463**: 103-107

Scott FL, Denault JB, Riedl SJ, Shin H, Renatus M, Salvesen GS (2005). XIAP inhibits caspase-3 and -7 using two binding sites: evolutionarily conserved mechanism of IAPs. *EMBO J* **24**: 645-655

Seifert A, Allan LA, Clarke PR (2008). DYRK1A phosphorylates caspase 9 at an inhibitory site and is potently inhibited in human cells by harmine. *FEBS J* **275**: 6268-6280

Shang L, Chen S, Du F, Li S, Zhao L, Wang X (2011). Nutrient starvation elicits an acute autophagic response mediated by Ulk1 dephosphorylation and its subsequent dissociation from AMPK. *Proc Natl Acad Sci U S A* **108**: 4788-4793

Shintani T, Mizushima N, Ogawa Y, Matsuura A, Noda T, Ohsumi Y (1999). Apg10p, a novel protein-conjugating enzyme essential for autophagy in yeast. *EMBO J* **18**: 5234-5241

Shiozaki EN, Chai J, Rigotti DJ, Riedl SJ, Li P, Srinivasula SM, . . . Shi Y (2003). Mechanism of XIAP-mediated inhibition of caspase-9. *Mol Cell* **11**: 519-527

Shiozaki EN, Chai J, Shi Y (2002). Oligomerization and activation of caspase-9, induced by Apaf-1 CARD. *Proc Natl Acad Sci U S A* **99**: 4197-4202

Snyder H, Mensah K, Theisler C, Lee J, Matouschek A, Wolozin B (2003). Aggregated and monomeric alpha-synuclein bind to the S6' proteasomal protein and inhibit proteasomal function. *J Biol Chem* **278**: 11753-11759

Sonoda E, Morrison C, Yamashita YM, Takata M, Takeda S (2001). Reverse genetic studies of homologous DNA recombination using the chicken B-lymphocyte line, DT40. *Philos Trans R Soc Lond B Biol Sci* **356**: 111-117

Sparreboom A, Chen H, Acharya MR, Senderowicz AM, Messmann RA, Kuwabara T, . . . Figg WD (2004). Effects of alpha1-acid glycoprotein on the clinical pharmacokinetics of 7-hydroxystaurosporine. *Clinical cancer research : an official journal of the American Association for Cancer Research* **10**: 6840-6846

Srinivasula SM, Ashwell JD (2008). IAPs: what's in a name? *Mol Cell* **30**: 123-135

Srinivasula SM, Hegde R, Saleh A, Datta P, Shiozaki E, Chai J, . . . Alnemri ES (2001). A conserved XIAP-interaction motif in caspase-9 and Smac/DIABLO regulates caspase activity and apoptosis. *Nature* **410**: 112-116

Stepczynska A, Lauber K, Engels IH, Janssen O, Kabelitz D, Wesselborg S, Schulze-Osthoff K (2001). Staurosporine and conventional anticancer drugs induce overlapping, yet distinct pathways of apoptosis and caspase activation. *Oncogene* **20**: 1193-1202

Strasser A, Cory S, Adams JM (2011). Deciphering the rules of programmed cell death to improve therapy of cancer and other diseases. *EMBO J* **30**: 3667-3683

Sun H, Kapuria V, Peterson LF, Fang D, Bornmann WG, Bartholomeusz G, . . . Donato NJ (2011). Bcr-Abl ubiquitination and Usp9x inhibition block kinase signaling and promote CML cell apoptosis. *Blood* **117**: 3151-3162

Suzuki K, Kirisako T, Kamada Y, Mizushima N, Noda T, Ohsumi Y (2001). The pre-autophagosomal structure organized by concerted functions of APG genes is essential for autophagosome formation. *EMBO J* **20**: 5971-5981

Suzuki K, Kubota Y, Sekito T, Ohsumi Y (2007). Hierarchy of Atg proteins in pre-autophagosomal structure organization. *Genes Cells* **12**: 209-218

Tamaoki T, Nomoto H, Takahashi I, Kato Y, Morimoto M, Tomita F (1986). Staurosporine, a potent inhibitor of phospholipid/Ca++dependent protein kinase. *Biochem Biophys Res Commun* **135**: 397-402

Tanida I, Minematsu-Ikeguchi N, Ueno T, Kominami E (2005). Lysosomal turnover, but not a cellular level, of endogenous LC3 is a marker for autophagy. *Autophagy* **1**: 84-91

Taylor JP, Tanaka F, Robitschek J, Sandoval CM, Taye A, Markovic-Plese S, Fischbeck KH (2003). Aggresomes protect cells by enhancing the degradation of toxic polyglutamine-containing protein. *Hum Mol Genet* **12**: 749-757

Tenev T, Bianchi K, Darding M, Broemer M, Langlais C, Wallberg F, . . . Meier P (2011). The Ripoptosome, a signaling platform that assembles in response to genotoxic stress and loss of IAPs. *Mol Cell* **43**: 432-448

Tepper AD, Cock JG, de Vries E, Borst J, van Blitterswijk WJ (1997). CD95/Fas-induced ceramide formation proceeds with slow kinetics and is not blocked by caspase-3/CPP32 inhibition. *J Biol Chem* **272**: 24308-24312

Tinel A, Tschopp J (2004). The PIDDosome, a protein complex implicated in activation of caspase-2 in response to genotoxic stress. *Science* **304**: 843-846

Tsukada M, Ohsumi Y (1993). Isolation and characterization of autophagy-defective mutants of Saccharomyces cerevisiae. *FEBS Lett* **333**: 169-174

van Delft MF, Wei AH, Mason KD, Vandenberg CJ, Chen L, Czabotar PE, . . . Huang DC (2006). The BH3 mimetic ABT-737 targets selective Bcl-2 proteins and efficiently induces apoptosis via Bak/Bax if Mcl-1 is neutralized. *Cancer Cell* **10**: 389-399

Vandenabeele P, Galluzzi L, Vanden Berghe T, Kroemer G (2010). Molecular mechanisms of necroptosis: an ordered cellular explosion. *Nat Rev Mol Cell Biol* **11**: 700-714

Vaux DL (2011). Apoptogenic factors released from mitochondria. *Biochim Biophys Acta* **1813**: 546-550

Vaux DL, Cory S, Adams JM (1988). Bcl-2 gene promotes haemopoietic cell survival and cooperates with c-myc to immortalize pre-B cells. *Nature* **335**: 440-442

Vaux DL, Silke J (2003). Mammalian mitochondrial IAP binding proteins. *Biochem Biophys Res Commun* **304**: 499-504

Walczak H, Miller RE, Ariail K, Gliniak B, Griffith TS, Kubin M, . . . Lynch DH (1999). Tumoricidal activity of tumor necrosis factor-related apoptosis-inducing ligand in vivo. *Nat Med* **5**: 157-163

Wang HQ, Zhang HY, Hao FJ, Meng X, Guan Y, Du ZX (2008). Induction of BAG2 protein during proteasome inhibitor-induced apoptosis in thyroid carcinoma cells. *Br J Pharmacol* **155**: 655-660

Wang S, Kollipara RK, Srivastava N, Li R, Ravindranathan P, Hernandez E, . . . Kittler R (2014). Ablation of the oncogenic transcription factor ERG by deubiquitinase inhibition in prostate cancer. *Proc Natl Acad Sci U S A*

Weber K, Osborn M (1969). The reliability of molecular weight determinations by dodecyl sulfate-polyacrylamide gel electrophoresis. *J Biol Chem* **244**: 4406-4412

Wick W, Puduvalli VK, Chamberlain MC, van den Bent MJ, Carpentier AF, Cher LM, . . . Fine HA (2010). Phase III study of enzastaurin compared with lomustine in the treatment of recurrent intracranial glioblastoma. *J Clin Oncol* **28**: 1168-1174

Wong E, Cuervo AM (2010). Integration of clearance mechanisms: the proteasome and autophagy. *Cold Spring Harb Perspect Biol* **2**: a006734

Wong PM, Puente C, Ganley IG, Jiang X (2013). The ULK1 complex: sensing nutrient signals for autophagy activation. *Autophagy* **9**: 124-137

Yin XM, Wang K, Gross A, Zhao Y, Zinkel S, Klocke B, . . . Korsmeyer SJ (1999). Bid-deficient mice are resistant to Fas-induced hepatocellular apoptosis. *Nature* **400**: 886-891

Yla-Anttila P, Vihinen H, Jokitalo E, Eskelinen EL (2009). 3D tomography reveals connections between the phagophore and endoplasmic reticulum. *Autophagy* **5**: 1180-1185

Young AR, Chan EY, Hu XW, Kochl R, Crawshaw SG, High S, . . . Tooze SA (2006). Starvation and ULK1-dependent cycling of mammalian Atg9 between the TGN and endosomes. *J Cell Sci* **119**: 3888-3900

Yu X, Acehan D, Menetret JF, Booth CR, Ludtke SJ, Riedl SJ, . . . Akey CW (2005). A structure of the human apoptosome at 12.8 A resolution provides insights into this cell death platform. *Structure* **13**: 1725-1735

Yuan S, Yu X, Topf M, Ludtke SJ, Wang X, Akey CW (2010). Structure of an apoptosome-procaspase-9 CARD complex. *Structure* **18**: 571-583

Zhong Y, Wang QJ, Li X, Yan Y, Backer JM, Chait BT, . . . Yue Z (2009). Distinct regulation of autophagic activity by Atg14L and Rubicon associated with Beclin 1-phosphatidylinositol-3-kinase complex. *Nat Cell Biol* **11**: 468-476

Zhou X, Babu JR, da Silva S, Shu Q, Graef IA, Oliver T, . . . Wang F (2007). Unc-51-like kinase 1/2-mediated endocytic processes regulate filopodia extension and branching of sensory axons. *Proc Natl Acad Sci U S A* **104**: 5842-5847

Zou H, Li Y, Liu X, Wang X (1999). An APAF-1.cytochrome c multimeric complex is a functional apoptosome that activates procaspase-9. *J Biol Chem* **274**: 11549-11556

8 Addendum

8.1 Publications

Parts of this thesis are accepted for publication

Drießen S, Berleth N, Friesen O, Löffler AS, Böhler P, Hieke N, Stuhldreier F, Peter C, Schink KO, Schultz SW, Stenmark H, Holland P, Simonsen A, Wesselborg S, Stork B (2015). Deubiquitinase inhibition by WP1130 leads to ULK1 aggregation and blockade of autophagy. *Autophagy*

Further Publications

Hieke N, Löffler AS, Kaizuka T, Berleth N, Böhler P, **Drießen S**, Stuhldreier F, Friesen O, Assani K, Schmitz K, Peter C, Diedrich B, Dengjel J, Holland P, Simonsen A, Wesselborg S, Mizushima N, Stork B (2015). Expression of an ULK1/2 binding-deficient ATG13 variant can partially restore autophagic activity in ATG13-deficient cells. *Autophagy* accepted for publication.

Dieterle AM, Böhler P, Keppeler H, Alers S, Berleth N, **Drießen S**, Hieke N, Pietkiewicz S, Löffler AS, Peter C, Gray A, Leslie NR, Shinohara H, Kurosaki T, Engelke M, Wienands J, Bonin M, Wesselborg S, Stork B (2014). PDK1 controls upstream PI3K expression and PIP3 generation. *Oncogene* 33(23): 3043-3053.

Beck D, Niessner H, Smalley KS, Flaherty K, Paraiso KH, Busch C, Sinnberg T, Vasseur S, Iovanna L, **Drießen S**, Stork B, Wesselborg S, Schaller M, Biedermann T, Bauer J, Lasithiotakis K, Weise B, Eberle J, Schittek B, Schadendorf D, Garbe C, Kulms D, Meier F (2013). Vemurafenib potently induces endoplasmic reticulum stress-mediated apoptosis in BRAFV600E melanoma cells. *Sci Signal* 6(260): ra7.

Manns J, Daubrawa M, **Driessen S**, Paasch F, Hoffmann N, Löffler A, Lauber K, Dieterle A, Alers S, Iftner K, Schulze-Osthoff K, Stork B, Wesselborg S (2011). Triggering of a novel intrinsic apoptosis pathway by the kinase inhibitor staurosporine: activation of caspase-9 in the absence of Apaf-1. *FASEB Journal* 25(9): 3250-3261.

Hübener J, Vauti F, Funke C, Wolburg H, Ye Y, Schmidt T, Wolburg-Buchholz K, Schmitt I, Gardyan A, **Driessen S**, Arnold HH, Nguyen HP, Riess O (2011). N-terminal ataxin-3 causes neurological symptoms with inclusions, endoplasmic reticulum stress and ribosomal dislocation. *Brain* 134: 1925-1942.